

Reply to Report #1 (Anonymous Referee #7)

Dear Reviewer,

Thank you for your insight comments and suggestions. We have modified the manuscript accordingly. We trust that all of your comments have been addressed accordingly in the revised manuscript. If you have further suggestions for changes, please let us know. The detailed corrections are listed below point by point:

All changes in the manuscript are marked with **red color**.

Major comments

The authors have substantially improved this version of the manuscript. They have taken all my suggestions into account and therefore, I recommend the publication of this manuscript after addressing the following points.

Answer: Thank you for your valuable comments. In addition, we updated the DOI of the resulting dataset.

The newly uploaded files are the results of precipitation bias adjustment by WHU-SGCC method about four seasons.

Shen, G. Y., Chen, N. C., Wang, W., and Chen, Z. Q.: Improving the Climate Hazards Group Infrared Precipitation (CHIRP) using WHU-SGCC method over the Jinsha River Basin from 1990 to 2014. PANGAEA, <https://doi.org/10.1594/PANGAEA.905376>, 2019.

In addition, these four files without gauge information are the results of the WHU-SGCC method with all gauges as the input. 1. Figure 5: Here the authors show Pearson's correlation coefficients. I believe that the legend is a bit misleading. Generally, the green is used to represent well performance but the authors use it in the range between 0.2 and 0.5. It would be better to use a two-color palette (e.g., from red to blue).

Answer: Thanks. We changed the color of legend.

Change:

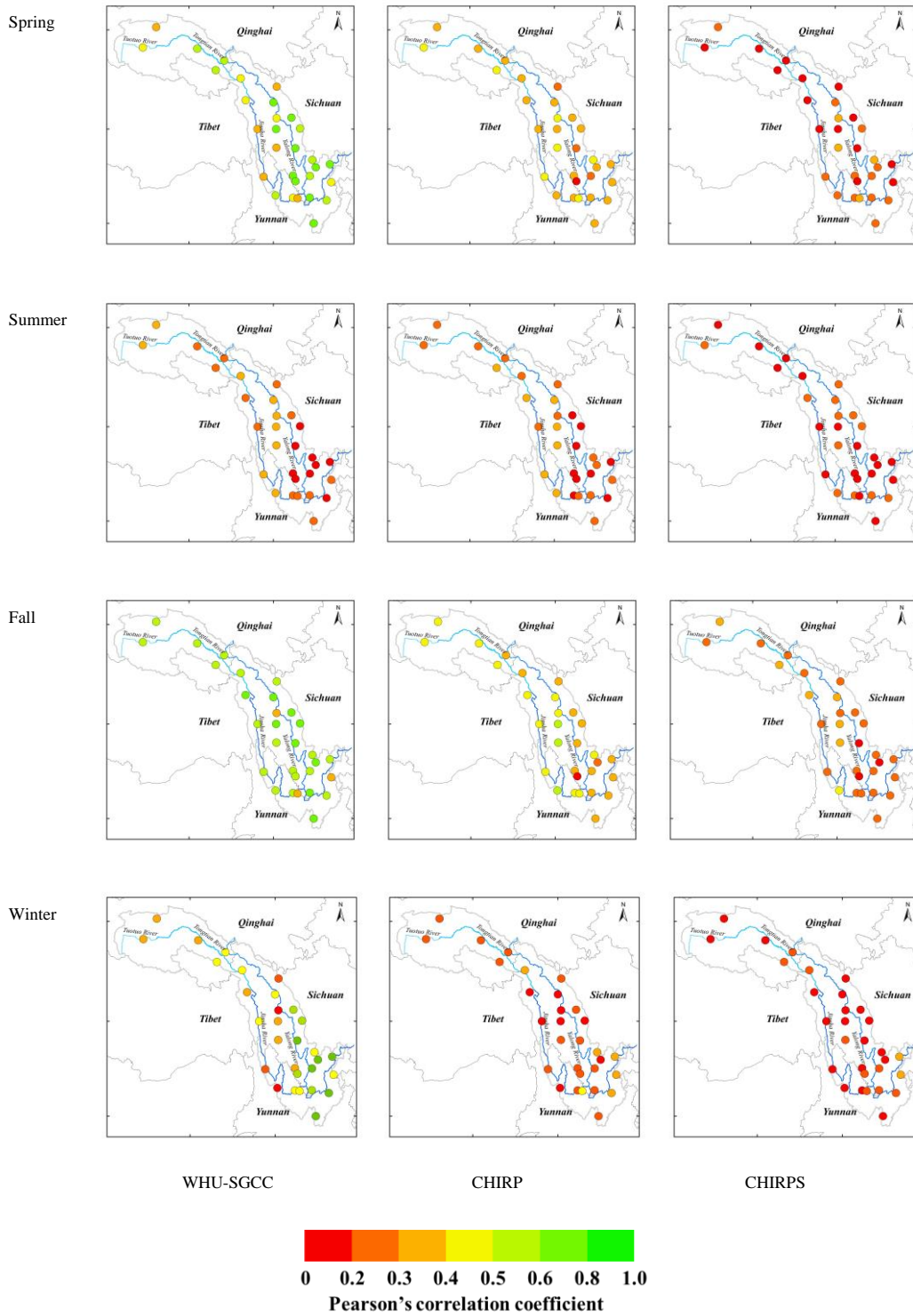


Figure 5 Spatial distribution of the Pearson's correlation coefficient of the overall agreement between observations and the WHU-SGCC, CHIRP and CHIRPS estimations in the four seasons from 1990 to 2014.

2. There is still not clear the influence in the number of gauge stations in the approach. I assume that the performance of this method will decrease with a reduction in the number of C1 pixels. The authors need to include an evaluation of the performance of

the method with a varying number of rain gauge stations.

Answer: Thank you for your valuable comments. In this study, the WHU-SGCC approach is to estimate the precipitation at every pixel by blending satellite estimates and rain gauge observations considering the terrain factors and precipitation characteristics. The leave-one-out cross validation step was applied to compute the out-of-sample adjusted error with the gauge stations. The WHU-SGCC algorithm was repeated 30 times, each time leaving one station as the validation station. The main objective of this study is to present a novel approach for reblending gauge observations and CHIRP satellite-based estimates.

The statistical comparisons between the different spatial distribution of observations and the WHU-SGCC, CHIRP and CHIRPS precipitation were conducted as shown in Fig. 5 and Fig. 6. The results show that, the variation in the PCC shows low correlations in areas with lower elevation, particularly in the southeast Jinsha River Basin, where there is higher precipitation and a greater density of rain gauges. The PCC is highest in the fall, followed by the spring and winter, and finally by summer. The higher correlations are located in the north-central area along the Tongtian River, Jinsha River and upstream part of the Yalong River, which has complex terrain and few rain gauges. The RMSE is lowest in the winter than in the spring, fall and summer, which can be attributed to the lower precipitation in the winter and the greatest in the summer. The spatial distribution of the RMSE shows that, the smaller errors are scattered in the northwest area of the river basin, with values lower than 5 mm, while the highest errors are located along the border between the lower reaches of the Jinsha River and the river basin. This is related to the climate regimes of the Jinsha River Basin, which includes more rainfall in the south and southeast areas than in the north, and northwest. **Therefore, the total rainfall and spatial distribution of rain gauges (C1 pixels) and will influence the estimates accuracy.** But we are not sure that the performance of this method will decrease with a reduction in the number of C1 pixels. In the future, we will further investigate the performance of the different number of C1 pixels on the WHU-SGCC adjustment.

3. One of my main concerns is that the main objective of this approach is to improve the characterization of precipitation over mountainous regions. However, ~50-60% of the pixels are classified as C4 and interpolated using IDW which does not account for the influence of elevation in the interpolation of precipitation. The authors may apply another interpolation method that accounts for the precipitation gradient related to elevation.

Answer: Thanks. It is reasonable to assume that some pixels are statistically similar to the historical precipitation characteristics of the C1 pixels within a certain area. Several studies indicate that the geographical location, elevation and other terrain information

influence the spatial distribution of rainfall, especially in mountainous areas with complex topography (Anders et al., 2006; Long and Singh, 2013). The size of the spatial range is an important parameter to distinguish the spatial similarity and heterogeneity. In the WHU-SGCC method, the fuzzy c-means (FCM) clustering approach was used to determine the spatial range considered for each pixel's terrain factors, including longitude, latitude, elevation, slope, aspect and curvature. Therefore, the elevation was considered into the process of the WHU-SGCC. In Rule 4, the IDW method was used to interpolate the unknown pixels based on C2 and C3 pixels. IDW is based on the concept of the first law of geography from 1970, which was defined as *everything is related to everything else, but near things are more related than distant things*. Therefore, the attribute value of an unsampled point is the weighted average of the known values within the neighbourhood, and the distance weighting can be determined by means of IDW (Lu and Wong, 2008). **Consider the quality of the results and the algorithm efficiency, the IDW method is applicable into the WHU-SGCC.**

In the future, we will further investigate another interpolation method that accounts for the precipitation gradient related to elevation when time is sufficient, such as geographically weighted regression.

Minor comments

1. Line 10: What do the authors mean with "existing fusion precipitation estimates"?

Answer: Thanks. "Existing fusion precipitation estimates" means the existing precipitation products of multi-source data fusion.

2. Line 27: might be due to the ...

Answer: Thanks. Done.

Change: changed from "which may due to the" to "**which might be due to the**".

3. Line 28: events.

Answer: Thanks. Done.

Change: changed from "rain event" to "rain **events**".

4. Please add a space between the references.

Answer: Thanks. Done.

Change: We added the space between the references.

5. Line 55: Please replace "spacing" with "spatial resolution".

Answer: Thanks. Done.

Change: changed from "spacing" to "**spatial resolution**".

6. Line 89: evaluated and indicated.

Answer: Thanks. Done.

Change: changed from “Moreover, Bai et al. (2018) evaluates CHIRPS over mainland China and indicates that” to “Moreover, Bai et al. (2018) **evaluated** CHIRPS over mainland China and **indicated** that”

7. Table 1: Some of the temporal resolutions of the products start with uppercase and some of them with lowercase. Also, the period of CMORPH is not complete.

Answer: Thanks. Done.

Changed: We changed the temporal resolutions of the products starting with lowercase and added the temporal resolutions of CMORPH.

Table 1 Coverage and spatiotemporal resolutions of major satellite precipitation datasets.

Product	Temporal resolution	Spatial resolution	Period	Coverage
TRMM 3B42-RT	3 Hourly	0.25°	1998-present	50°S-50°N
CMORPH	0.5 Hourly /3 Hourly/Daily	8 km/0.25°	1998-	60°S-60°N
PERSIANN-CDR	Daily	0.25°	1983-(delayed) present	60°S-60°N
GsMaP-NRT	Hourly	0.01°	2007	60°S-60°N
GsMaP-MVK	Hourly	0.01°	2000	60°S-60°N
	0.5 Hourly/ Hourly/			60°S-60°N
GPM	3 Hourly/Daily/3 Day/ 7 Day/Monthly	0.1°/0.25°/0.05°/5°	2014-present	70°N-70°S 90°N-90°S
MSWEP	3 Hourly/Daily/Monthly	0.1°	1979-2017	90°N-90°S
CHIRPS	Daily/Pentad/Dekad/ Monthly/Annual	0.05°/0.25°	1981- present	50°S-50°N

8. Line 112: probably present fits better than demonstrate.

Answer: Thanks. Done.

Changed: changed “demonstrate” to “**present**”.

9. Line 121: replace the comma with "is".

Answer: Thanks. We replaced the comma with “is”.

Change: changed from “The Yangtze River, one of the largest and most important rivers in Southeast Asia, originates on the Tibetan Plateau and extends approximately 6300 km eastward to the East China Sea.” to “The Yangtze River **is** one of the largest and most important rivers in Southeast Asia, **originating** on the Tibetan Plateau and **extending** approximately 6300 km eastward to the East China Sea.”

10. Lines 135-136: I think that now that the research is not focused in summer, it is better to remove this sentence.

Answer: Thanks. We removed this sentence about the summer precipitation.

11. Line 178: Recommendation, replace "in situ" with ground-based.

Answer: Thanks. Done.

Change: changed from “in situ” to “ground-based”.

12. Line 194: remove "is to".

Answer: Thanks. We removed “is to”.

Changed: changed from “the WHU-SGCC approach estimates the precipitation at every pixel by blending satellite estimates” to “**the WHU-SGCC approach estimates** the precipitation at every pixel by blending satellite estimates”.

13. Recommendation: change "multi-year" for "multi-annual" throughout the manuscript

Answer: Thanks. We changed "multi-year" for "multi-annual" throughout the manuscript

Reply to Report #3 (Anonymous Referee #4)

Dear Reviewer,

Thank you for your insight comments and suggestions. We have modified the manuscript accordingly. We trust that all of your comments have been addressed accordingly in the revised manuscript. If you have further suggestions for changes, please let us know. The detailed corrections are listed below point by point:

All changes in the manuscript are marked with **red color**.

After the last review stage, the authors largely revised the manuscript to improve its quality and to show quantitatively what are the qualities of WHU-SGCC vs CHIRP and CHIRPS datasets. I think the manuscript has reached a fair quality and it can be subject to minor revisions, though a few of the comments reported below, if not seriously address, can definitely affect the consistency of the manuscript and contains serious mistakes.

Answer: Thank you for your valuable comments. In addition, we updated the DOI of the resulting dataset.

The newly uploaded files are the results of precipitation bias adjustment by WHU-SGCC method about four seasons.

Shen, G. Y., Chen, N. C., Wang, W., and Chen, Z. Q.: Improving the Climate Hazards Group Infrared Precipitation (CHIRP) using WHU-SGCC method over the Jinsha River Basin from 1990 to 2014. PANGAEA, <https://doi.org/10.1594/PANGAEA.905376>, 2019.

Major comments

1. First of all, concepts of errors and uncertainties are still not correctly used in the manuscript and I have the impression the use of the word “error” is sometimes abused by the authors which also mention in their reply the words “more errors”, which definitely makes no sense.

Error is the difference between the true value of the measurand and the measured value. Accuracy is an expression of the lack of error. Uncertainty characterizes the range of values within which the true value is asserted to lie with some level of confidence.

Looking at the abstract I am amazed to see at line 17 the term “error adjustment”. Error is error and cannot be adjusted. Values of climate variables can be adjusted if the presence of systematic effects is detected. At line 23-24, the authors state that “precipitation errors” can be reduced. May be the authors are talking about the RMSE

which is not the error. Going through, the text I can provide other examples.

I recommend again to define all the quantities discussed in the manuscript in a proper way. This is mandatory to my opinion and the authors can also check the GUM (<https://www.bipm.org/en/publications/guides/gum.html>) to stay consistent.

Answer: Thank you for your valuable comments. We misunderstood the concepts of “errors” and “bias”.

Change: changed from “error adjustment” to “**bias adjustment**”;

Changed from “precipitation errors” to “**precipitation bias**”

2. It is also not clear to me why a few information reported in the reply to the reviewers are not provided also in the manuscript. For example, the authors could describe the way CMA imposes strict quality control on rain gauge observations.

In their comments the authors say:

“The process of quality control is as follows:

- (1) Climate threshold or allowable value check;
- (2) Extreme values at gauge stations check;
- (3) Internal consistency check between fixed value, daily average value and daily extreme value;
- (4) Time consistency check;
- (5) Manual verification and correction;

this quality control approach is provided by the official document from CMA. So, the daily rain gauge observations were used as the “Reference dataset”.

I think the information above must be provided when the CMA dataset is introduced in the manuscript to increase confidence in this dataset.

Answer: Thanks. We have added the description of strict quality on rain gauge observations in the manuscript.

Change: Added “**The process of quality control conducted by the CMA is as follows: (1) Climate threshold or allowable value check; (2) Extreme values at gauge stations check; (3) Internal consistency check between fixed value, daily average value and daily extreme value; (4) Time consistency check; and (5) Manual verification and correction.**” in to section 2.2.1.

3. The authors spent an appropriate effort to improve the quality of the analysis used and to smooth the tone of the writing which was often too enthusiastic in the previous version. Issues which may affect the quality of the dataset are now better highlighted though this is done still in a qualitative way. Generally, this may be sufficient to allow the reader to properly use the WHU-SGCC dataset; nevertheless, wherever possible, I

recommend the authors to be more quantitative.

For example, when the authors say: “In addition, the spatial distribution of C2 and C3 pixels also significantly impact the overall accuracy in different seasons that the most uniform in the fall, while the sparsest in the winter.”, it would be desirable to report a quantification of the impact which the authors are referring to. This happens also in other parts of the manuscript.

Answer: Thank you for your valuable comments.

Change:

(1) This sentence is not right, so we changed from “In addition, the spatial distribution of C2 and C3 pixels also significantly impact the overall accuracy in different seasons that the most uniform in the fall, while the sparsest in the winter.” to “**In addition, the spatial distribution of C2 and C3 pixels might slightly impact the overall accuracy in different seasons that the sparsest in the winter, while more uniform in the summer. However, the performances of PCC, RMSE, MAE and NSE in the winter are better than those in the summer.** The worst errors of forecasting performance in the summer may be attributed to the highest precipitation. The limited precipitation **events** detection in the winter could also be explained by the lowest precipitation (Xu et al., 2019).”

(2) Changed from “The WHU-SGCC method provides an obvious improvement in the NSE relative to CHIRP and CHIRPS, though the median and average values are still less than 0, which may be due to the inherent uncertainty in the CHIRP” to “The WHU-SGCC method provides an obvious improvement in the NSE, **with average improvements of 0.1742-13.8322 and 2.0131-14.7052 relative to CHIRP and CHIRPS,** though the median and average values are still less than 0, which may be due to the inherent uncertainty in the CHIRP”

(3) Changed from “The estimates of extreme rain events might also be attenuated during the process of WHU-SGCC adjustment.” to “**Besides the WHU-SGCC dataset has almost always a negative bias, while CHIRP and CHIRPS has a positive bias in the different rain events. After bias correction of the WHU-SGCC, some precipitation estimates are lower than observations.** The estimates of extreme rain events might also be attenuated during the process of WHU-SGCC adjustment.”

Other comments:

1. I am not sure why the authors speak about "attenuating the simulation" of extreme rain events at line 29 and other times thereafter; I'd simply write “attenuating extreme rain events”.

Answer: Thanks. We changed the sentence.

Change: changed from “which may due to the homogenization attenuating the simulation of extreme rain event.” to “**which might be due to the homogenization attenuating the extreme rain events estimates.**”

2. Check if all the acronyms are reported, for example NSE is not introduced in the abstract

Answer: Thanks. We added the full name of NSE in the abstract.

Change: changed from “the NSE of the WHU-SGCC” to “**the Nash-Sutcliffe efficiency coefficient (NSE)** of the WHU-SGCC”.

3. At line 235-236 the sentence could be clearer, adding the term “separately” at the end of the sentence.

Answer: Thanks. Done.

Change: changed from “Because there are 30 gauge stations in the study area, 30 regression relationships at the C1 pixels were derived from Rule 1.” to “**In the process of Rule 1, the regression relationships at the C1 pixels were established at 30 gauge stations separately.**”

4. At line 260, there is the assumption of “no long-held outliers”, whose impact is anyhow not assessed in the manuscript. A few words more to demonstrate the robustness of this assumption would be useful.

Answer: Thanks. “no long-held outliers” means no abnormal values during the long time series.

Change: changed from “There are no long-held outliers at one pixel in the CHIRP dataset” to “**There are no abnormal values at one pixel in the CHIRP dataset during the long time series**”

5. Table 3 shows interesting information which if reported in a plot style would be much clearer and useful for the reader, otherwise is quite confusing

Answer: Thanks. We added the spatial distribution of C1-C3 pixels in **Figure D1**.

Change: Added the sentence in the first paragraph in section 4.

“Besides, the pixel type of the validation gauge stations is shown in Table D1 **and the spatial distribution of C1-C3 pixels in Figure D1 with the most uniform in the fall, while the sparsest in the winter.**”

6. Line 627-632: this is one of the points where the limitations affecting the WHU-SGCC dataset are discussed. I think that, at least for this case, the paragraph should be reported also in the conclusions to give the right balance to the final section of the manuscript.

Answer: Thanks. We added these sentences to the conclusions.

Change: “**As for the results of the WHU-SGCC, the assessments of POD and CSI are the best in the summer, followed by the fall, spring, and winter, which are related to the**

seasonal rainfall pattern of more rain in the summer and less in the winter. In spite of the corrections, the performance of the WHU-SGCC for short intense and extreme rain events was poorer than those of CHIRP and CHIRPS, and the bias in the precipitation forecasts in the summer are still large, which may due to the homogenization attenuating the extreme rain events estimates.”

7. Figure 8: this is the core of the presented analysis and it is not clear why the WHU-SGCC dataset has almost always a negative bias, while CHIRP and CHIRPS has a positive bias. The authors should comment more on this important aspect of their homogenization approach.

Answer: Thanks. The equation of BIAS is as follows:

$$\text{BIAS} = \frac{\sum_{i=1}^n (C_i - Y_{oi})}{\sum_{i=1}^n Y_{oi}}$$

In different rain events, the WHU-SGCC dataset has almost always a negative bias, while CHIRP and CHIRPS has a positive bias. After bias correction of the WHU-SGCC, some precipitation estimates are lower than observations. The estimates of extreme rain events might also be attenuated during the process of WHU-SGCC adjustment.

Change: Added more comments on this important aspect of their homogenization approach. “Besides the WHU-SGCC dataset has almost always a negative bias, while CHIRP and CHIRPS has a positive bias in the different rain events. After bias correction of the WHU-SGCC, some precipitation estimates are lower than observations. The estimates of extreme rain events might also be attenuated during the process of WHU-SGCC adjustment.”

8. In addition, Figure 8 clearly states that CHIRP and WHU-SGCC have very similar performance, expect for the bias (which for WHU-SGCC is slightly better in absolute value). This should be clearly stated in the analysis and in the conclusions.

Answer: Thanks. As shown in Fig. 8, the WHU-SGCC approach had lower errors than CHIRP and CHIRPS, as indicated by the RMSE, MAE and BIAS, but the performance of WHU-SGCC is not promising for events with total rainfall greater than 25 mm in the summer. Besides, the POD and CSI results of CHIRPS are the worst, while the results of the WHU-SGCC are the highest, which indicate its superiority for the detection of precipitation events. As for the results of the WHU-SGCC, the assessments of POD and CSI are the best in the summer, followed by the fall, spring, and winter, which are related to the seasonal rainfall pattern of more rain in the summer and less in the winter. Therefore, the WHU-SGCC approach is applicable for the detection of rainfall events in the Jinsha River Basin, while in the summer it is better with rainfall less than or approximately equal to the average daily precipitation. Due to the homogenization of the WHU-SGCC method, its performance for short intense and extreme rain events was

poorer than those of CHIRP and CHIRPS, which should be improved in a future study. **And we have added the relevant analysis in the conclusion** “The leave-one-out cross validation of WHU-SGCC on daily rain events confirmed that the model is effective in the detection of precipitation events that are less than or approximately equal to the average annual precipitation in the Jinsha River Basin. The WHU-SGCC approach achieves reductions of the RMSE, MAE and BIAS metrics, while on rain events less than 25 mm in the summer. Specifically, the WHU-SGCC has the best ability to reduce precipitation errors for daily accuracy evaluations, with average reductions of 15% and 34% for compared to CHIRP and CHIRPS, respectively. **As for the results of the WHU-SGCC, the assessments of POD and CSI are the best in the summer, followed by the fall, spring, and winter, which are related to the seasonal rainfall pattern of more rain in the summer and less in the winter. In spite of the corrections, the performance of the WHU-SGCC for short intense and extreme rain events was poorer than those of CHIRP and CHIRPS, and the bias in the precipitation forecasts in the summer are still large, which may due to the homogenization attenuating the extreme rain events estimates.”**

9. Finally, I recommend an appropriate use of decimal places throughout the presented analysis. The manuscript can also benefit from a final English review (I recommend).

Answer: Thanks. We retain **four decimal**.

1 WHU-SGCC: A novel approach for blending daily satellite (CHIRP) 2 and precipitation observations over the Jinsha River Basin

3 Gaoyun Shen¹, Nengcheng Chen^{1,2}, Wei Wang^{1,2}, Zeqiang Chen^{1,2}

4 ¹ State Key Laboratory of Information Engineering in Surveying, Mapping and Remote Sensing, Wuhan University, 129 Luoyu
5 Road, Wuhan 430079, China

6 ² Collaborative Innovation Center of Geospatial Technology, Wuhan 430079, China

7 *Correspondence to:* ZeqiangChen@whu.edu.cn; Tel.: +86 13871025965; Fax: +86 27 68778229.

8 **Abstract.** Accurate and consistent satellite-based precipitation estimates blended with rain gauge data are important for
9 regional precipitation monitoring and hydrological applications, especially in regions with limited rain gauges. However, the
10 existing fusion precipitation estimates often have large uncertainties over mountainous areas with complex topography and
11 sparse rain gauges, and most of the existing data blending algorithms are not good at removing the day-by-day errors. Therefore,
12 the development of effective methods for high-accuracy precipitation estimates over complex terrain and at a daily scale is of
13 vital importance for mountainous hydrological applications. This study aims to offer a novel approach for blending daily
14 precipitation gauge data and the Climate Hazards Group Infrared Precipitation (CHIRP; daily, 0.05°) satellite-derived
15 precipitation developed by UC Santa Barbara over the Jinsha River Basin from 1994 to 2014. This method is called the Wuhan
16 University Satellite and Gauge precipitation Collaborated Correction (WHU-SGCC). The results show that the WHU-SGCC
17 method is effective for liquid precipitation ~~error-bias~~ adjustments from points to surfaces as evaluated by multiple error
18 statistics and from different perspectives. Compared with CHIRP and CHIRP with station data (CHIRPS), the precipitation
19 adjusted by the WHU-SGCC method has greater accuracy, with overall average improvements of the Pearson's correlation
20 coefficient (PCC) by 0.01-0.23 and 0.06-0.32, respectively, and decreases in the root mean square error (RMSE) by 0.06-0.1
21 mm and 0.2-3 mm, respectively. In addition, the Nash-Sutcliffe efficiency coefficient (NSE) of the WHU-SGCC provides
22 substantial improvements than CHIRP and CHIRPS, which reached 0.2836, 0.2944 and 0.1853 in the spring, fall and winter.
23 Daily accuracy evaluations indicate that the WHU-SGCC method has the best ability to reduce precipitation ~~error+bias~~, with
24 average reductions of 15% and 34% compared to CHIRP and CHIRPS, respectively. Moreover, the accuracy of the spatial
25 distribution of the precipitation estimates derived from the WHU-SGCC method is related to the complexity of the topography.
26 The validation also verifies that the proposed approach is effective at detecting major precipitation events within the Jinsha
27 River Basin. In spite of the correction, the uncertainties in the seasonal precipitation forecasts in the summer and winter are
28 still large, which ~~may-might be~~ due to the homogenization attenuating the ~~simulation of~~ extreme rain events ~~estimates~~. However,
29 the WHU-SGCC approach may serve as a promising tool to monitor daily precipitation over the Jinsha River Basin, which
30 contains complicated mountainous terrain with sparse rain gauge data, based on the spatial correlation and the historical
31 precipitation characteristics. The daily precipitation estimations at the 0.05° resolution over the Jinsha River Basin during all
32 four seasons from 1990 to 2014, derived from WHU-SGCC are available at the PANGAEA Data Publisher for Earth &
33 Environmental Science portal (<https://doi.pangaea.de/10.1594/PANGAEA.900620>).

34 1 Introduction

35 Accurate and consistent estimates of precipitation are vital for hydrological modelling, flood forecasting and climatological
36 studies in support of better planning and decision making (Agutu et al., 2017; Cattani et al., 2018; Roy et al., 2017). In general,
37 ground-based gauge networks include a substantial number of liquid precipitation observations measured with high accuracy,
38 high temporal resolution, and long historical records. However, the sparse distribution and point measurements limit the
39 accurate estimation of spatially gridded rainfall (Martens et al., 2013).

40 Due to the sparseness and uneven spatial distribution of rain gauges and the high proportion of missing data, satellite-derived
41 precipitation data are an attractive supplement offering the advantage of plentiful information with high spatio-temporal
42 resolution over widespread regions, particularly over oceans, high elevation mountainous regions, and other remote regions
43 where gauge networks are difficult to deploy. However, satellite estimates are susceptible to systematic biases that can
44 influence hydrological modelling and the retrieval algorithms are relatively insensitive to light rainfall events, especially in
45 complex terrain, resulting in underestimations of the magnitudes of precipitation events (Behrangi et al., 2014; Thiemig et al.,
46 2013; Yang et al., 2017). Without adjustments, inaccurate satellite-based precipitation estimates will lead to unreliable
47 assessments of risk and reliability (AghaKouchak et al., 2011).

48 Accordingly, many kinds of precipitation estimates combining multiple sources and datasets are available. Table 1 shows
49 the temporal and spatial resolution of current major satellite-based precipitation datasets. Since 1997, the Tropical Rainfall
50 Measurement Mission (TRMM) has improved satellite-based rainfall retrievals over tropical regions (Kummerow et al., 1998;
51 Simpson et al., 1988). High spatial and temporal resolution multi-satellite precipitation products have been developed
52 continuously during the TRMM era (Maggioni et al., 2016), including: (1) the TRMM Multisatellite Precipitation Analysis
53 (TMPA) products, which are derived from gauge-satellite fusing (Huffman et al., 2010; Vila et al., 2009); (2) the Climate
54 Prediction Center (CPC) morphing technique (Joyce et al., 2004; Joyce and Xie, 2011; Xie et al., 2017), which integrates
55 geosynchronous infrared (GEO IR) and polar-orbiting microwave (PMW) sensor data and is available three-hourly on a grid
56 with a spatial resolution spacing of 0.25° ; (3) the Precipitation Estimation from Remotely Sensed Information using Artificial
57 Neural Networks - Climate Data Record (PERSIANN-CDR) produced by the PERSIANN algorithm, which has daily temporal
58 and $0.25^\circ \times 0.25^\circ$ spatial resolutions (Ashouri et al., 2015); and (4) the Global Satellite Mapping of Precipitation (GSMaP)
59 project, which produces global rainfall estimates in near-real time and applies the motion vector Kalman filter based
60 on physical models (GSMaP-NRT and GSMaP-MVK, respectively) (Aonashi et al., 2009; Ushio et al., 2009; Ushio and
61 Kachi, 2010). In 2014, the Global Precipitation Measurement (GPM) satellite was launched after the success of the TRMM
62 satellite by a cooperation between the National Aeronautics and Space Administration (NASA) and Japan Aerospace
63 Exploration Agency (JAXA) (Mahmoud et al., 2018; Ning et al., 2016). The main core observatory satellite (GPM) integrates
64 advanced radar and radiometer systems to obtain the precipitation physics and takes advantages of TMPA, the Climate
65 Prediction Center morphing technique (CMORPH), and PERSIANN algorithms to offer high spatiotemporal resolution
66 products ($0.1^\circ \times 0.1^\circ$, half-hourly) of global real-time precipitation estimates (Huffman et al., 2018; Skofronick-Jackson et al.,
67 2017; Hou et al., 2014). Nevertheless, the major aforementioned products have only been available since 1998, which limits
68 long-term climatological studies. Only the PERSIANN-CDR data set has temporal coverage since 1983. However, the spatial
69 resolution of PERSIANN-CDR is relatively coarse, and the data resolution must be degraded to achieve high accuracy in
70 precipitation monitoring. To fill the gap in high resolution and long-term global multi-satellite precipitation monitoring, the
71 Multi-Source Weighted-Ensemble Precipitation (MSWEP) product (Beck et al., 2017; Beck et al., 2019), and the Climate
72 Hazards Group Infrared Precipitation with Station data (CHIRPS) product from UC Santa Barbara (Funk et al., 2015 a) were
73 developed. MSWEP is a precipitation data set with global coverage available at 0.1° spatial resolution and at three-hourly,
74 daily, and monthly temporal resolutions. MSWEP is multi-source data that takes advantage of the complementary strengths of
75 gauge-, satellite-, and reanalysis-based data. However, to provide precipitation estimates at a higher spatial resolution, the
76 CHIRPS data set is used in this study.

77 CHIRPS is a longer length precipitation data series with a higher spatial resolution (0.05°) that, merges three types of
78 information: global climatology, satellite estimates and in situ observations. The CHIRPS precipitation dataset with several
79 temporal and spatial scales has been evaluated in Brazil (Nogueira et al., 2018; Paredes-Trejo et al., 2017), Chile (Yang et al.,
80 2016; Zambrano-Bigiarini et al., 2017), China (Bai et al., 2018), Cyprus (Katsanos et al., 2016a; Katsanos et al., 2016b), India
81 (Ali and Mishra, 2017; Prakash, 2019) and Italy (Duan et al., 2016). However, the temporal resolutions of these applications

82 were mainly at seasonal and monthly scales, lacking the evaluation and correction of daily precipitation. Additionally, despite
 83 the great potential of gauge-satellite fusing products for large-scale environmental monitoring, there are still large
 84 discrepancies with ground observations at the sub-regional level where these data have been applied. Furthermore, the CHIRPS
 85 product's reliability has not been analysed in detail over the Jinsha River Basin in China, particularly at a daily scale. The
 86 Jinsha River Basin is a typical study area with complex and varied terrain, an uneven spatial distribution of precipitation, and
 87 a sparse spatial distribution of rain gauges, which limit high accuracy precipitation monitoring. The existing research indicates
 88 that estimations over mountainous areas with complex topography often have large uncertainties and ~~errors-bias~~ due to the
 89 topography, seasonality, climate impact and sparseness of rain gauges (Derin et al., 2016; Maggioni and Massari, 2018;
 90 Zambrano-Bigiarini et al., 2017). Moreover, Bai et al. (2018) evaluates ~~s-d~~ CHIRPS over mainland China and indicates ~~s-d~~ that the
 91 performance of CHIRPS is poor over the Sichuan Basin and the Northern China Plain, which have complex terrain with
 92 substantial variations in elevation. Additionally, Trejo et al. (2016) shows that CHIRPS overestimates low monthly rainfall and
 93 underestimates high monthly rainfall using several numerical metrics and that the rainfall event frequency is overestimated
 94 outside the rainy season.

95 **Table 1** Coverage and spatiotemporal resolutions of major satellite precipitation datasets.

Product	Temporal resolution	Spatial resolution	Period	Coverage
TRMM 3B42-RT	3 hourly Hourly	0.25°	1998-present	50°S-50°N
CMORPH	30 min/3 Hourly/Daily	8 km/0.25°	1998-	60°S-60°N
PERSIANN-CDR	Daily daily	0.25°	1983-(delayed) present	60°S-60°N
GsMaP-NRT	hourly Hourly	0.01°	2007	60°S-60°N
GsMaP-MVK	hourly Hourly	0.01°	2000	60°S-60°N
GPM	30 min/Hourly/ 3 hourly Hourly/Daily/3_Day/ 7 Day/Monthly	0.1°/0.25°/0.05°/5°	2014-present	60°S-60°N 70°N-70°S 90°N-90°S
MSWEP	3 hourly Hourly/Daily/Monthly Annual Monthly/	0.1°	1979-2017	90°N-90°S
CHIRPS	Dekad / Pentad / Daily Daily/ Pentad / Dekad / Monthly/Annual	0.05°/0.25°	1981- present	50°S-50°N

96 To overcome these limitations, many studies have focused on proposing effective methodologies for blending rain gauge
 97 observations, satellite-based precipitation estimates, and sometimes radar data to take advantage of each dataset. Many
 98 numerical models have been established with these datasets for high-accuracy precipitation estimations, such as bias
 99 adjustment by a quantile mapping (QM) approach (Yang et al., 2016), Bayesian kriging (BK) (Verdin et al., 2015) and a
 100 conditional merging technique (Berndt et al., 2014). The QM approach is a distribution-based approach, which works with
 101 historical data for bias adjustment and is effective at reducing the systematic bias of regional climate model precipitation
 102 estimates at monthly or seasonal scales (Chen et al., 2013). However, the QM approach offers very limited improvement in
 103 removing day-by-day errors. The BK approach provides very good model fit with precipitation observations, but the Gaussian
 104 assumption of the BK model is invalid for daily scales. Overall, there is a lack of effective methods for high-accuracy
 105 precipitation estimates over complex terrain at a daily scale.

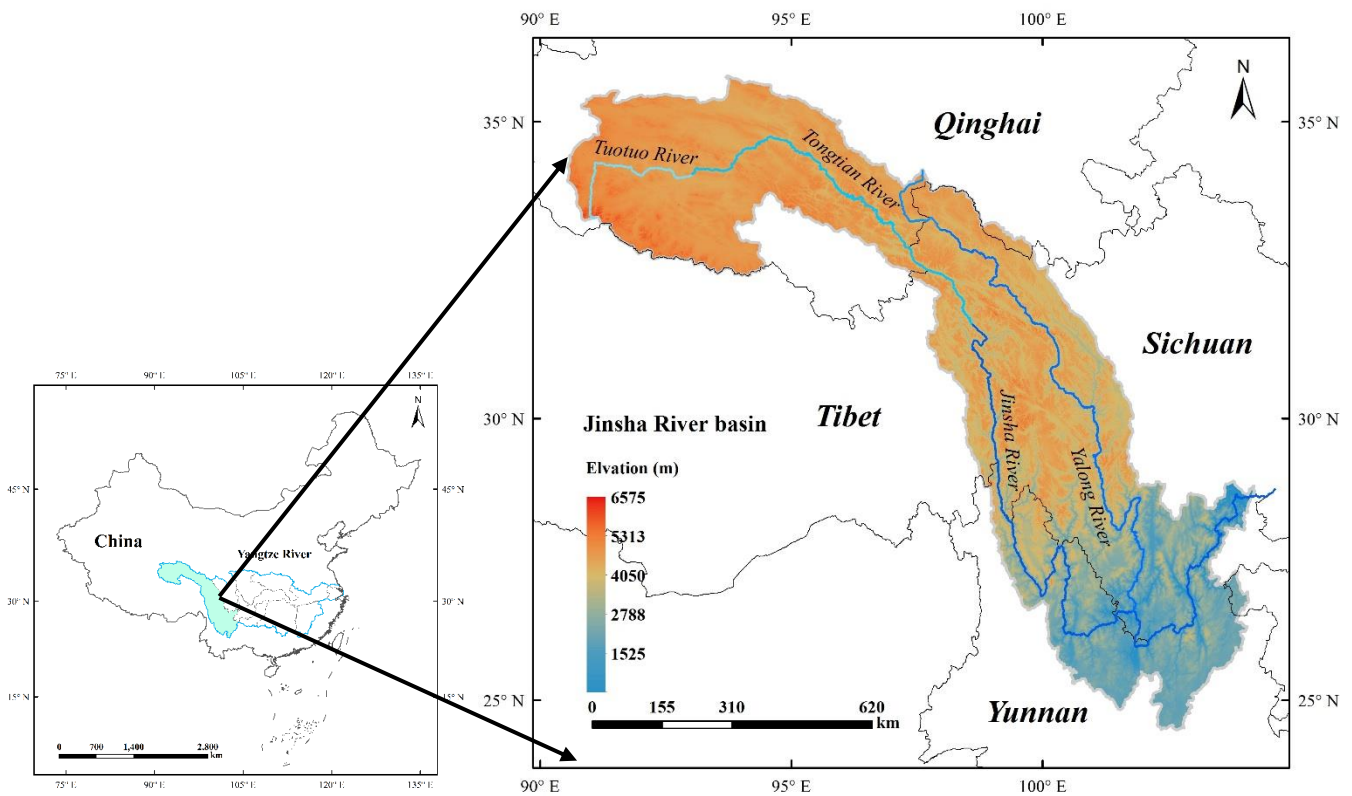
106 As such, due to the poor performance at the sub-regional scale, the gauge-satellite fusing algorithms can be assumed to limit
 107 high accuracy estimations in the process of CHIRPS data production. Therefore, the aim of this article is to present a novel
 108 approach for reblending daily liquid precipitation gauge data and the Climate Hazards Group Infrared Precipitation (CHIRP)
 109 satellite-derived precipitation estimates developed by UC Santa Barbara, over the Jinsha River Basin. We use precipitation to
 110 denote liquid precipitation throughout the text. The CHIRP data are the raw data of CHIRPS before blending with the rain
 111 gauge data. The objective is to build corresponding precipitation models that consider terrain factors and precipitation
 112 characteristics to produce high-quality precipitation estimates. This novel method is called the Wuhan University Satellite and
 113 Gauge precipitation Collaborated Correction (WHU-SGCC) method. We ~~demonstrate-present~~ this method by applying it to
 114 daily precipitation over the Jinsha River Basin in the different seasons from 1990 to 2014. The results support the validity of
 115 the proposed approach for producing refined satellite-gauge precipitation estimates over mountainous areas.

116 The remainder of this paper is organized as follows: Section 2 describes the study region, rain gauges and CHIRPS dataset
117 used in this study. Section 3 presents the principle of the WHU-SGCC approach for high-accuracy daily precipitation estimates.
118 The results and discussion are analysed in Section 4, the data available are described in Section 5, and the conclusions and
119 future work are presented in Section 6.

120 2 Study Region and Data

121 2.1 Study Region

122 The Yangtze River is, one of the largest and most important rivers in Southeast Asia, originates ing on the Tibetan Plateau and
123 extends ing approximately 6300 km eastward to the East China Sea. The river's catchment covers an area of approximately
124 $\sim 180 \times 10^4$ km² and the average annual precipitation is approximately 1100 mm (Zhang et al., 2019). The Yangtze River is
125 divided into nine sub-basins, the upper drainage basin is the Jinsha River Basin, which flows through the provinces of Qinghai,
126 Sichuan, and Yunnan in western China. Within the Jinsha River Basin, the total river length is 3486 km, accounting for 77%
127 of the length of the upper Yangtze River, and covering a watershed area of 460×10^3 km². The location of the Jinsha River
128 Basin is shown in Fig. 1, and it covers the eastern part of the Tibetan Plateau and part of the Hengduan Mountains. The southern
129 portion of the river basin is the Northern Yunnan Plateau and the eastern portion includes a wide area of the southwestern
130 margin of the Sichuan Basin. Crossing complex and varied terrains, the elevation of the Jinsha River ranges from 263 to 6575
131 m above sea level, which results in significant temporal and spatial climate and weather variations inside the basin. The average
132 annual precipitation of the Jinsha River Basin is approximately 710 mm, the average annual precipitation of the lower reaches
133 is approximately 900-1300 mm, and the average annual precipitation of the middle and upper reaches is approximately 600-
134 800 mm (Yuan et al., 2018). The Jinsha River Basin has four seasons: spring (March-April-May), summer (June-July-August),
135 fall (September-October-November) and winter (December-January-February). ~~The climate of the Jinsha River Basin is~~
136 ~~affected by oceanic southwest and southeast monsoons, resulting in more precipitation during the summer.~~ Therefore, the
137 blending of satellite estimations with gauge observations during the different seasons is the main focus of this research.



138 **Figure 1** Location of the study area with key topographic features.
139

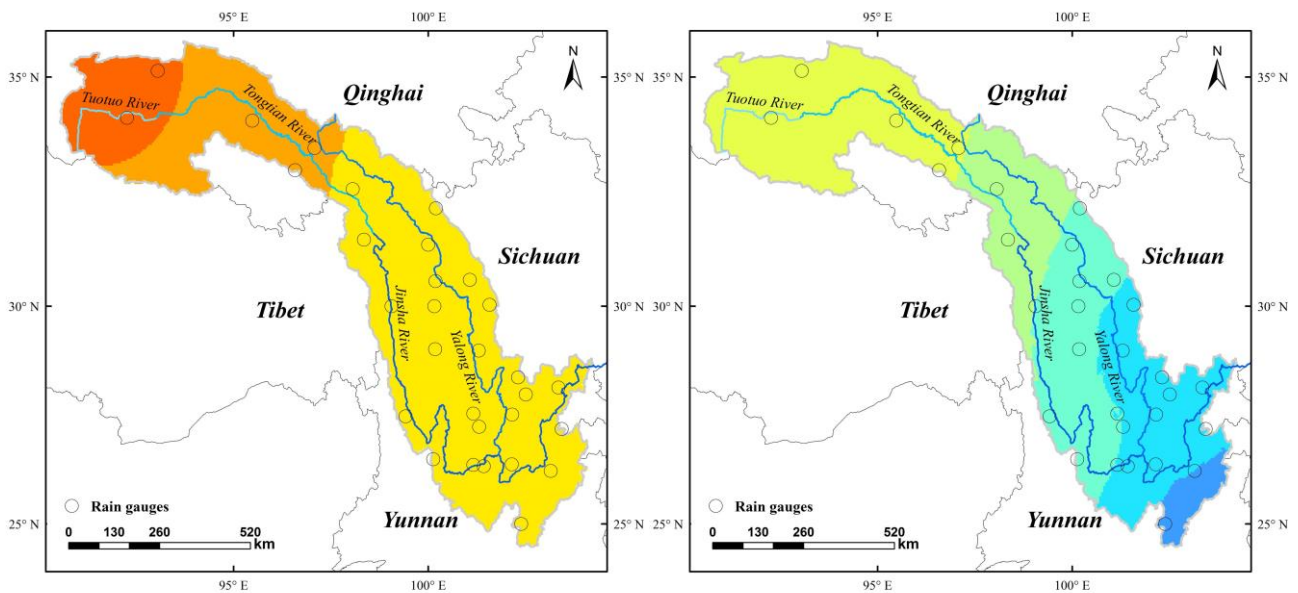
140 **2.2 Study Data**

141 **2.2.1 Precipitation gauge observations**

142 Daily rain gauge observations at 30 national standard rain stations within the Jinsha River Basin from 1 March 1990 to February
143 2015 were provided by the National Climate Centre (NCC) of the China Meteorological Administration (CMA)
144 (http://data.cma.cn/data/cdcdetail/dataCode/SURF_CLI_CHN_MUL_DAY_V3.0.html, last access: 10 December, 2018),
145 which imposes strict quality control at the station, provincial and state levels. The process of quality control conducted by the
146 CMA is as follows: (1) Climate threshold or allowable value check; (2) Extreme values at gauge stations check; (3) Internal
147 consistency check between fixed value, daily average value and daily extreme value; (4) Time consistency check; and (5)
148 Manual verification and correction. The station identification numbers and relevant geographical characteristics are shown in
149 Appendix A, and their uneven spatial distribution is shown in Fig. 2. The selected rain gauges are located in Qinghai, Tibet,
150 Sichuan and Yunnan Provinces but are mainly scattered in Sichuan Province, and the northern river basin contains fewer rain
151 gauges than the southern river basin. In this study, the daily rain gauge observations were used as the reference data for the
152 error-bias adjustment-correction of satellite precipitation estimations.

153 The multi-year-annual (1990-2014) average seasonal precipitation over the Jinsha River Basin increases from north to south
154 (Fig. 2). The dynamic and uneven distribution of precipitation is influenced distinctly by the seasonal climate. Most of the
155 precipitation falls in the summer, with the average seasonal precipitation ranging from less than 250 mm to more than 600 mm,
156 while the average seasonal precipitation during the winter is no more than 50 mm. The average seasonal precipitation and
157 spatial distribution in the spring are similar with those in the fall, with values concentrated in the range of 50 mm to 200 mm.

158



159

160

(a) Spring

(b) Summer

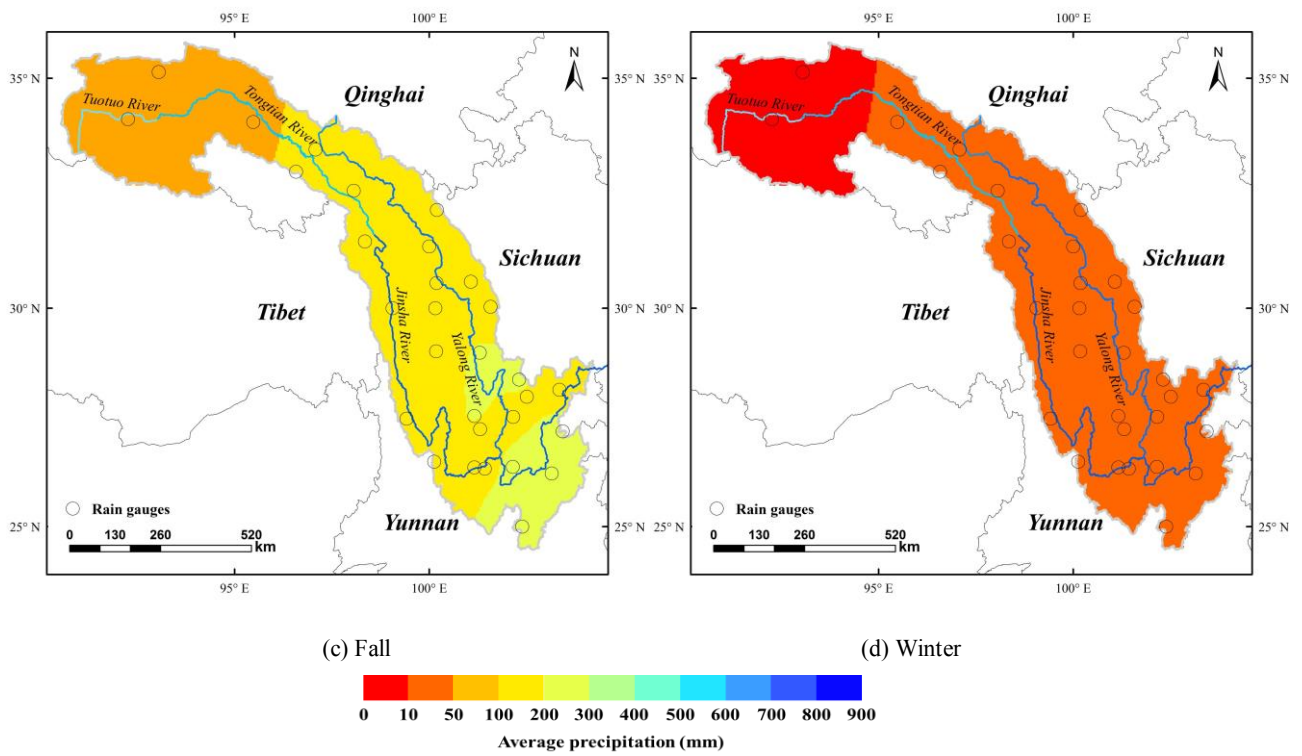


Figure 2 The multi-year-annual (1990-2014) average seasonal precipitation over the Jinsha River Basin interpolated from 30 rain gauges downloaded from the China Meteorological Administration stations.

2.2.2 CHIRPS satellite-gauge fusion precipitation estimates

The CHIRPS v.2 dataset, a satellite-based daily rainfall product, is available online at ftp://ftp.chg.ucsb.edu/pub/org/chg/products/CHIRPS-2.0/global_daily/tifs/p05/ (last access: 10 December, 2018). It covers a quasi-global area (land only, 50° S-50° N) a several temporal scales (daily, pentad, dekad, monthly and annual temporal resolutions) and a high spatial resolution (0.05°) (Rivera et al., 2018). This dataset contains a wide variety of satellite-based rainfall products derived from a multiple data sources and incorporates five data types: (1) the monthly precipitation from CHPClim v.1.0 (Climate Hazards Group's Precipitation Climatology version 1) derived from a combination of satellite fields, gridded physiographic indicators, and in situ climate normal with the geospatial modelling approach based on moving window regressions and inverse distance weighting interpolation (Funk et al., 2015 b); (2) quasi-global geostationary thermal infrared (IR) satellite observations; (3) the TRMM 3B42 product (Huffman et al., 2007); (4) the CFS (Climate Forecast System, version 2) atmospheric model rainfall fields from NOAA; and (5) surface-based precipitation observations from various sources including national and regional meteorological services. The differences from other frequently used precipitation products are the higher resolution of 0.05°, wider coverage and longer length data series from 1981 to near-real time (Funk et al., 2015 a).

CHIRPS is the blended product of a two-part process. First, IR precipitation (IRP) pentad rainfall estimates are fused with corresponding CHPClim pentad data to produce an unbiased gridded estimate, called CHIRP, which is available online at <ftp://ftp.chg.ucsb.edu/pub/org/chg/products/CHIRP/daily/> (last access: 10 December, 2018). In the second part of the process, the CHIRP data are blended with in-situ-ground-based precipitation observations obtained from a variety of sources, including national and regional meteorological services by means of a modified inverse-distance weighting algorithm to create the final blended product, CHIRPS (Funk et al., 2014). The daily CHIRP satellite-based data over the Jinsha River Basin from 1990.02 to 2015.02 were selected as the input for WHU-SGCC blending with rain observations, and the corresponding daily CHIRPS blended data was used for comparisons of the precipitation accuracy.

The blended in situ daily precipitation observations of the CHIRPS data come from a variety of sources, such as the daily GHCN archive (Durre et al., 2010), the Global Summary of the Day dataset (GSOD) provided by NOAA's National Climatic Data Center, the World Meteorological Organization's Global Telecommunication System (GTS) daily archive provided by

190 NOAA CPC, and more than a dozen national and regional meteorological services. However, the stations for daily CHIRPS
191 data have a different spatial distribution than those downloaded from the CMA, and the precipitation values used for CHIRPS
192 production are the monthly values available online ([ftp://ftp.chg.ucsb.edu/pub/org/chg/products/CHIRPS-
193 2.0/diagnostics/monthly_station_data/](ftp://ftp.chg.ucsb.edu/pub/org/chg/products/CHIRPS-2.0/diagnostics/monthly_station_data/)). For the daily precipitation adjustments over the Jinsha River Basin, the daily gauge
194 observations from the CMA are blended with the daily CHIRP data due to the unknown spatial distribution and precipitation
195 values of gauge stations used in the process of daily CHIRPS merging.

196 **3 Methods**

197 **3.1 The WHU-SGCC approach**

198 In this study, the WHU-SGCC approach ~~is to~~ estimates the precipitation at every pixel by blending satellite estimates and rain
199 gauge observations considering the terrain factors and precipitation characteristics. Due to the significant seasonal difference
200 of precipitation, the WHU-SGCC method was applied in the different seasons. Four steps were used to establish the numerical
201 relationship between the gauge stations and the corresponding satellite pixels and for the interpolation of the remaining pixels.
202 The WHU-SGCC method identifies the geographical locations and topographical features of each pixel and applies the four
203 classification and blending rules. A flowchart of the WHU-SGCC method is shown in Fig. 3. The proposed approach was
204 evaluated over the Jinsha River Basin based on 30 gauge stations and CHIRP satellite-based precipitation estimations in the
205 different seasons from 1990 to 2014. The leave-one-out cross validation step was applied to compute the out-of-sample
206 adjusted ~~error-bias~~ with the gauge stations. The WHU-SGCC algorithm was repeated 30 times, each time leaving one station
207 as the validation station.

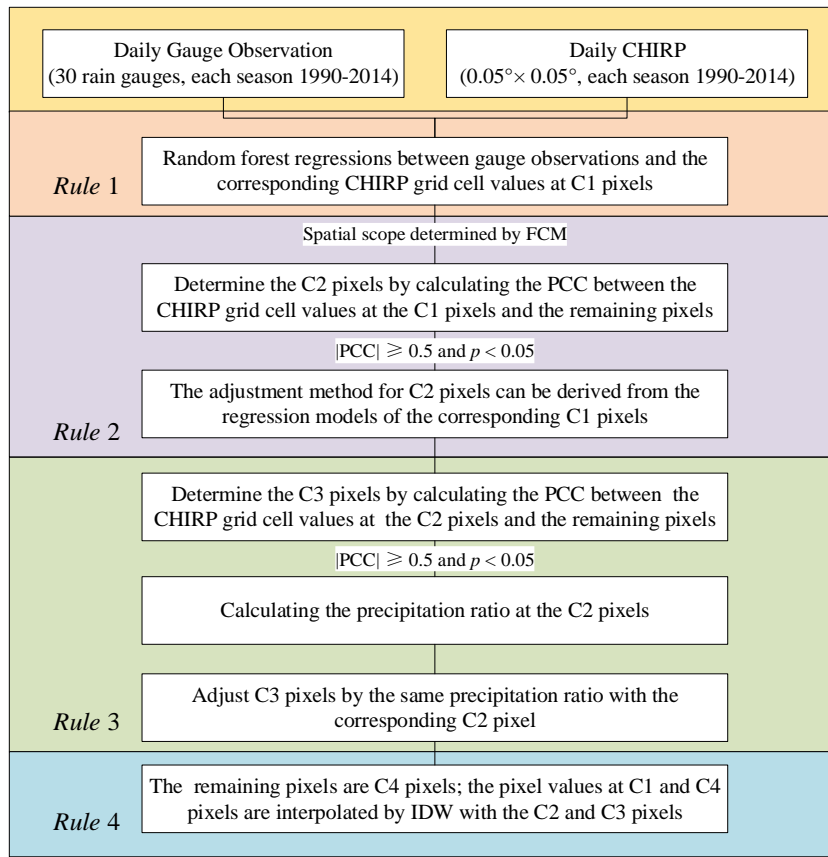
208 The basic description of the WHU-SGCC method is given below, and the details are illustrated separately in later sections:

209 (1) Classify all regional pixels into four types: C1 (pixels including one gauge station in their area), C2 (pixels statistically
210 similar to C1), C3 (pixels statistically similar to C2) and C4 (remaining pixels).

211 (2) Analyze the relationships between the precipitation observations and the C1, C2, and C3 pixel types, and interpolate for
212 the C4 pixels. These relationships are described by four rules, which are described below as Rules 1 through 4.

213 (3) Establish statistical models and screen the target pixels based on the four rules.

214 (4) Correct all of the precipitation pixels in the daily regional precipitation images.



215

216

Figure 3 Flowchart of the WHU-SGCC approach with the four rules applied in this study.

217

3.1.1 Assumptions

218

(1) Gauge observations are the most accurate, or “true”, values for reference purposes. However, the sparseness of the gauges, their uneven spatial distribution, and the high proportion of missing data may limit high accuracy estimation in rainfall monitoring.

221

(2) No major terrain changes occurred during the twenty years (Appendix B).

222

(3) There are no long-held outliers at one pixel in the CHIRP dataset, so Pearson’s Correlation Coefficient (PCC) can represent the statistical similarity of the rainfall characteristics among the pixels in a certain spatial area at a seasonal scale.

223

224

3.1.2 Rule 1 of the WHU-SGCC method

225

In general, the satellite precipitation estimations deviated from the ground-based measurements, which were assumed to be the true values. Rule 1 aims to establish a regression model between the historical observations at each gauge and the corresponding CHIRP grid cell values. The regression relationship was derived by random forest regression (RFR) at each gauge station. RFR is a machine-learning algorithm for a predictive model with a large set of regression trees in which each tree in the ensemble is grown from a bootstrap sample (Johnson, 1998) drawn with a replacement from the training set. In the process of establishing regression trees, a subset of variables for each node is selected to avoid overfitting. The final prediction is obtained by combining the results of the prediction methods applied to each bootstrap sample (Genuer et al., 2017). The predicted value is calculated by the average of the values from all of the decision trees. Each tree can be expressed as

232

233

$$Tree_k = f_{RFR}(Y_o, \Theta_{Y_{s_k}}), \quad k=1 \dots n \quad (1)$$

234

where Y_o denotes the historical observations at each gauge at the C1 pixels, $\Theta_{Y_{s_k}}$ is a randomly selected vector from Y_s ,

235

Y_s denotes the corresponding CHIRP grid cell values at the C1 pixels, n is the number of trees, and f_{RFR} is constructed

236

from the time series Y_o (dependent variable) and Y_s (independent variable) by means of RFR. The bootstrap sample will

be the training set used for growing the tree. The error rate (out-of-bag, OOB) left out of one-third of the training data is also monitored to determine the number of decision trees. In this study, the minimum OOB error rate was reached when the number of decision trees n was less than 500 (Appendix C).

Rule 1 builds the statistical relationships between the gauge observations and the corresponding CHIRP grid cell values, which is the key idea in correcting the satellite-based precipitation estimations in the entire study area. ~~In the process of Rule 1, the regression relationships at the C1 pixels were established at 30 gauge stations separately. Because there are 30 gauge stations in the study area, 30 regression relationships at the C1 pixels were derived from Rule 1.~~ The values of the C1 pixels are not corrected in Rule 1 but are interpolated in Rule 4.

3.1.3 Rule 2 of the WHU-SGCC method

It is reasonable to assume that some pixels are statistically similar to the historical precipitation characteristics of the C1 pixels within a certain area. Therefore, it is feasible to adjust the satellite estimation bias of the C2 pixels by referring to the appropriate regression relationships at the corresponding C1 pixels based on Rule 1.

First, the spatial area in which pixels may have highly similar characteristics is established. Several studies indicate that the geographical location, elevation and other terrain information influence the spatial distribution of rainfall, especially in mountainous areas with complex topography (Anders et al., 2006; Long and Singh, 2013). The size of the spatial range is an important parameter to distinguish the spatial similarity and heterogeneity. In the WHU-SGCC method, the fuzzy c-means (FCM) clustering approach was used to determine the spatial range considered for each pixel's terrain factors, including longitude, latitude, elevation, slope, aspect and curvature. The FCM method was developed by J.C. Dunn in 1973 (Dunn, 1973), and improved in 1983 (Wang, 1983). It is an unsupervised fuzzy clustering method and its steps are as follows (Pessoa et al., 2018):

1) Choose the number of clusters c . The optimum number of clusters is determined by $L(c)$, which is derived from the inter-distance and inner distance of the samples in Eq. (2). It is ensured that the distance between similar samples is smaller, while the distance between different samples is larger.

$$L(c) = \frac{\sum_{i=1}^c \sum_{j=1}^n w_{ij}^m \|c_i - \bar{x}\|^2 / (c-1)}{\sum_{i=1}^c \sum_{j=1}^n w_{ij}^m \|x_j - c_i\|^2 / (n-c)} \quad (2)$$

In Eq. (2), the denominator is the inner-distance, and the numerator is the inter-distance. The initial value of c is 1 and the maximum value of c is the number of gauge stations in the study area. The optimum number of clusters was optimized to maximize $L(c)$. For this reason, the value of c is varied from 1 to the number of gauge stations with an increment of 1 in this study.

2) Assign coefficients randomly to each data point x_i for the degree to which it belongs in the i -th cluster $w_{ij}(x_i)$:

$$c_i^{(t)} = \frac{\sum_{j=1}^n w_{ij}^m x_j}{\sum_{j=1}^n w_{ij}^m} \quad (3), \quad w_{ij} = \frac{1}{\sum_{k=1}^c \left(\frac{\|x_i - c_i\|}{\|x_i - c_k\|} \right)^{\frac{2}{m-1}}} \quad (4), \quad \bar{x} = \frac{\sum_{i=1}^c \sum_{j=1}^n w_{ij}^m x_j}{n} \quad (5)$$

where x is a finite collection of n elements that will be partitioned into a collection of c fuzzy clusters, c_i is the centre of each cluster, m is the hyper-parameter that controls the level of cluster fuzziness, w_{ij} is the degree to which element x_i belongs to c_j , and \bar{x} is the centre vector of the collection. In Eq. (3), $c_j^{(t)}$ represents the cluster centre in iteration t . If the

270 minimum improvement in the objective function between two consecutive iterations satisfies the following equation, the
 271 algorithm terminates in iteration t (Eq. (6)):

$$272 \quad \|c_i^{(t)} - c_i^{(t+1)}\| < \varepsilon \quad (6)$$

273 3) Minimize the objective function F_c to achieve data partitioning.

$$274 \quad F_c = \sum_{j=1}^n \sum_{i=1}^c w_{ij}^m \|x_j - c_i\|^2 \quad (7)$$

275 The results of the FCM are the degree of membership of each pixel to the cluster centre as represented by numerical values.
 276 The pixels in each cluster have similar terrain features and precipitation characteristics.

277 Second, as mentioned above, the aim of Rule 2 is to derive an adjustment method for the C2 pixels based on learning from
 278 Rule 1. With the establishment of a regression relationship between the gauge observations and the corresponding CHIRP grid
 279 cell values of the C1 pixels by the RFR method, the determination of the C2 pixels follows a complicated procedure. With the
 280 exception of the C1 pixels, the remaining pixels in each cluster represent potential C2 pixels, which are called R pixels. The
 281 Pearson's correlation coefficient (PCC) and p -values between the satellite estimations (multi-year-annual daily CHIRP grid
 282 cell values) at the R pixels and the C1 pixels are the criteria for the final determination of the C2 pixels. The PCC is defined
 283 as follows:

$$284 \quad PCC_{x,y} = \frac{\sum_{i=1}^n (x_i - \bar{x})(y_i - \bar{y})}{\sqrt{\sum_{i=1}^n (x_i - \bar{x})^2} \sqrt{\sum_{i=1}^n (y_i - \bar{y})^2}} \quad (8)$$

285 where n is the number of samples, x_i and y_i are individual samples (CHIRP grid cell values at the C1 and C2 pixels,
 286 respectively), \bar{x} is the arithmetic mean of x calculated by $\bar{x} = \frac{1}{n} \sum_{i=1}^n x_i$, and \bar{y} is the arithmetic mean of y calculated by

$$287 \quad \bar{y} = \frac{1}{n} \sum_{i=1}^n y_i.$$

288 The PCC ranges between -1 and +1. If there are no repeated data values, a perfect PCC of +1 or -1 occurs when each of the
 289 variables is a perfect monotonic function of the other. However, if the value is close to zero, there is zero correlation. In
 290 addition, the correlation is not only determined by the value of the correlation coefficient but also by the correlation test's p -
 291 value. The critical values for the PCC and p -value are 0.5 and 0.05, respectively; thus, a PCC value higher than 0.5 and a p -
 292 value lower than 0.05 indicate that the data are significantly correlated (Zhang and Chen, 2016). Therefore, the final
 293 determination of the C2 pixels must meet the following criteria:

$$294 \quad |PCC| \geq 0.5 \quad \text{and} \quad p < 0.05 \quad (9)$$

295 Each R pixel has m PCC and p -values (the number of C1 pixels in the cluster), and the subset of C2 pixels is identified by
 296 excluding the data that failed the correlation test and retaining both the data with a maximum PCC of at least 0.5 and a p -value
 297 lower than 0.05, and the corresponding index of C1 pixels. The selected C2 pixels can then be considered statistically similar
 298 to the precipitation characteristics of the corresponding C1 pixels in their defined spatial area.

299 After identifying the C2 pixels and their corresponding C1 pixels, the adjustment method for the C2 pixels is derived from
 300 the regression model for the C1 pixels:

$$301 \quad C2_{as} = \frac{1}{n} \sum_{k=1}^n Tree_{k_{C1}}(Y_{s_{C2}}) \quad (10)$$

302 where $Tree_{k_{C1}}$ is the decision tree derived from the RFR algorithm at the corresponding C1 pixel, $Y_{s_{C2}}$ is the CHIRP grid cell

303 value at the C2 pixels, and $C2_{as}$ is the adjusted satellite precipitation estimate calculated by the average of the values from
 304 the RFR decision trees.

305

306 3.1.4 Rule 3 of the WHU-SGCC method

307 Recognizing that precipitation has a spatial distribution, the assumption that the C3 pixels are statistically similar to the
 308 precipitation characteristics of the C2 pixels is adopted to establish the adjustment method for the C3 pixels.

309 First, the determination of the C3 pixels in each spatial cluster is based on the selection of C2 pixels. The satellite-based
 310 estimation values at the pixels other than the C1 and C2 pixels are used to calculate the PCC and p -value with the satellite-
 311 based estimation values at the C2 pixels in the same cluster. The results of each pixel's k PCC and p -value (the number of C2
 312 pixels in the cluster) are evaluated based on the correlation test (Eq. (9)) that the pixels have a maximum PCC of at least 0.5
 313 and a p -value is of no more than 0.05, and the corresponding index of C2 pixels is retained. The selected pixels are called C3
 314 pixels, which are statistically similar to the precipitation characteristics of the corresponding C2 pixels in the defined spatial
 315 area.

316 After identifying the C3 pixels, a method for merging the CHIRP grid cell values at the C3 pixels (Y_s) and the target reference
 317 values of $C2_{as}$ at the corresponding C2 pixels is applied to estimate the adjusted precipitation values at the C3 pixels. This
 318 method combines the Y_s and $C2_{as}$ values into one variable, as shown in Eq. (11):

$$319 \quad w_i = \frac{C2_{as_i} + \lambda}{Y_{s_i} + \lambda} \quad i=1, \dots, n \quad (11)$$

320 where λ is a positive constant set to 10 mm (Sokol, 2003), $C2_{as}$ is the adjusted precipitation values at the C2 pixels, Y_s is
 321 extracted from the CHIRP grid cell values at the corresponding location of the C2 pixels, and n is the number of C2 pixels in
 322 each spatial cluster.

323 Each w of the C3 pixels is assigned the same value as the corresponding C2 pixel. Therefore, the values of the C3 pixels are
 324 derived from Eq. (12):

$$325 \quad C3_{as} = \max(w \times (Y_s + \lambda) - \lambda, 0) \quad (12)$$

326 where $C3_{as}$ is the adjusted target precipitation value at one C3 pixel, and Y_s is the corresponding CHIRP grid cell value. To
 327 avoid precipitation estimates below 0, Eq. (12) sets negative values to 0.

328 3.1.5 Rule 4 of the WHU-SGCC method

329 The pixels other than the C1, C2 and C3 pixels are called C4 pixels and they are adjusted by inverse distance weighting (IDW).
 330 IDW is based on the concept of the first law of geography from 1970, which was defined as *everything is related to everything*
 331 *else, but near things are more related than distant things*. Therefore, the attribute value of an unsampled point is the weighted
 332 average of the known values within the neighbourhood, and the distance weighting can be determined by means of IDW (Lu
 333 and Wong, 2008). In Rule 4, IDW is used to interpolate the unknown spatial precipitation data from the adjusted precipitation
 334 values at the C2 and C3 pixels. The IDW formulas are given as Eq. (13) and Eq. (14).

$$335 \quad R_{as} = \sum_{i=1}^n w_i R_i \quad (13)$$

$$336 \quad w_i = \frac{d_i^{-\alpha}}{\sum_{i=1}^n d_i^{-\alpha}} \quad \text{with} \quad \sum_{i=1}^n w_i = 1 \quad (14)$$

337 where R_{as} is the unknown spatial precipitation data, R_i is the adjusted precipitation values at the C2 and C3 pixels, n is the
 338 number of C2 and C3 pixels, d_i is the distance from each C2 or C3 pixel to the unknown grid cell, and α is the power which
 339 is generally specified as a geometric form for the weight. Several studies (Simanton and Osborn 1980; Tung 1983) have
 340 experimented with variations in the power; a the small α tends to estimate values with the averages of sampled grids in the
 341 neighbourhood, while a large α tends to give larger weights to the nearest points and increasingly down-weights points
 342 farther away (Chen and Liu, 2012; Lu and Wong, 2008). The value of α has an influence on the spatial distribution of the
 343 information from precipitation observations. For this reason, α is varied in the range of 0.1 to three (0.1, 0.3, 0.5, 1.0, 1.5,
 344 2.0, 2.5 and 3.0) in this study.

345 Note that the unknown spatial precipitation data include C1 and C4 pixels because the C1 pixels values were not adjusted
 346 in Rule 1.

347 After applying these four rules, we obtained complete daily adjusted regional precipitation maps for the four seasons over
 348 the Jinsha River basin.

349 3.2 Accuracy assessment

350 The performance of the WHU-SGCC adjusted precipitation estimates was evaluated by eight mathematic metrics: the
 351 Pearson's correlation coefficient (PCC), root mean square error (RMSE), mean absolute error (MAE), relative bias (BIAS),
 352 Nash-Sutcliffe efficiency coefficient (NSE), probability of detection (POD), false alarm ratio (FAR) and critical success index
 353 (CSI). The results of accuracy assessment are the average values validated by the leave-one-out cross method. Each validated
 354 pixel will probably be a C2, C3 or C4 pixel in the process of the WHU-SGCC algorithm. The PCC, RMSE, MAE and BIAS
 355 were used to evaluate how well the WHU-SGCC method adjusted the satellite estimation bias, while POD, FAR and CSI were
 356 used to evaluate the performance of precipitation forecasting (Su et al., 2011). The PCC measures the strength of the correlation
 357 relationship between the satellite estimations and observations. The RMSE is an absolute measurement used to compare the
 358 difference between the satellite estimations and observations, and the MAE represents the average magnitude of error
 359 estimations considering both systematic and random errors. The NSE (Nash and Sutcliffe, 1970) determines the relative
 360 magnitude of the variance of the residuals compared to the variance of the observations, bounded by minus infinity and 1; a
 361 negative value indicates a poor precipitation estimate, and a value of 1 indicates an optimal estimate. The BIAS measures the
 362 mean tendency of the estimated precipitation to be larger (positive values) or smaller (negative values) than the observed
 363 precipitation and has an optimal value of 0. The POD, also known as the hit rate, represents the probability of rainfall detection,
 364 and the FAR is defined as the ratio of the false alarm of rainfall to the total number of rainfall events. All of the accuracy
 365 assessment metrics are shown in Table 2.

366 **Table 2** Accuracy assessment metrics.

Accuracy assessment Index	Unit	Formula	Range	Optimal value
Pearson's Correlation Coefficient (PCC)	NA	$PCC = \frac{\sum_{i=1}^n (Y_{oi} - \bar{Y}_o)(C_i - \bar{C})}{\sqrt{\sum_{i=1}^n (Y_{oi} - \bar{Y}_o)^2} \cdot \sqrt{\sum_{i=1}^n (C_i - \bar{C})^2}}$	[-1,1]	1
Root Mean Square Error (RMSE)	mm	$RMSE = \sqrt{\frac{1}{n} \sum_{i=1}^n (C_i - Y_{oi})^2}$	[0,+∞)	0
Mean Absolute Error (MAE)	mm	$MAE = \frac{1}{n} \sum_{i=1}^n C_i - Y_{oi} $	[0, +∞)	0
Relative Bias (BIAS)	NA	$BIAS = \frac{\sum_{i=1}^n (C_i - Y_{oi})}{\sum_{i=1}^n Y_{oi}}$	(-∞, +∞)	0
Nash-Sutcliffe Efficiency Coefficient (NSE)	NA	$NSE = 1 - \frac{\sum_{i=1}^n (C_i - Y_{oi})^2}{\sum_{i=1}^n (C_i - \bar{Y}_o)^2}$	(-∞,1]	1
Probability of Detection (POD)	NA	$POD = H/(H+M)$	[0,1]	1

False Alarm Ratio (FAR)	NA	$FAR=F/(H+F)$	[0,1]	0
Critical Success Index (CSI)	NA	$CSI=H/(H+M+F)$	[0,1]	1

367 Note: Y_{oi} is the observation data; C_i is the adjusted value using the WHU-SGCC method for the test sample pixel; \bar{Y}_o is
368 the arithmetic mean of Y_o and is given by $\bar{Y}_o = \frac{1}{n} \sum_{i=1}^n Y_{oi}$; \bar{C} is the arithmetic mean of C and is given by $\bar{C} = \frac{1}{n} \sum_{i=1}^n C_i$; H
369 represents the number of both observed and estimated precipitation events (successfully forecasted); F is the number of false
370 alarms when the observed precipitation was below the threshold and estimated precipitation was above threshold (false alarms;
371 and. M is the number of events in which the estimated precipitation was below the threshold and observed precipitation was
372 above the threshold (missed forecasts). The POD and FAR values are dimensionless numbers ranging from 0 to 1. The
373 precipitation threshold (event/no event) was set to 0.1 mm/day.

374 4 Results and Discussion

375 A total of 18,482 daily pixels were adjusted by blending the satellite estimations (CHIRP) and observations (rain gauge stations)
376 using the WHU-SGCC approach over the Jinsha River Basin from 1990 to 2014. The percentage of pixels adjusted by each
377 rule in the WHU-SGCC method is shown in Table 3. The number of C1 pixels was the number of training gauge stations,
378 which accounted for 0.16% of the total pixels (18,482) within the basin. Due to the leave-one-out cross validation step, the
379 different training samples will have different numbers of C2, C3 and C4 pixels within the Jinsha River Basin. The percentage
380 of C2 and C3 pixels are highest in fall, followed by summer, spring and winter. In the spring, the average percentage of C2
381 pixels was approximately 21%, the average percentage of C3 pixels was approximately 17%, and the percentage of C4 pixels
382 was approximately 61%. In the summer, the percentage of C2 pixels was ranging from 15.59% to 18.36%, the percentage of
383 C3 pixels was ranging from 21.72% to 24.40%, and the percentage of C4 pixels was approximately 60%. In the full, the
384 average percentage of C2 pixels was approximately 31%, the average percentage of C3 pixels was approximately 22%, and
385 the average percentage of C4 pixels was approximately 47%. In the winter, the average percentage of C2 pixels was
386 approximately 16%, the average percentage of C3 pixels was approximately 19%, and the average percentage of C4 pixels
387 was approximately 65%. Besides, the pixel type of the validation gauge station is shown in Table D1 and the spatial distribution
388 of C1-C3 pixels in Figure D1 with the most uniform in the fall and, while the sparsest in the winter. Each validation gauge
389 station could be identified as either C2, C3 or C4 pixels to evaluate the performances of all the rules in the WHU-SGCC
390 method.

391 **Table 3** The percentage of each class pixels adjusted by each rule using the WHU-SGCC method within the Jinsha River Basin.

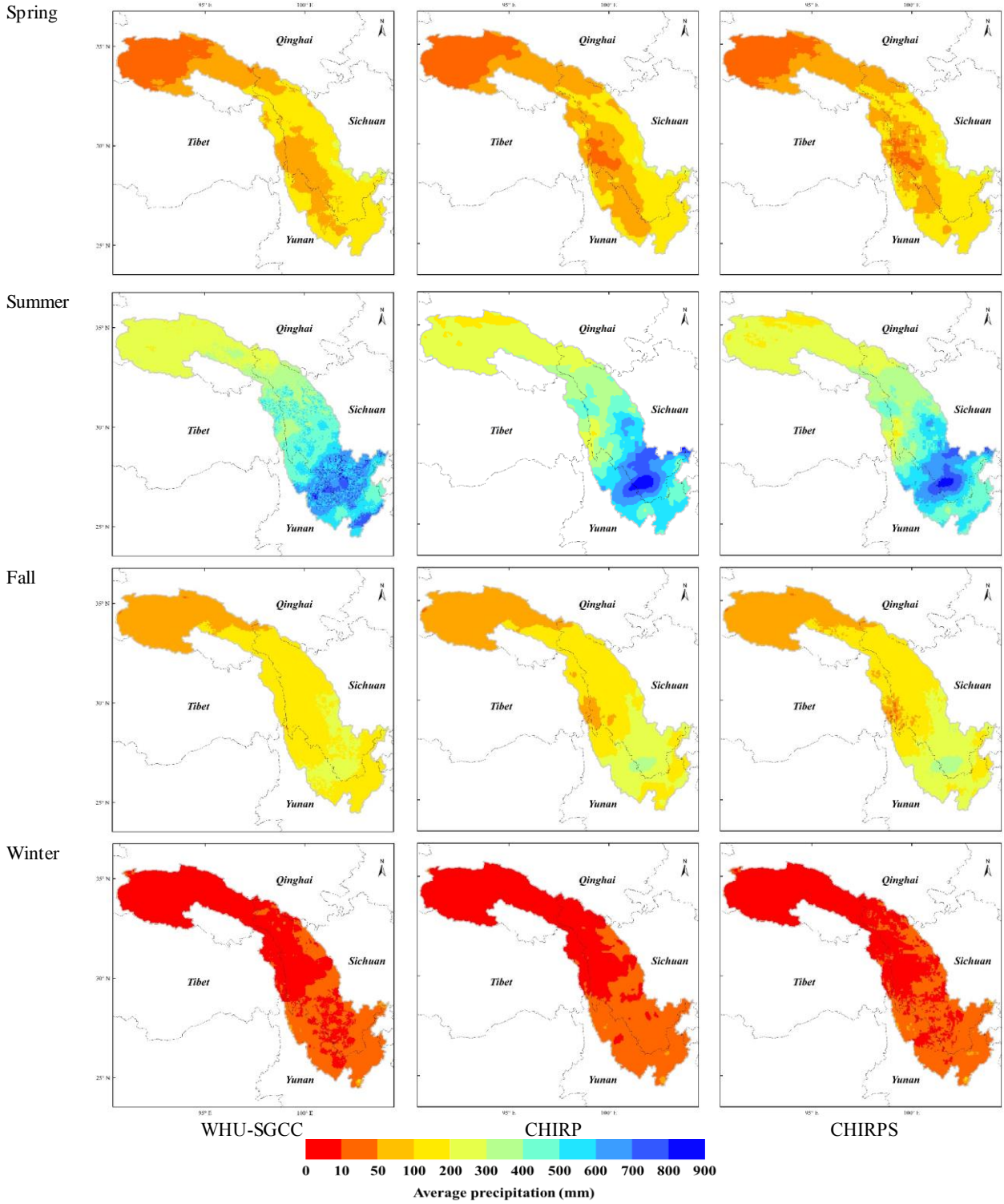
Validation gauge station	C2 Pixels (%)				C3 Pixels (%)				C4 Pixels (%)			
	Spring	Summer	Fall	Winter	Spring	Summer	Fall	Winter	Spring	Summer	Fall	Winter
52908	20.80%	16.59%	29.15%	15.52%	17.76%	22.85%	20.82%	18.16%	61.29%	60.40%	49.87%	66.16%
56004	20.89%	15.59%	29.40%	15.65%	16.29%	22.24%	20.64%	18.83%	62.66%	62.01%	49.81%	65.36%
56021	21.38%	17.91%	32.46%	15.65%	17.55%	24.40%	21.85%	19.91%	60.91%	57.53%	45.53%	64.28%
56029	21.77%	18.06%	32.60%	16.03%	17.31%	24.06%	21.61%	19.64%	60.76%	57.72%	45.63%	64.18%
56034	21.09%	17.86%	31.22%	14.86%	17.78%	23.95%	23.07%	20.19%	60.97%	58.03%	45.55%	64.79%
56038	20.48%	17.36%	30.72%	15.56%	16.12%	21.72%	23.74%	17.63%	63.23%	60.76%	45.39%	66.65%
56144	21.42%	18.11%	31.97%	16.00%	16.46%	24.03%	21.78%	19.38%	61.96%	57.70%	46.09%	64.46%
56146	21.33%	17.22%	31.77%	15.70%	17.12%	24.24%	21.42%	18.34%	61.39%	58.38%	46.65%	65.81%
56152	21.32%	17.17%	31.27%	15.57%	17.56%	22.59%	22.32%	18.94%	60.96%	60.08%	46.26%	65.34%
56167	21.46%	18.19%	32.36%	15.84%	16.90%	23.51%	21.72%	19.03%	61.48%	58.14%	45.76%	64.98%
56247	21.66%	18.32%	31.44%	16.10%	17.16%	23.89%	22.19%	19.55%	61.03%	57.63%	46.21%	64.20%
56251	21.09%	17.86%	31.28%	15.73%	17.39%	23.53%	22.88%	18.50%	61.36%	58.46%	45.68%	65.62%

56257	21.17%	17.93%	30.99%	15.95%	16.15%	21.88%	23.55%	19.13%	62.53%	60.04%	45.30%	64.77%
56357	21.62%	18.14%	31.59%	15.64%	17.12%	23.75%	22.54%	19.52%	61.10%	57.95%	45.71%	64.68%
56374	21.52%	18.08%	31.92%	14.32%	17.38%	23.23%	21.90%	19.20%	60.95%	58.53%	46.02%	66.32%
56459	21.30%	18.10%	32.14%	15.64%	16.92%	23.45%	21.16%	19.17%	61.62%	58.29%	46.54%	65.03%
56462	21.67%	18.29%	32.68%	15.92%	17.28%	23.68%	21.55%	19.14%	60.90%	57.87%	45.61%	64.78%
56475	21.49%	18.10%	32.49%	15.98%	16.36%	23.50%	22.08%	19.53%	62.00%	58.24%	45.28%	64.33%
56479	20.42%	17.88%	31.34%	15.69%	16.35%	22.79%	19.36%	18.74%	63.07%	59.17%	49.14%	65.41%
56485	21.44%	18.36%	32.78%	15.64%	17.43%	23.91%	21.82%	19.85%	60.97%	57.57%	45.24%	64.35%
56543	21.52%	18.25%	32.51%	15.87%	16.97%	23.72%	21.78%	18.90%	61.35%	57.87%	45.56%	65.06%
56565	21.21%	17.54%	30.93%	15.52%	17.81%	24.08%	23.55%	19.96%	60.83%	58.23%	45.36%	64.37%
56571	21.62%	17.89%	31.31%	14.94%	17.03%	23.07%	20.83%	18.94%	61.19%	58.89%	47.70%	65.97%
56586	21.73%	18.33%	21.73%	15.49%	17.35%	23.99%	17.35%	19.59%	60.76%	57.53%	60.76%	64.77%
56651	20.90%	18.07%	32.46%	15.38%	17.78%	23.98%	22.13%	19.95%	61.16%	57.79%	45.25%	64.51%
56664	20.94%	18.22%	32.43%	15.50%	16.64%	23.06%	21.00%	18.70%	62.26%	58.56%	46.42%	65.64%
56666	21.06%	17.98%	31.59%	15.39%	18.03%	23.97%	22.41%	19.64%	60.76%	57.89%	45.84%	64.82%
56671	20.71%	18.16%	32.55%	15.67%	16.53%	23.63%	21.89%	20.03%	62.61%	58.06%	45.41%	64.14%
56684	21.36%	18.04%	32.65%	15.46%	17.72%	23.15%	21.95%	19.28%	60.76%	58.65%	45.24%	65.10%
56778	21.63%	18.11%	32.25%	15.91%	17.31%	23.14%	22.11%	19.52%	60.90%	58.59%	45.48%	64.41%

392

393 **4.1 Model performance based on overall accuracy evaluations**

394 The multi-year-annual (1990-2014) average seasonal precipitation over the Jinsha River Basin interpolated from WHU-SGCC,
 395 CHIRP and CHIRPS is shown in Fig. 4. There exist some differences in the spatial pattern of precipitation estimates. Overall,
 396 the WHU-SGCC method exhibits the similar spatial distribution of precipitation to the CHIRP and CHIRPS, while the WHU-
 397 SGCC method attenuated the intense rain in the central area. The statistical accuracy evaluations are needed to further analyze
 398 the performance of the WHU-SGCC method.



399 **Figure 4** The multi-year-annual (1990-2014) average seasonal precipitation over the Jinsha River Basin interpolated from WHU-SGCC,
 400 CHIRP and CHIRPS.
 401

402 To test the performance of the WHU-SGCC method for precipitation estimates, the PCC, RMSE, BAE, BIAS, NSE, POD,

403 FAR, and CSI were calculated and are presented in Table 4 (the results were derived from the 22 clusters for the FCM in Rule
 404 2, as shown in Appendix E, and $\alpha = 0.1$ for the IDW in Rule 4 after the comparison of the RMSE). After the correction, the
 405 PCC in the WHU-SGCC method shows an improvement relative to the CHIRP and CHIRPS estimates. The spring and fall
 406 have better correlations than the summer and winter. In addition, the NSE of the WHU-SGCC provides substantial
 407 improvements over CHIRP and CHIRPS, especially in the spring and fall which were better than the summer and winter. The
 408 RMSE and MAE are the largest in the summer, followed by the fall, spring, and winter; however, the performances of the
 409 BIAS in the summer and fall are better than those in the spring and winter, which might be influenced by the greater
 410 precipitation in the summer and fall than in the spring and winter. The assessments of the POD and CSI are lowest, and the
 411 FAR is largest in the winter due to the overestimation of no rain events estimated by the satellite-based data set.

412 Compared with the estimates of CHIRP and CHIRPS, the PCCs of the WHU-SGCC method are improved to more than 0.5
 413 in the spring and fall and to approximately 0.5 in the winter. In addition, the RMSE and MAE of the WHU-SGCC were all
 414 lower than those of CHIRP and CHIRPS. The absolute values of the BIAS of the WHU-SGCC are substantially improved in the
 415 spring, followed by the summer, winter and fall. Although the absolute value of the BIAS of the WHU-SGCC in fall are not
 416 significantly better than those of CHIRP and CHIRPS, all of the values are approximately 0. The NSEs of the WHU-SGCC
 417 reached 0.2836, 0.2944 and 0.1853 in the spring, fall and winter, respectively, which are substantially better than the negative
 418 or zero values of CHIRP and CHIRPS. In the summer, the NSE of the WHU-SGCC is still negative, but it is improved to be
 419 nearly zero, which indicates that the adjusted results are similar to the average level of the rain gauge observations. It is worth
 420 noting that in the spring, summer and fall, the POD values of the WHU-SGCC are in the range of 0.95 to 1, better than CHIRP
 421 and CHIRPS, and the FAR values of the WHU-SGCC are no more than 0.3, lower than CHIRP and CHIRPS; these results
 422 represent the better ability of the WHU-SGCC method to predict precipitation events. The rainfall detection ability is the worst
 423 in the winter compared to the other seasons. This can be explained by the seasonal distribution of precipitation in the Jinsha
 424 River Basin, in which the most rainfall occurs in the summer, followed by the fall, spring and winter. In addition, the spatial
 425 distribution of C2 and C3 pixels ~~might slightly also significantly~~ impact the overall accuracy in different seasons that the
 426 ~~sparsest in the winter most uniform in the fall~~, while ~~more uniform in the summer the sparsest in the winter~~. However, the
 427 performances of PCC, RMSE, MAE and NSE in the winter are better than those in the summer. The worst errors of forecasting
 428 performance in the summer may be attributed to the highest precipitation. The limited precipitation events detection in the
 429 winter could also be explained by the lowest precipitation (Xu et al., 2019).

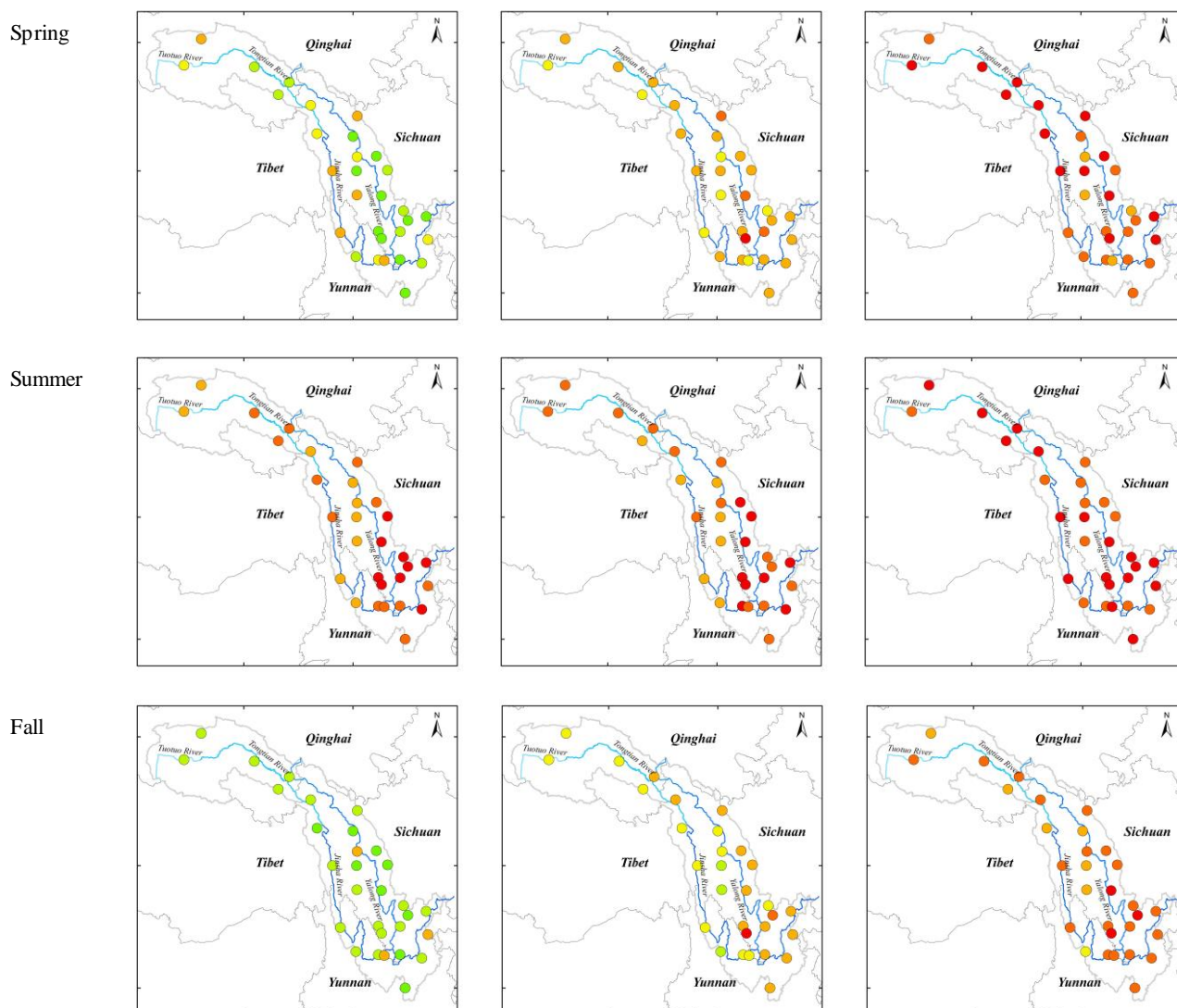
430 **Table 4** Overall accuracy assessments for the four seasons from 1990 to 2014.

Statistic	Spring			Summer			Fall			Winter		
	WHU-SGCC	CHIRP	CHIRPS									
PCC	0.5376	0.3644	0.2132	0.2536	0.2454	0.1924	0.5508	0.3889	0.2661	0.4722	0.2490	0.1716
RMSE	2.9526	3.4332	5.1926	8.7608	9.4108	11.3354	4.7981	4.9038	7.7506	0.8120	0.9042	1.0569
MAE	1.3380	1.5426	1.9948	5.4564	5.8415	7.0088	2.0973	2.2943	2.9925	0.2093	0.7398	0.6905
BIAS	-0.1148	-0.2490	-0.1783	-0.0167	-0.0443	-0.0134	-0.0566	-0.0563	-0.0231	-0.1775	-0.2083	-0.3093
NSE	0.2836	0.0745	-1.0817	-0.0139	-0.2083	-0.8293	0.2944	0.0168	-1.4692	0.1853	0.0161	-0.3098
POD	0.9605	0.8572	0.2918	0.9932	0.9578	0.4351	0.9612	0.9047	0.2326	0.6988	0.5786	0.2076
FAR	0.2416	0.4515	0.3888	0.1146	0.2323	0.1601	0.2386	0.4301	0.2638	0.5242	0.7082	0.6381
CSI	0.6928	0.5001	0.2335	0.8799	0.7405	0.401	0.7089	0.5303	0.2144	0.3668	0.2210	0.1352

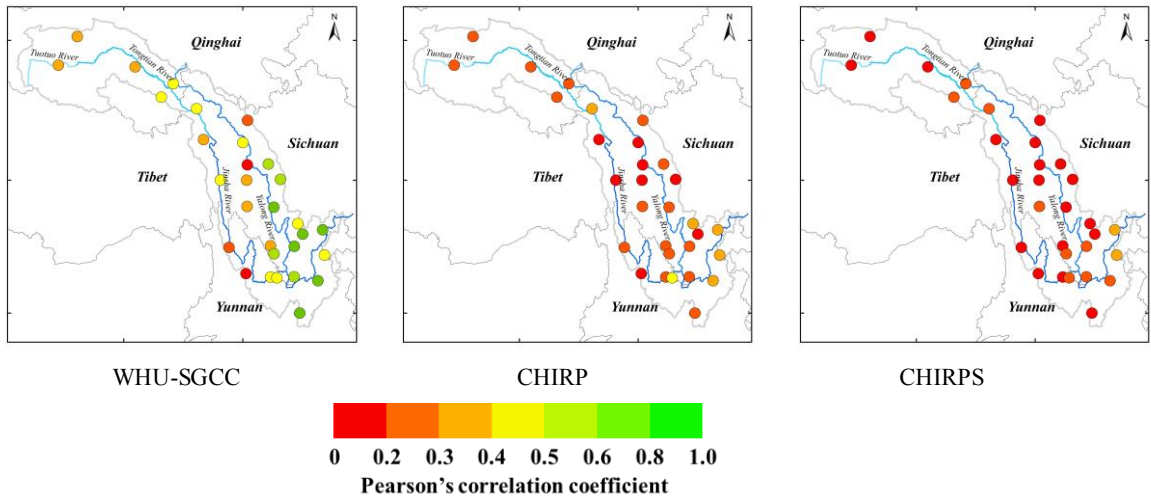
431 The spatial distributions of the statistical comparisons between the observations and the WHU-SGCC precipitation
 432 estimations are shown in Fig. 5 and Fig. 6. Overall, the variation in the PCC shows low correlations in areas with lower
 433 elevation, particularly in the southeast Jinsha River Basin, where there is higher precipitation and a greater density of rain
 434 gauges. The PCC is highest in the fall, followed by the spring and winter, and finally by summer. The higher correlations are
 435 located in the north-central area along the Tongtian River, Jinsha River and upstream part of the Yalong River, which has

436 complex terrain and few rain gauges. The RMSE is lowest in the winter than in the spring, fall and summer, which can be
 437 attributed to the lower precipitation in the winter and the greatest in the summer. The spatial distribution of the RMSE shows
 438 that, the smaller errors are scattered in the northwest area of the river basin, with values lower than 5 mm, while the highest
 439 errors are located along the border between the lower reaches of the Jinsha Jiang River and the river basin. This is related to
 440 the climate regimes of the Jinsha River Basin, which includes more rainfall in the south and southeast areas than in the north,
 441 and northwest.

442 The results show that the WHU-SGCC method improves the correlation relative to CHIRP and CHIRPS, especially in
 443 central and southeast river basin during the spring, fall and winter, with most of the PCC values falling between 0.4 and 0.8
 444 (Fig. 5). As shown by the RMSE (Fig. 6), the WHU-SGCC can also correct the precipitation errors-bias in the central and
 445 southeast river basin, especially along the downstream part of the Yalong River. In addition, the WHU-SGCC slightly
 446 improved the RMSE around the convergence of the rivers, where it is less than 5 mm in the spring and fall, and most of RMSE
 447 values are less than 1 mm in the winter. In spite of the correction, the RMSE values in the summer are still substantial.



Winter

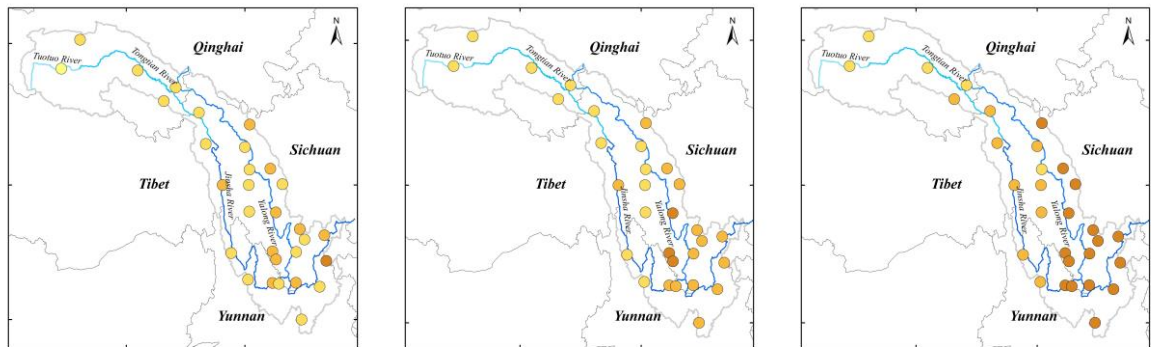


448
449
450

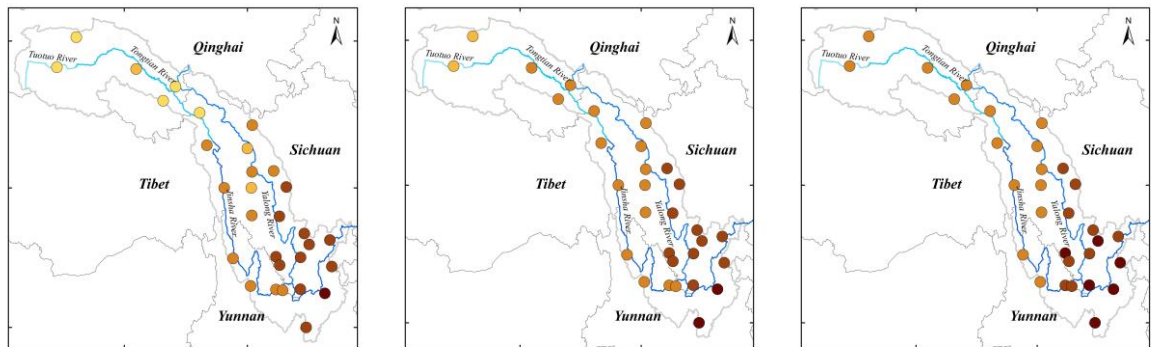
Figure 5 Spatial distribution of the Pearson's correlation coefficient of the overall agreement between observations and the WHU-SGCC, CHIRP and CHIRPS estimations in the four seasons from 1990 to 2014.

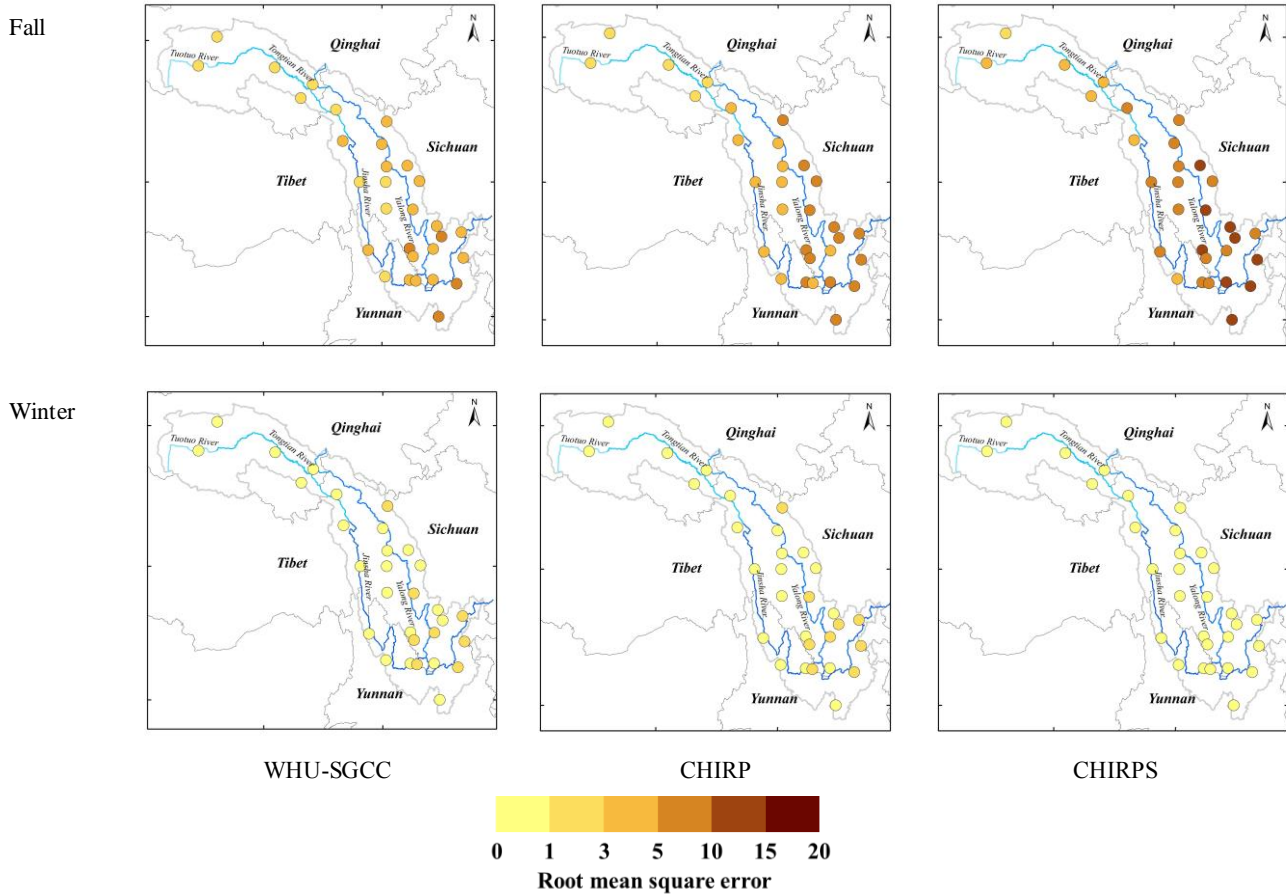
451 All of the spatial distribution statistics indicate that the statistical relationships established during the process of the WHU-SGCC method are susceptible to the mode values of the rain gauge stations data, especially in the summer. Although the average summer precipitation in the southern Jinsha River Basin was more than 600 mm (Fig. 2), days of light rain still represent a large percentage, which causes large biases and limits the performance over the south, while there are sufficient data with similar precipitation features for the WHU-SGCC in the north. Nevertheless, the WHU-SGCC approach is still effective at adjusting the satellite biases by blending the data with the observations, particularly in the complicated mountainous regions, where higher PCCs correspond to lower RMSEs.

Spring



Summer





458

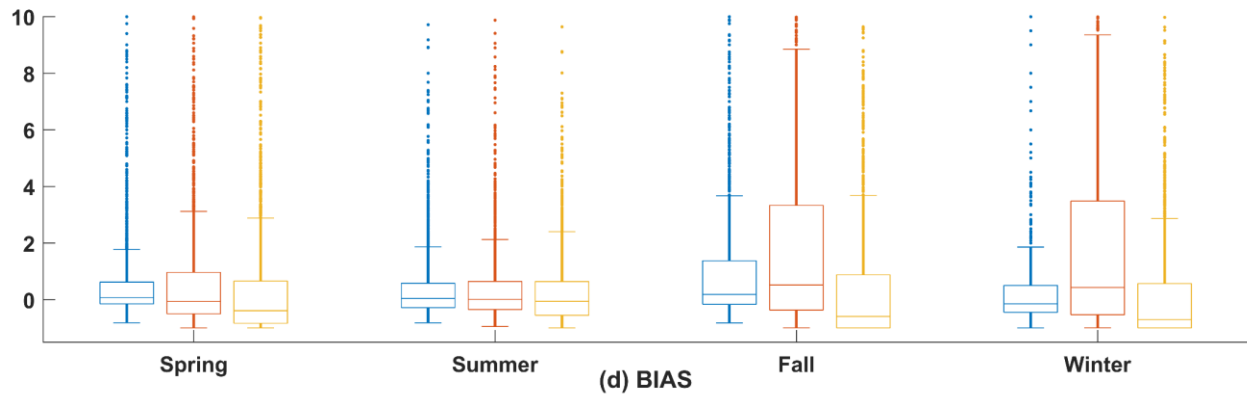
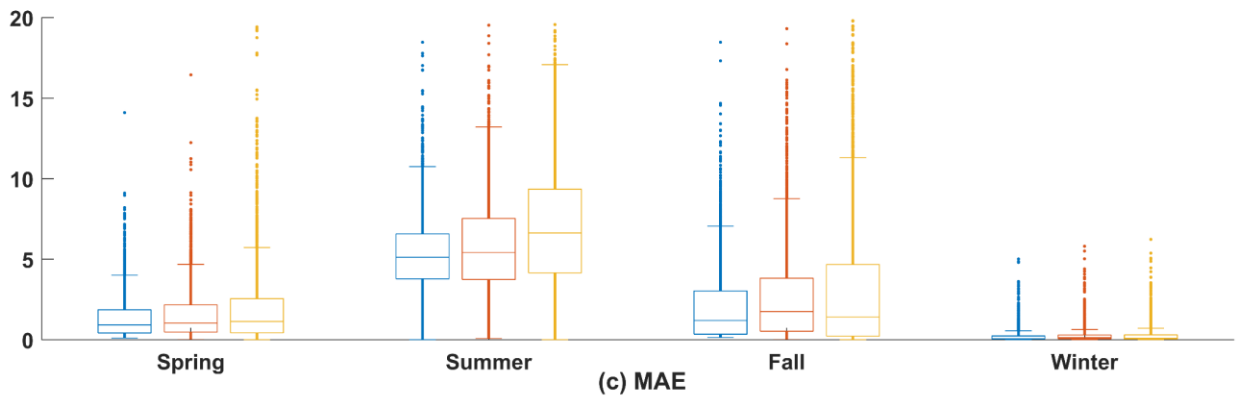
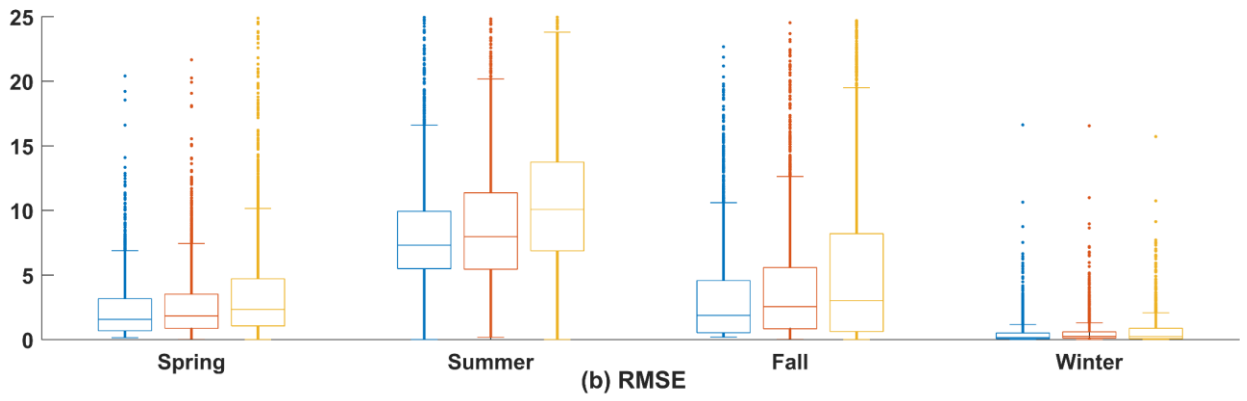
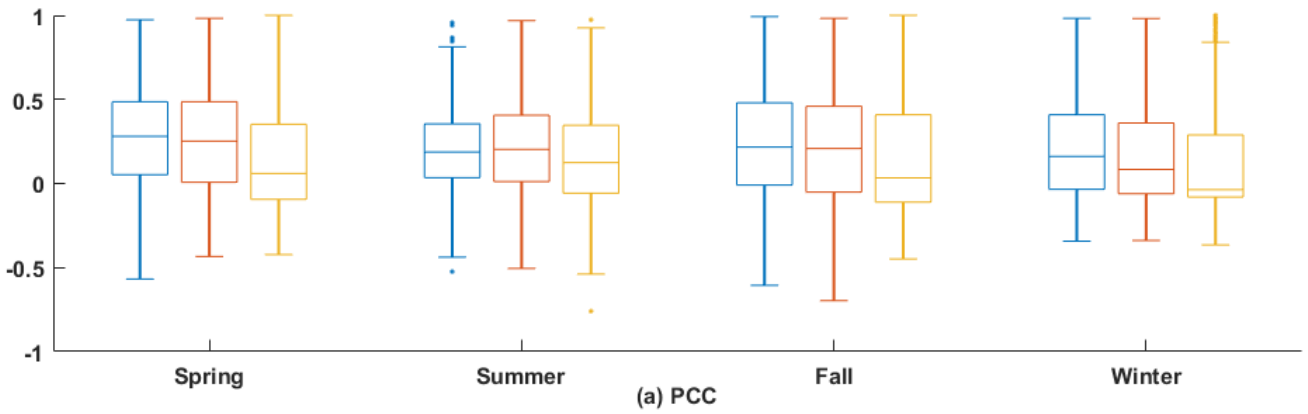
459 **Figure 6** Spatial distribution of the root mean square errors of the overall agreement between observations and the WHU-SGCC, CHIRP
 460 and CHIRPS estimations in the four seasons from 1990 to 2014.

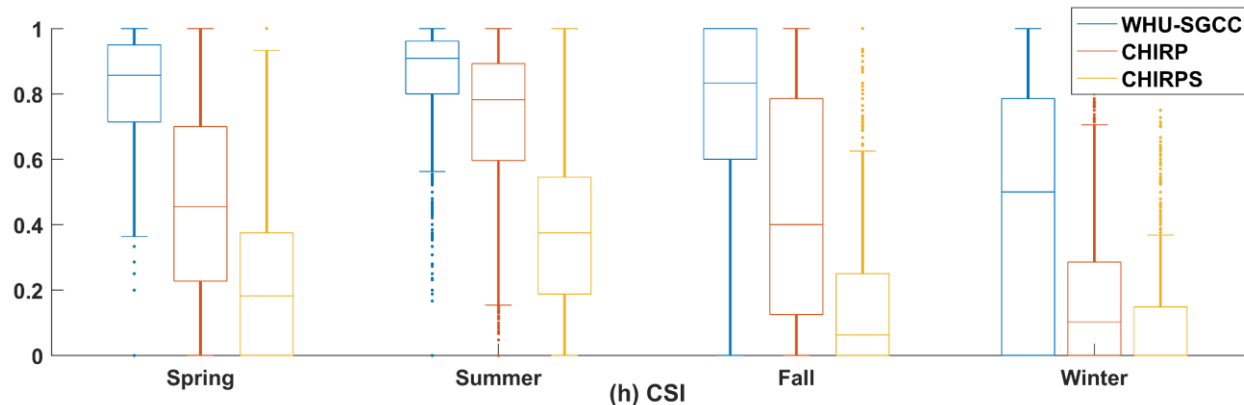
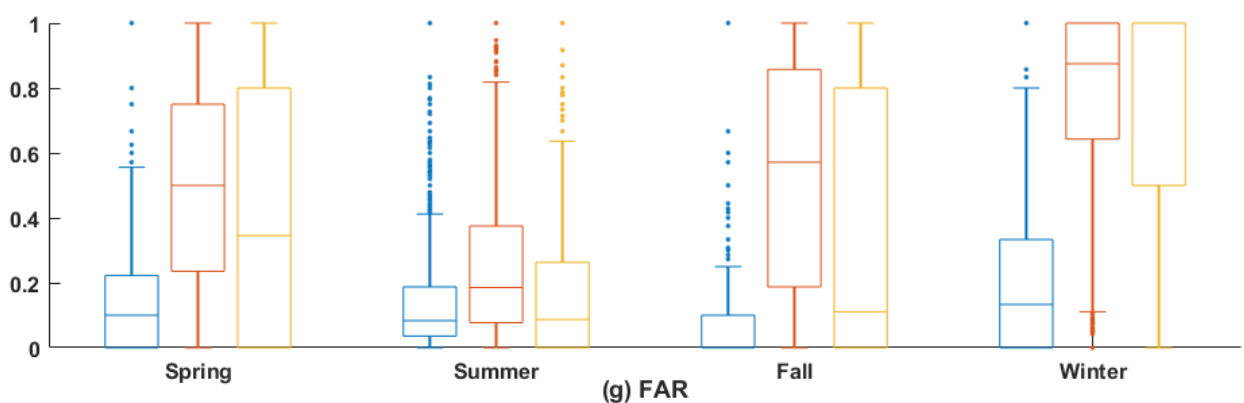
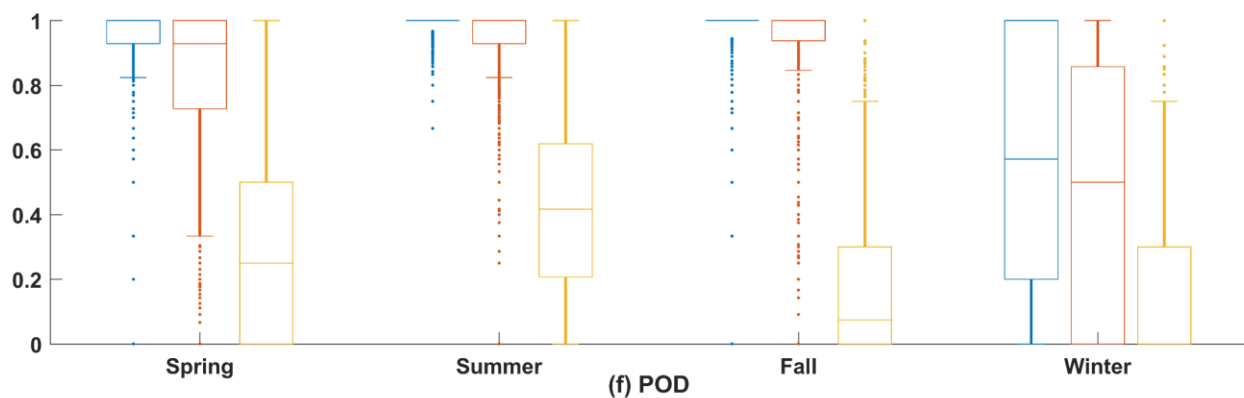
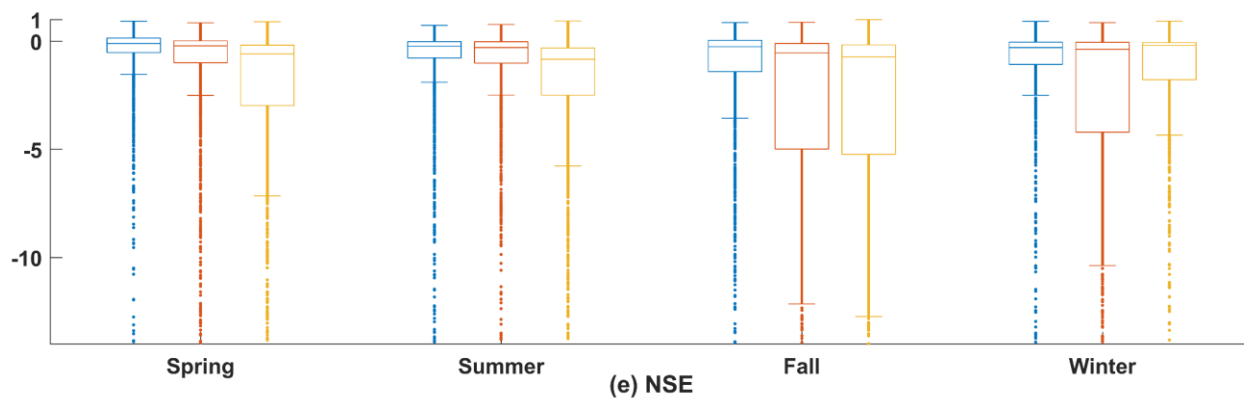
461 **4.2 Model performance based on daily accuracy evaluations**

462 After the overall accuracy evaluations were conducted, further evaluations of the daily accuracy in the four seasons were
 463 conducted, and the results are shown in Fig. 7. The evaluation of the daily accuracy indicates that the PCCs of the WHU-
 464 SGCC were slightly better than those of CHIRP and CHIRPS in the spring, fall and winter but were not as good in the summer
 465 and winter. The WHU-SGCC had lower RMSEs and MAEs than CHIRP and CHIRPS, especially compared to CHIRPS. The
 466 daily RMSE and MAE in the summer are the highest, although the WHU-SGCC still corrects the errors bias. Figure 7 indicates
 467 that there is a slight increase in the PCC, with average improvements of 0.02-0.04 and 0.04-0.14, respectively; however, the
 468 PCC is a relative metric of the magnitude of the association between paired variables, and a relative consistency may not
 469 indicate absolute proximity. Thus, the absolute measure indicated by the RMSE may be more reasonable. In this study, the
 470 RMSE and MAE derived from the WHU-SGCC are reduced by approximately 15% and 34% on average compared to CHIRP
 471 and CHIRPS, respectively. As for BIAS, WHU-SGCC method can correct the CHIRP precipitation bias in the spring, fall and
 472 winter, but the results are not as good compared with CHIRPS. The larger BIAS values and higher PCCs in the spring and fall
 473 may be attributed to the seasonal variations, when the CHIRP is highly consistent with the observations but subject to large
 474 biases. After the correction, a substantial decrease in BIAS occurs in the winter, and there is no significant reduction in the
 475 summer; all of the median and average adjusted values are approximately 0. The WHU-SGCC method provides an obvious
 476 improvement in the NSE, with average improvements of 0.20-3.00 and 0.25-4.00 relative to CHIRP and CHIRPS, though
 477 the median and average values are still less than 0, which may be due to the inherent uncertainty in the CHIRP. Moreover, in
 478 terms of the POD, FAR and CSI, except for the results in winter, the WHU-SGCC method appears to be better at detecting
 479 precipitation than CHIRP and CHIRPS; the results of POD and CSI are closest to 1, although FAR is worse than CHIRPS on
 480 some days. However, the overall result of FAR is the best in the WHU-SGCC. The POD and FAR results are the worst in the

481 winter, and the CSI is slightly higher, which may be attributed to the overestimation of no-rain events and the inherent
482 uncertainty in the CHIRP.

483 Overall, the WHU-SGCC approach can be regarded as an effective tool for daily precipitation adjustments.





492 **Figure 7** Statistical analysis of the agreement between the daily observations and the WHU-SGCC, CHIRP and CHIRPS estimates with the
 493 leave-one-out cross validation: a) Pearson's correlation coefficient, b) root mean square error, c) mean absolute error, d) relative bias, e)
 494 Nash-Sutcliffe efficiency coefficient, f) probability of detection, g) false alarm ratio, and h) critical success index.

495 **4.3 Model performance on rain events predictions**

496 To measure the WHU-SGCC performance on predicting rain events, daily precipitation thresholds of 0.1, 10, 25, and 50 mm
 497 were considered, and the results are shown in Table 5 and Table 6. The average percentage of each class of rain events at the

498 validation gauge station during the four seasons from 1990 to 2014 are shown in Table 5. The major rain events within the
 499 Jinsha River Basin were no rain (<0.1 mm) and light rain (0.1-10 mm), which accounted for more than 80% of the total days
 500 (the average percentage of rain event days of the total days at each gauge station), while the number of days with daily
 501 precipitation greater than the 50 mm was the smallest (no more than 1% of the total days) and fewer than 5% of the days had
 502 daily precipitation in the range of 25 mm to 50 mm. In the spring, fall and summer, significantly more no-rain days occurred
 503 than rainy days, and approximately 5% of the days had daily precipitation of 10-50 mm. The seasonal distribution of rainfall
 504 was concentrated in the summer, and 54.76%, 14.01% and 3.62% of the days had daily precipitation of 0.1-10, 10-25, and 25-
 505 50 mm, respectively. The results indicated that the average daily precipitation was less than 10 mm throughout the years of
 506 the study.

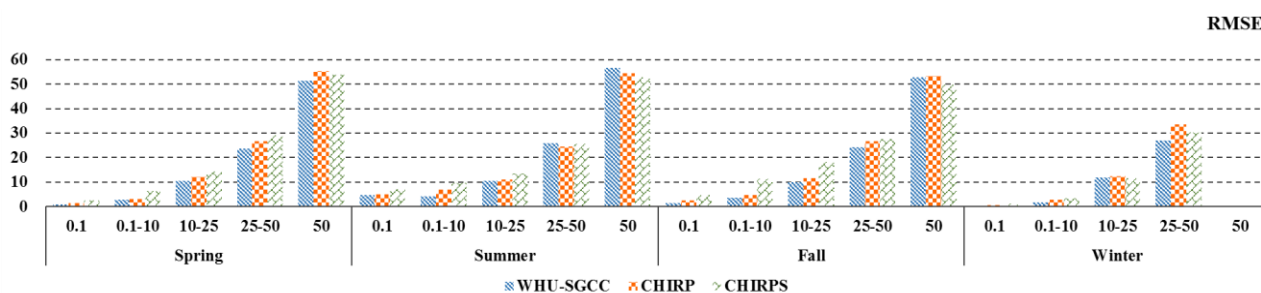
507 **Table 5** The average percentage of each class of rain events at the validation gauge station during the four seasons from 1990 to 2014 within
 508 the Jinsha River Basin.

Season	Rain event (mm)				
	<0.1	[0.1,10)	[10,25)	[25,50)	>=50
Spring	57.87%	38.43%	3.29%	0.39%	0.02%
Summer	26.89%	54.76%	14.01%	3.62%	0.72%
Fall	57.32%	36.62%	4.99%	0.93%	0.14%
Winter	85.78%	13.99%	0.21%	0.01%	0.00%

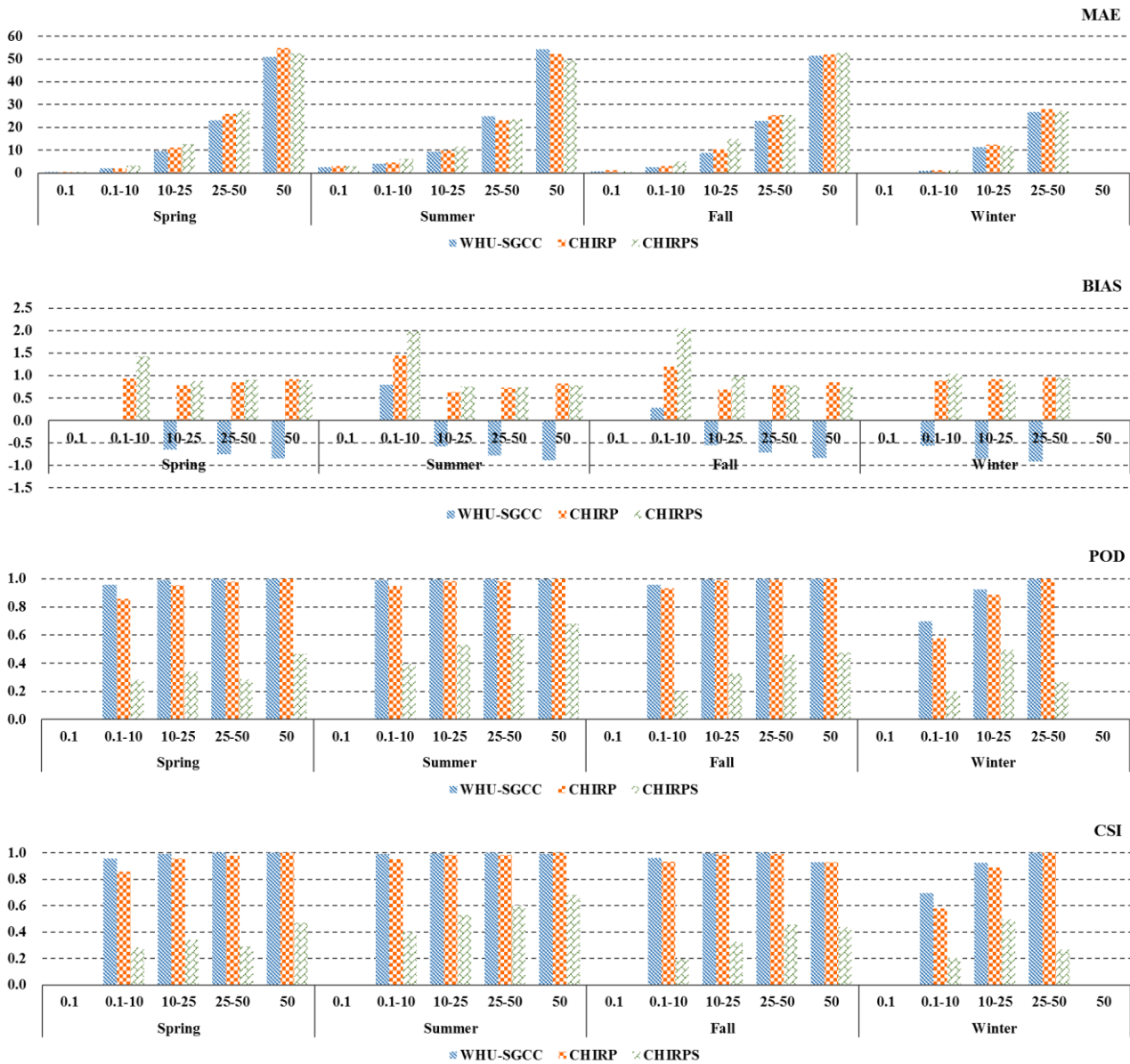
509 The WHU-SGCC approach had lower errors than CHIRP and CHIRPS, as indicated by the RMSE, MAE and BIAS, but the
 510 performance of WHU-SGCC is not promising for events with total rainfall greater than 25 mm in the summer (Fig. 8). This
 511 negative performance for total rainfall higher than 25 mm in the summer might be attributed to the overestimation of rainfall
 512 by CHIRP and CHIRPS. For the seasonal distribution of precipitation (Table 5), the average daily precipitation within the
 513 basin less than 10 mm over the study period, which results in numerous rain gauge station data with values lower than 10 mm,
 514 which had a significant impact on the establishment of statistical relationships for the WHU-SGCC. Besides the WHU-SGCC
 515 dataset has almost always a negative bias, while CHIRP and CHIRPS has a positive bias in the different rain events. After bias
 516 correction of the WHU-SGCC, some precipitation estimates are lower than observations. The estimates of extreme rain events
 517 might also be attenuated during the process of WHU-SGCC adjustment.

518 Besides, the POD and CSI results of CHIRPS are the worst, while the results of the WHU-SGCC are the highest, which
 519 indicate its superiority for the detection of precipitation events. As for the results of the WHU-SGCC, the assessments of POD
 520 and CSI are the best in the summer, followed by the fall, spring, and winter, which are related to the seasonal rainfall pattern
 521 of more rain in the summer and less in the winter.

522 Therefore, the WHU-SGCC approach is applicable for the detection of rainfall events in the Jinsha River Basin, while in
 523 the summer it is better with rainfall less than or approximately equal to the average daily precipitation. Due to the
 524 homogenization of the WHU-SGCC method, its performance for short intense and extreme rain events was poorer than those
 525 of CHIRP and CHIRPS, which should be improved in a future study.



526



527

528

529

530
531

Figure 8 Accuracy assessment of liquid precipitation events from 1990 to 2014.

532 **5 Data availability**

533 All the resulting dataset derived from the WHU-SGCC approach is available on PANGAEA, with the following DOI:
534 <https://doi.pangaea.de/10.1594/PANGAEA.900620> (Shen et al., 2019). The high-resolution (0.05°) daily precipitation
535 estimation data over the Jinsha River Basin from 1990 to 2014 can be downloaded in TIFF format.

536 **6 Conclusions**

537 This study provides a novel approach, the WHU-SGCC method, for merging daily satellite-based precipitation estimates with
538 observations. A case study of the Jinsha River Basin was conducted to verify the effectiveness of the WHU-SGCC approach
539 during all four seasons from 1990 to 2014, and the adjusted precipitation estimates were compared to CHIRP and CHIRPS.
540 The WHU-SGCC method aims to reduce the errors-bias and uncertainties in CHIRP data over regions with complicated
541 mountainous terrain and sparse rain gauges. To the best of the authors' knowledge, this study is the first to use daily CHIRP
542 and CHIRPS data in this area.

543 According to our findings, the following conclusions can be drawn: (1) The WHU-SGCC method is effective for the

544 adjustment of precipitation biases from points to surfaces. The precipitation adjusted by the WHU-SGCC method can achieve
545 greater accuracy compared with CHIRP and CHIRPS, with average improvements of Pearson's correlation coefficient (PCC)
546 of 0.01-0.23 and 0.06-0.32, respectively. The PCCs were improved to more than 0.5 in the spring and fall and to approximately
547 0.5 in the winter, and they were the worst in the summer, which may be attributed to the greater precipitation in the summer
548 and lower precipitation in the winter. In addition, the NSE of the WHU-SGCC provides substantial improvements over CHIRP
549 and CHIRPS, which reached 0.2836, 0.2944 and 0.1853 in the spring, fall and winter, respectively. In the summer, the NSE
550 of the WHU-SGCC is still negative, but it is improved to be nearly zero, which indicates that the adjusted results are similar
551 to the average level of the rain gauge observations. All of the measured errors were reduced except for the BIAS, which showed
552 no significant improvement in the summer but was approximately 0. Overall, the WHU-SGCC approach achieves good
553 performance in error correction of CHIRP and CHIRPS. (2) The spatial distribution of the precipitation estimate accuracy
554 derived from the WHU-SGCC method is related to the topographic complexity. These errors over the lower elevation regions
555 and the large size of light precipitation events with short durations resulted in a limited improvement in accuracy, with PCC
556 values less than 0.3. However, higher PCCs and lower errors were observed over the north-central part of the river basin, which
557 is a drier region with complex terrain and sparse rain gauges. The spatial distribution statistics indicate that the WHU-SGCC
558 method is promising for the adjustment of satellite biases by blending with the observations over regions of complex terrain.
559 (3) The leave-one-out cross validation of WHU-SGCC on daily rain events confirmed that the model is effective in the
560 detection of precipitation events that are less than or approximately equal to the average annual precipitation in the Jinsha
561 River Basin. The WHU-SGCC approach achieves reductions of the RMSE, MAE and BIAS metrics, while on rain events less
562 than 25 mm in the summer. Specifically, the WHU-SGCC has the best ability to reduce precipitation ~~errors-bias~~ for daily
563 accuracy evaluations, with average reductions of 15% and 34% for compared to CHIRP and CHIRPS, respectively. As for the
564 results of the WHU-SGCC, the assessments of POD and CSI are the best in the summer, followed by the fall, spring, and
565 winter, which are related to the seasonal rainfall pattern of more rain in the summer and less in the winter. In spite of the
566 corrections, the ~~uncertainties in the precipitation forecasts in the summer are still large~~ performance of the WHU-SGCC for
567 ~~short intense and extreme rain events was poorer than those of CHIRP and CHIRPS, and the bias in the precipitation forecasts~~
568 ~~in the summer are still large~~, which may due to the homogenization attenuating the ~~simulation of~~ extreme rain events ~~estimates~~.

569 In conclusion, the WHU-SGCC approach can help adjust the biases of daily satellite-based precipitation estimates over the
570 Jinsha River Basin, which contains complicated mountainous terrain with sparse rain gauges. This approach is a promising
571 tool to monitor daily precipitation over the Jinsha River Basin, considering the spatial correlation and historical precipitation
572 characteristics between raster pixels in regions with similar topographic features. Future development of the WHU-SGCC
573 approach will focus on the following three aspects: (1) the improvement of the adjusted precipitation quality to better monitor
574 extreme rainfall events by blending multiple data sources for different rain events; (2) the introduction of more climatic factors
575 and multi-model ensembles to achieve more accurate spatial distributions of precipitation; and (3) investigations of the
576 performance over other areas and for particular hydrological cases to validate the applicability of WHU-SGCC approach.

577 **Appendix A: Geographical characteristics of rain stations**

578 The station identification numbers and relevant geographical characteristics are shown in Table A1.

579

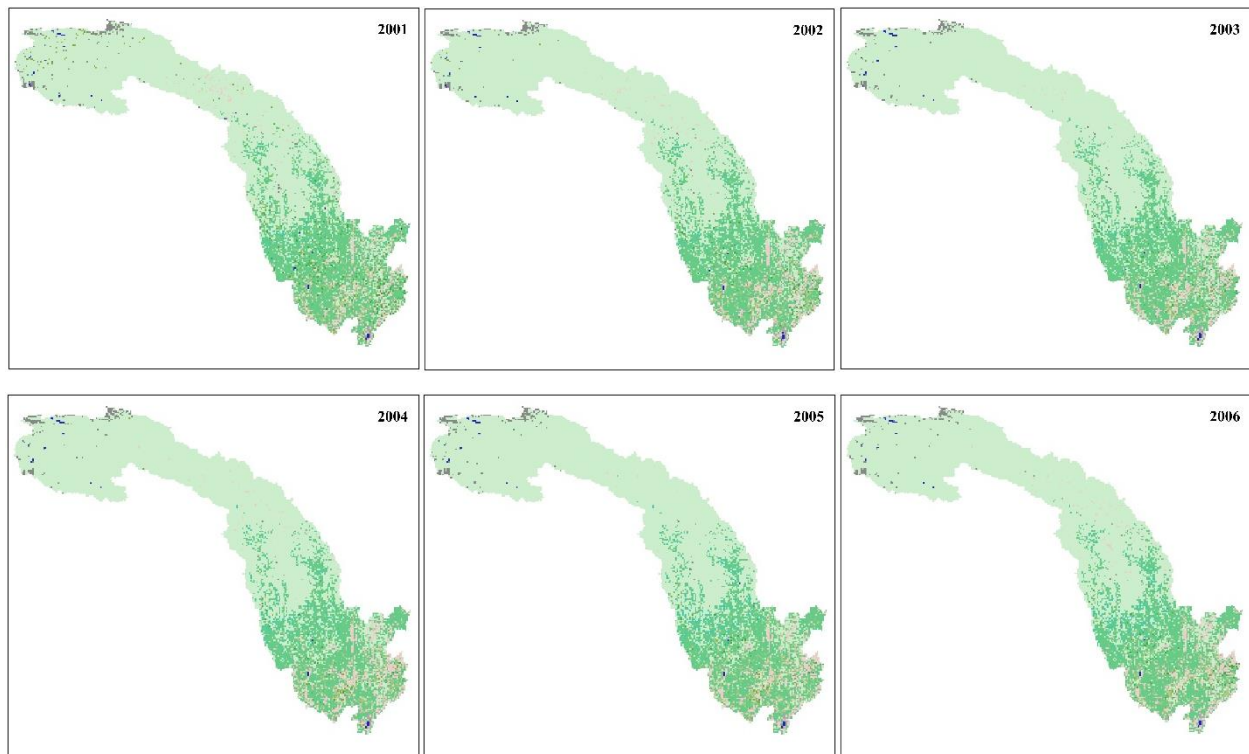
Table A1 Geographical characteristics of the rain stations.

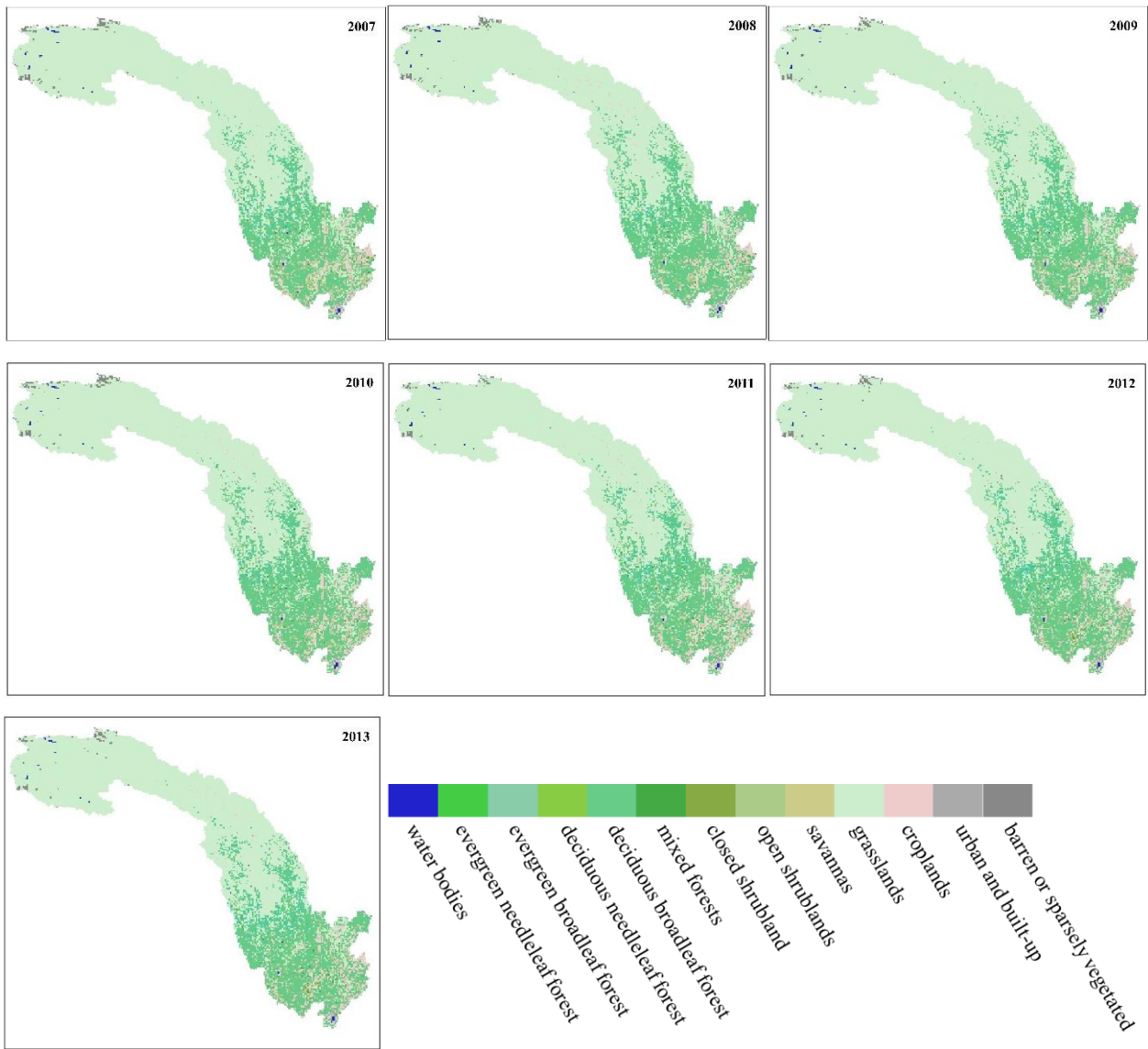
Station number	Province	Lat (°N)	Lon (°E)	Elevation (m)
52908	Qinghai	35.13	93.05	4823
56004	Qinghai	34.13	92.26	4744
56021	Qinghai	34.07	95.48	5049
56029	Qinghai	33.00	96.58	4510
56034	Qinghai	33.48	97.08	4503
56144	Tibet	31.48	98.35	4743

56038	Sichuan	32.59	98.06	4285
56146	Sichuan	31.37	100.00	4703
56152	Sichuan	32.17	100.20	4401
56167	Sichuan	30.59	101.07	3374
56247	Sichuan	30.00	99.06	2948
56251	Sichuan	30.56	100.19	4284
56257	Sichuan	30.00	100.16	3971
56357	Sichuan	29.03	100.18	4280
56374	Sichuan	30.03	101.58	3902
56459	Sichuan	27.56	101.16	3002
56462	Sichuan	29.00	101.30	4019
56475	Sichuan	28.39	102.31	1850
56479	Sichuan	28.00	102.51	2470
56485	Sichuan	28.16	103.35	2060
56565	Sichuan	27.26	101.31	2578
56571	Sichuan	27.54	102.16	1503
56666	Sichuan	26.35	101.43	1567
56671	Sichuan	26.39	102.15	1125
56543	Yunnan	27.50	99.42	3216
56586	Yunnan	27.21	103.43	2349
56651	Yunnan	26.51	100.13	2449
56664	Yunnan	26.38	101.16	1540
56684	Yunnan	26.24	103.15	2184
56778	Yunnan	25.00	102.39	1975

Appendix B: Multi-year annual land cover type

The multi-year annual land cover types in the Jinsha River Basin from 2001 to 2013 are shown in Fig. B1. All of the land cover type maps were derived from the MODIS/Terra+Aqua Land Cover Type Yearly L3 Global 500 m SIN Grid V051 data set, which is available online at https://search.earthdata.nasa.gov/search/granules?p=C200106111-LPDAAC_ECS&q=MCD12&ok=MCD12 (last access: 23 July 2019). Fig. B1 shows that the land use had no obvious changes over the study period. In addition, the upstream area of the Jinsha River is an untraversed region that has not been affected significantly by human activities. Thus, the land use in the study area has hardly changed.





589

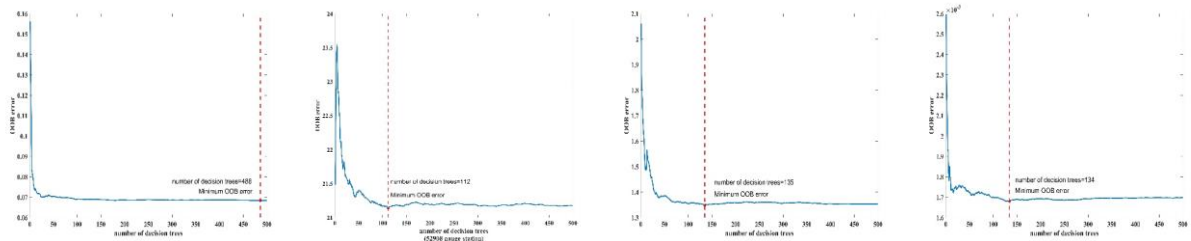
590

591

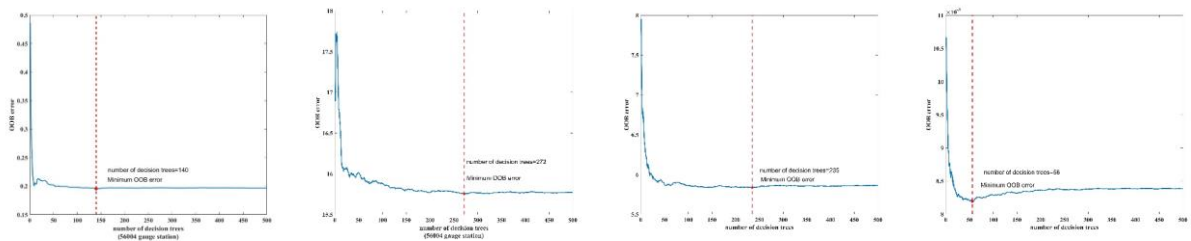
592 **Figure B1** Land cover types over the Jinsha River Basin from 2001 to 2013.

593 **Appendix C: Selection of decision trees for random forest regression**

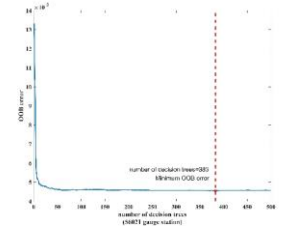
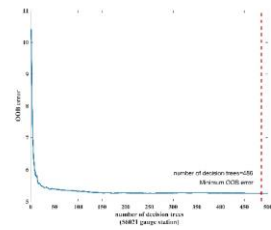
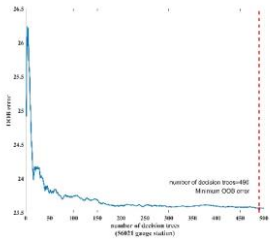
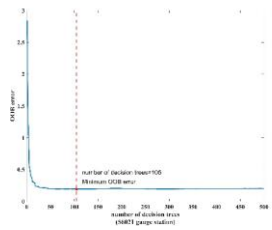
52908



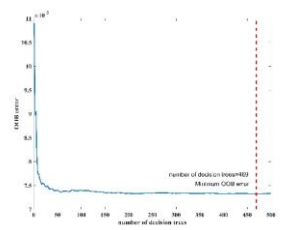
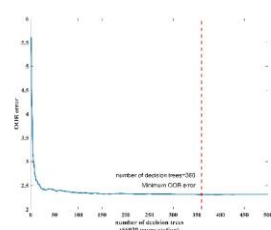
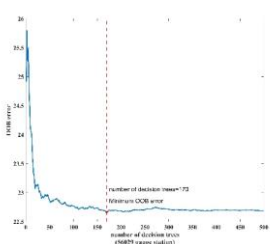
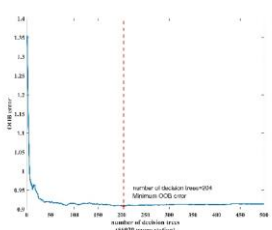
56004



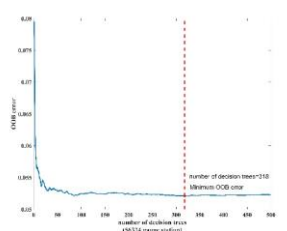
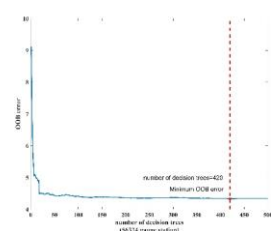
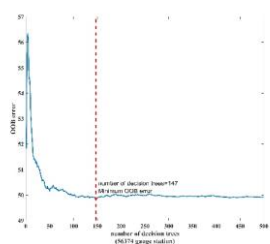
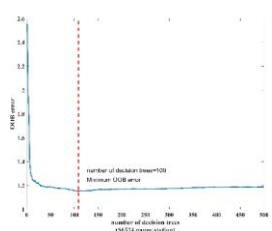
56021



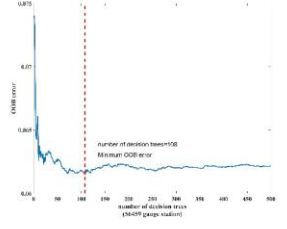
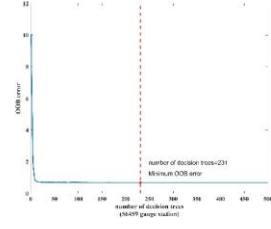
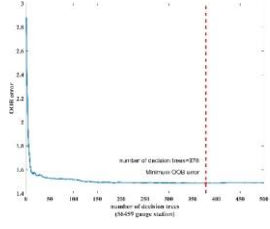
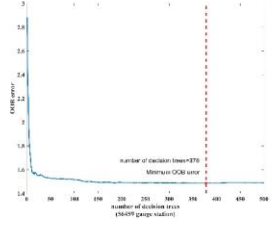
56029



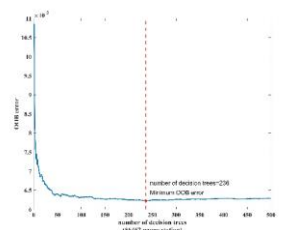
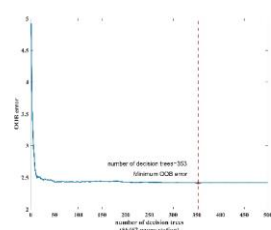
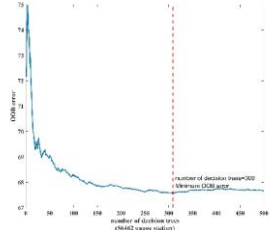
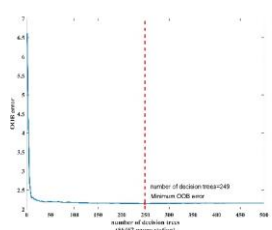
56374



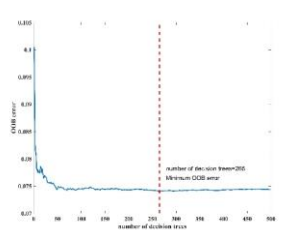
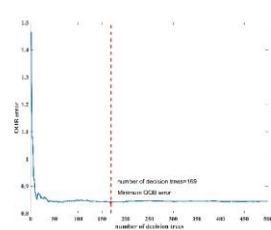
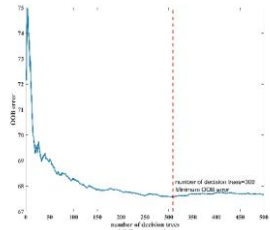
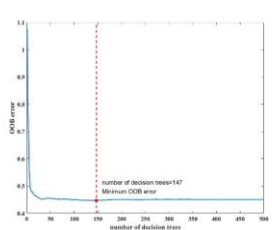
56459



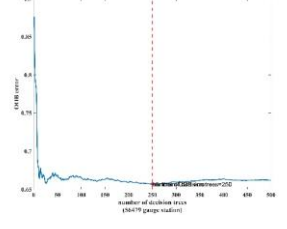
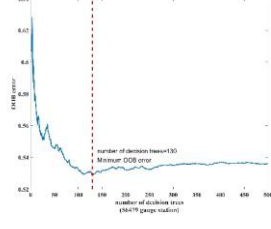
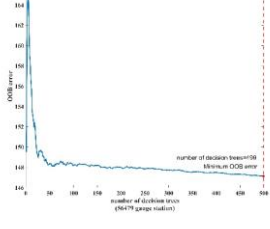
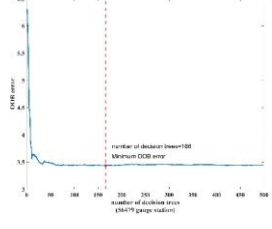
56462



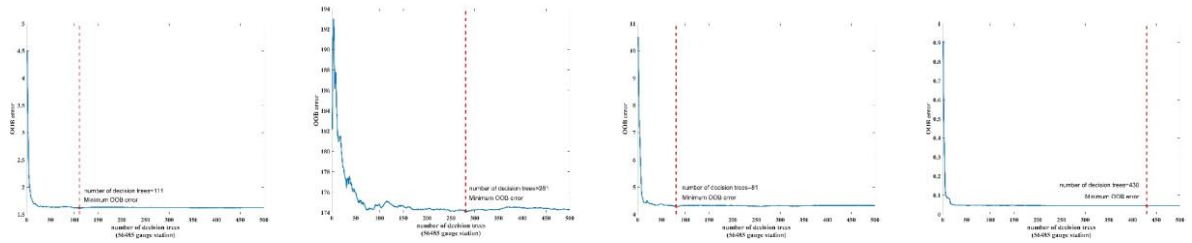
56475



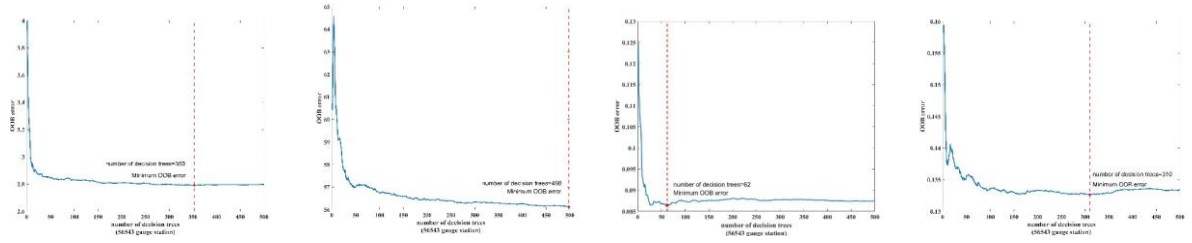
56479



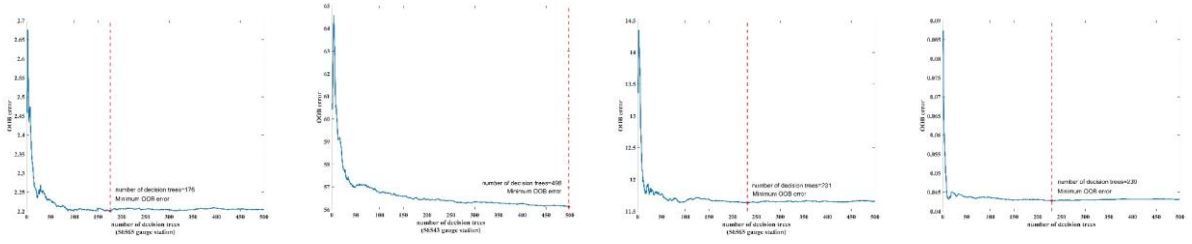
56485



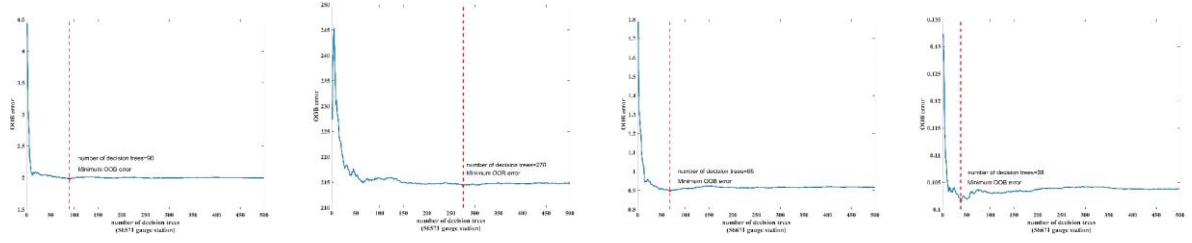
56543



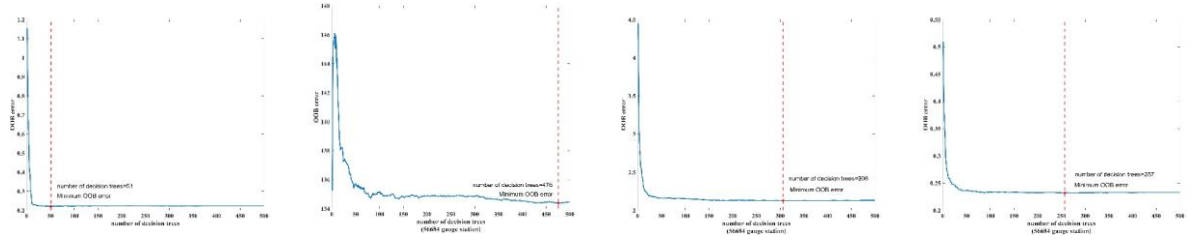
56565



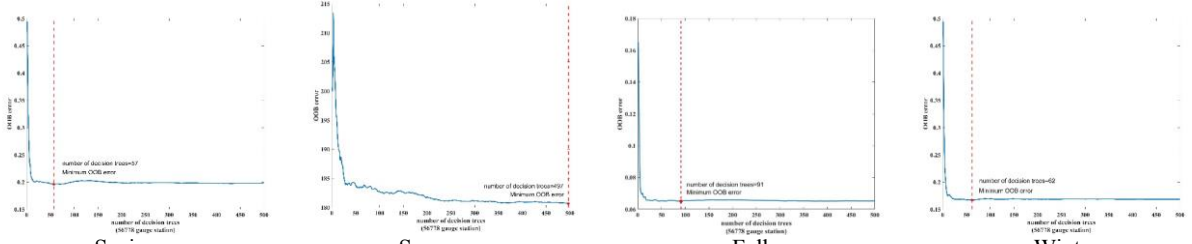
56571



56684



56778



Spring

Summer

Fall

Winter

594 **Figure C1** Changes in the out-of-bag (OOB) error with increasing number of decision trees by means of random forest regression at each
595 gauge station.

596

597

598

599

600

601

602

603

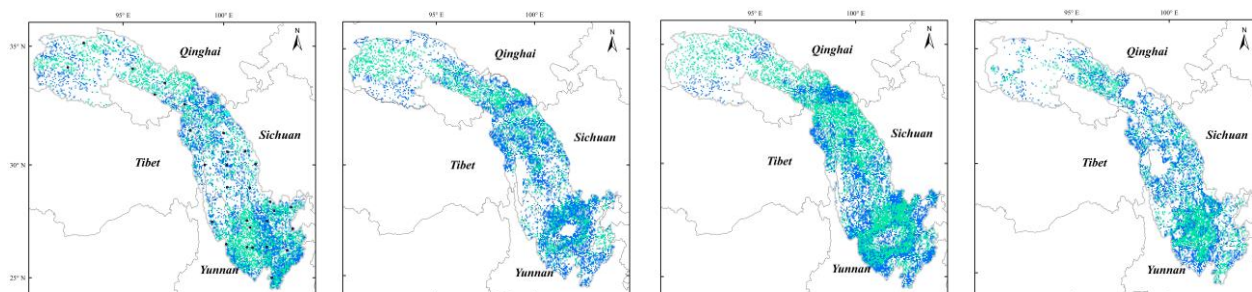
605

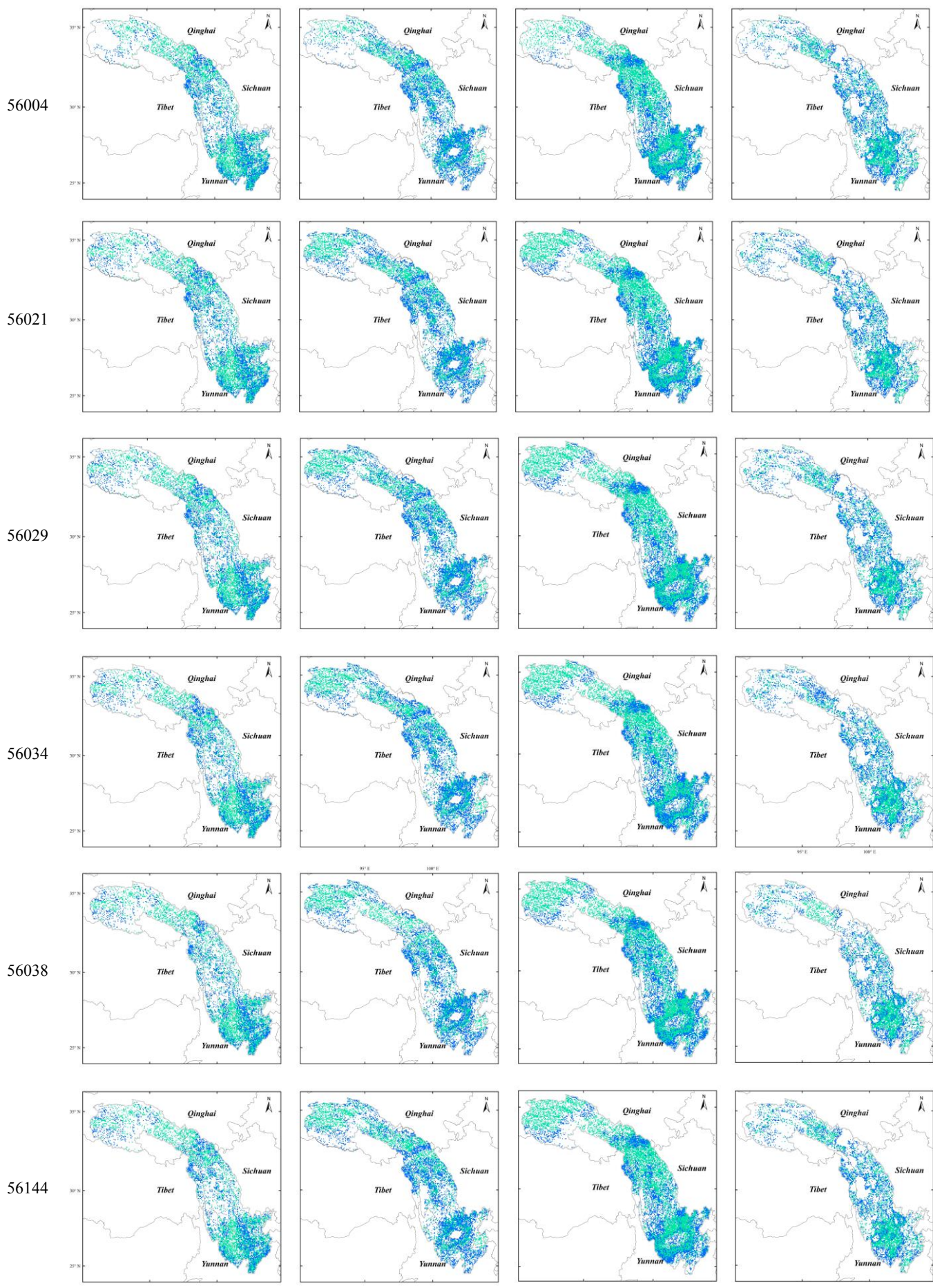
Table D1 Pixel type of the validation gauge station.

Validation gauge station	Pixel type			
	Spring	Summer	Fall	Winter
52908	C4	C4	C4	C4
56004	C4	C4	C4	C4
56021	C2	C2	C2	C3
56029	C2	C3	C2	C3
56034	C2	C3	C2	C3
56038	C4	C4	C4	C4
56144	C4	C4	C4	C4
56146	C4	C4	C4	C4
56152	C2	C3	C3	C4
56167	C4	C2	C2	C4
56247	C4	C4	C4	C4
56251	C2	C2	C3	C3
56257	C4	C4	C4	C4
56357	C4	C4	C4	C4
56374	C4	C4	C3	C4
56459	C4	C4	C4	C4
56462	C4	C4	C4	C4
56475	C4	C3	C3	C3
56479	C4	C4	C4	C4
56485	C3	C2	C2	C3
56543	C3	C3	C4	C4
56565	C2	C2	C3	C3
56571	C2	C4	C4	C4
56586	C2	C3	C2	C3
56651	C3	C2	C2	C3
56664	C4	C4	C4	C4
56666	C3	C3	C3	C3
56671	C3	C2	C2	C3
56684	C2	C2	C2	C4
56778	C4	C3	C3	C4

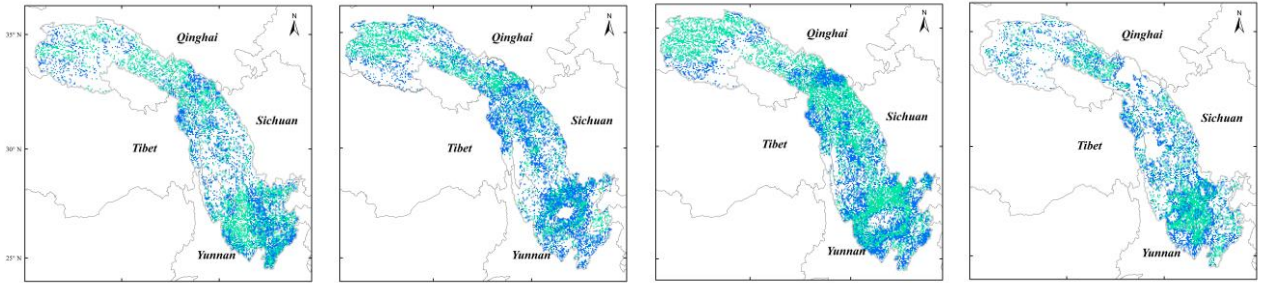
606
607

52908

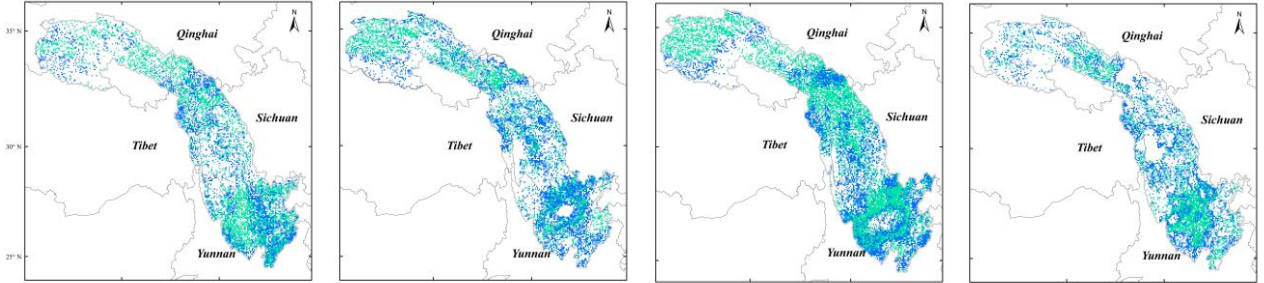




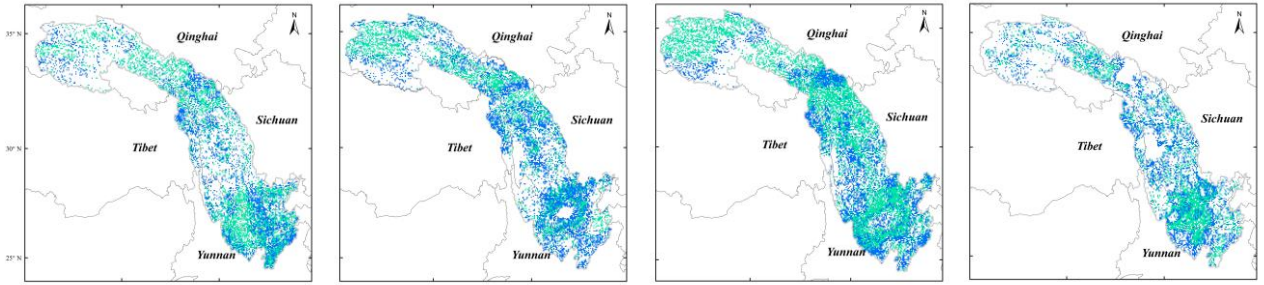
56146



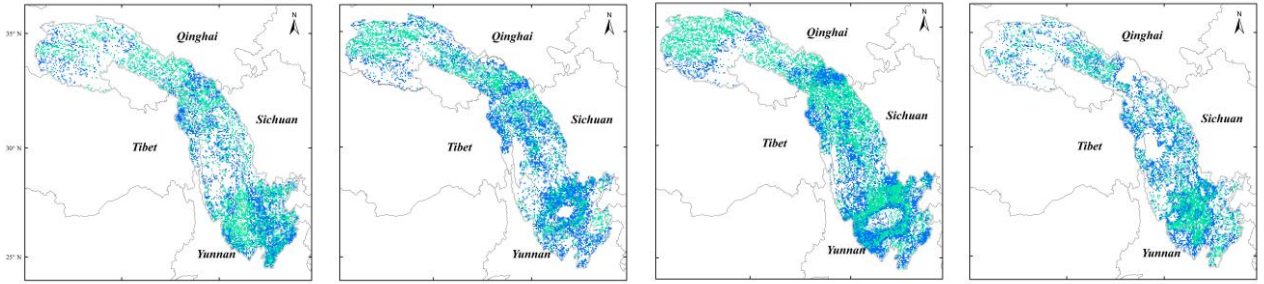
56152



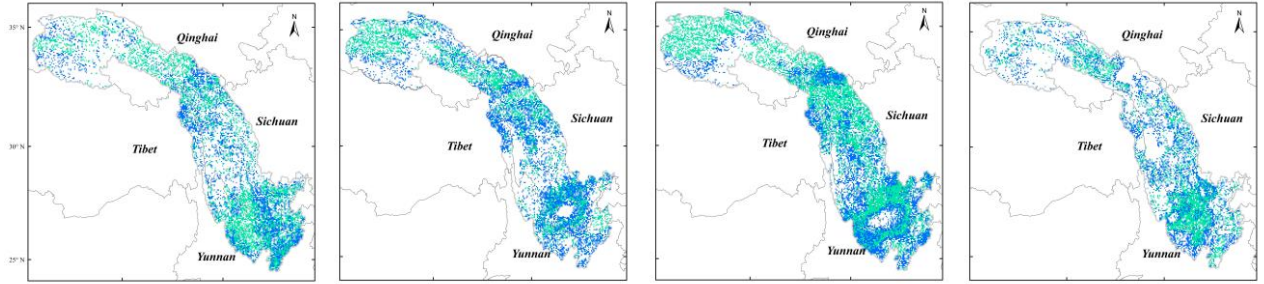
56167



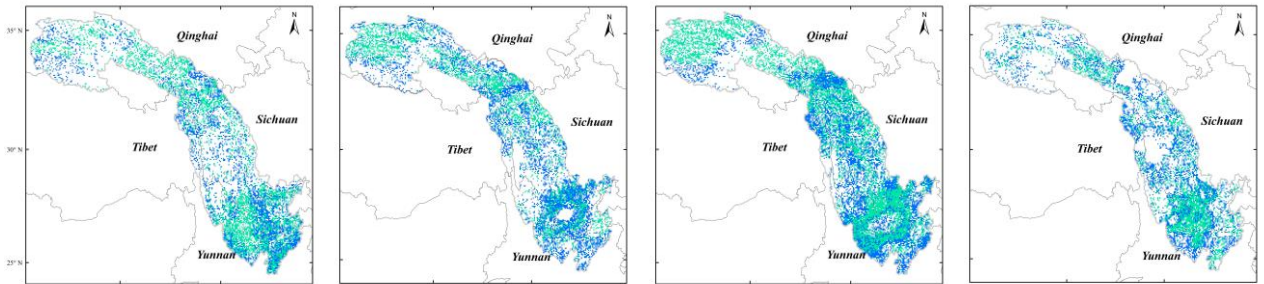
56247



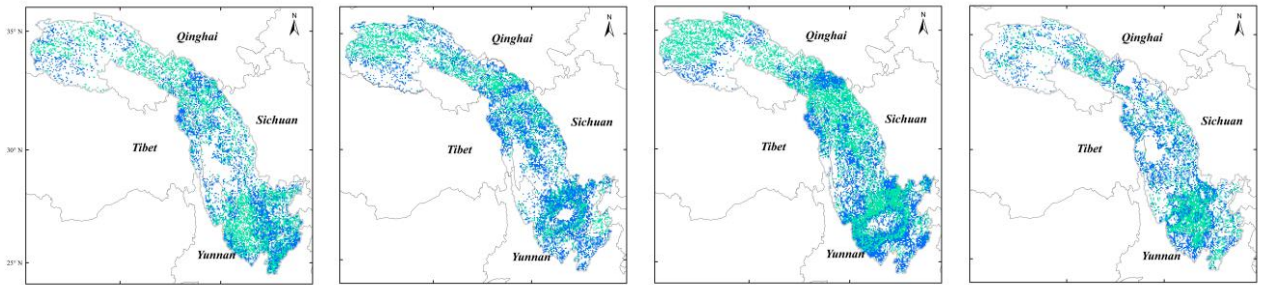
56251



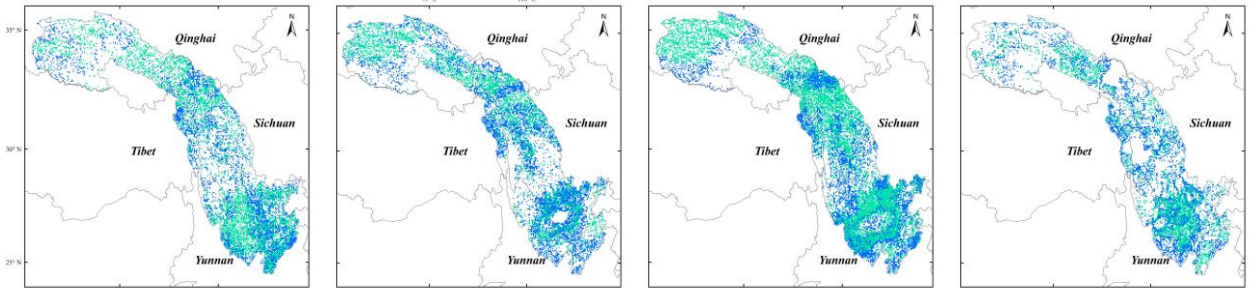
56257



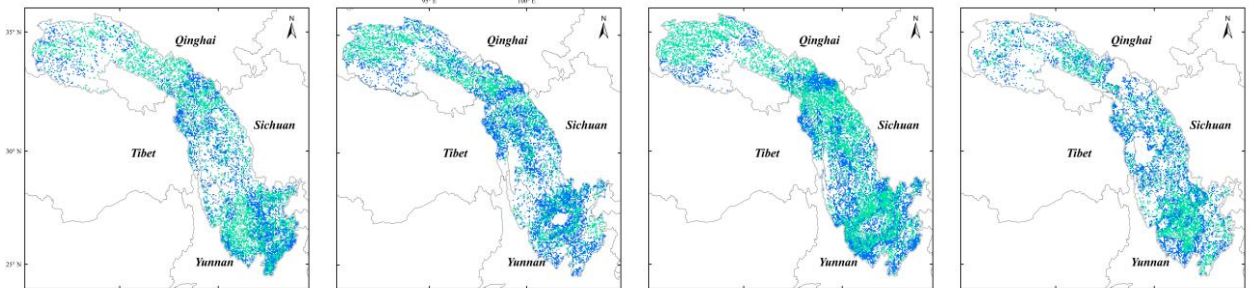
56357



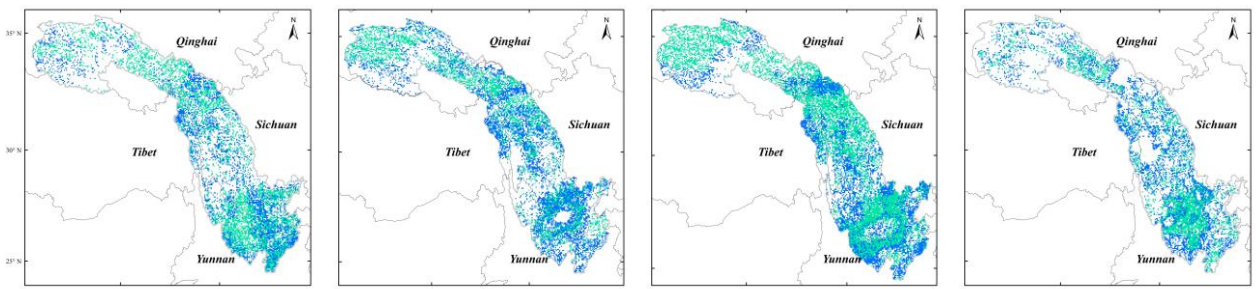
56374



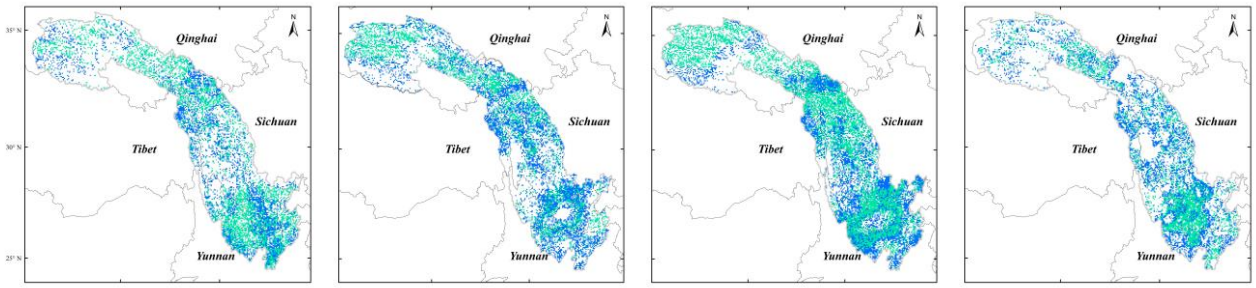
56459



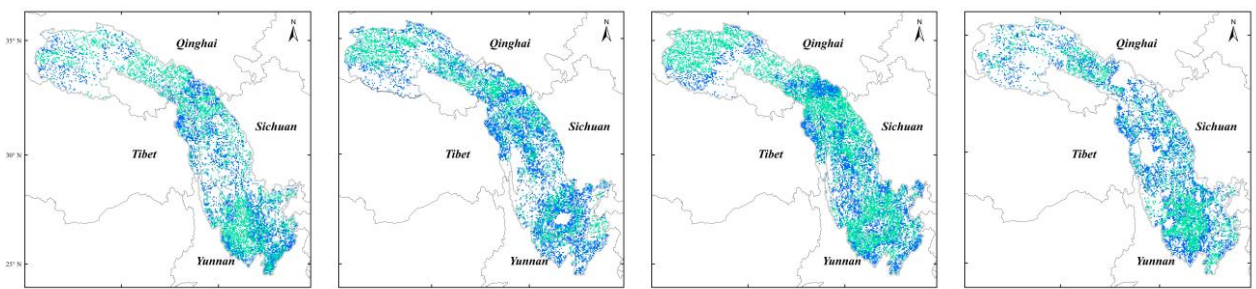
56462



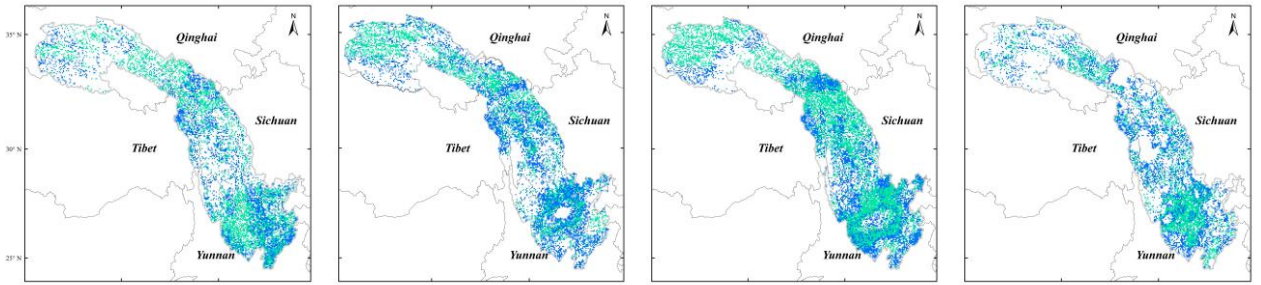
56475



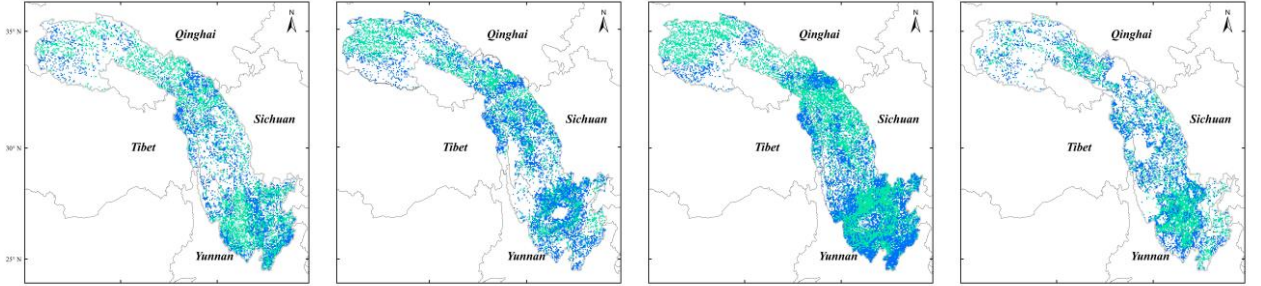
56479



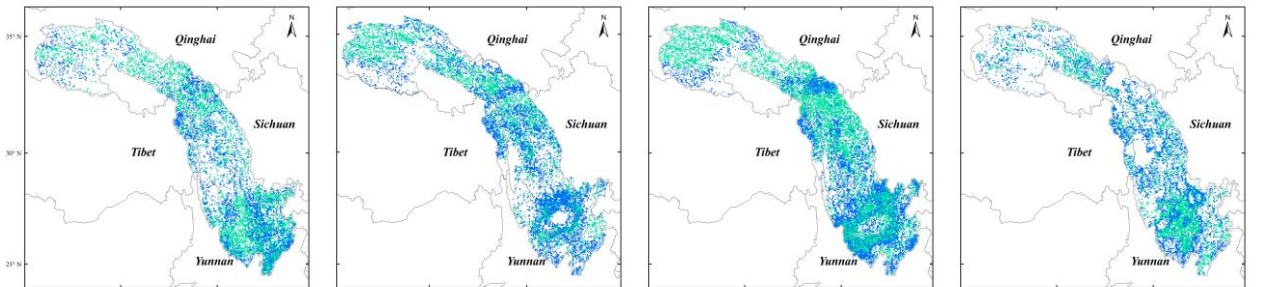
56485



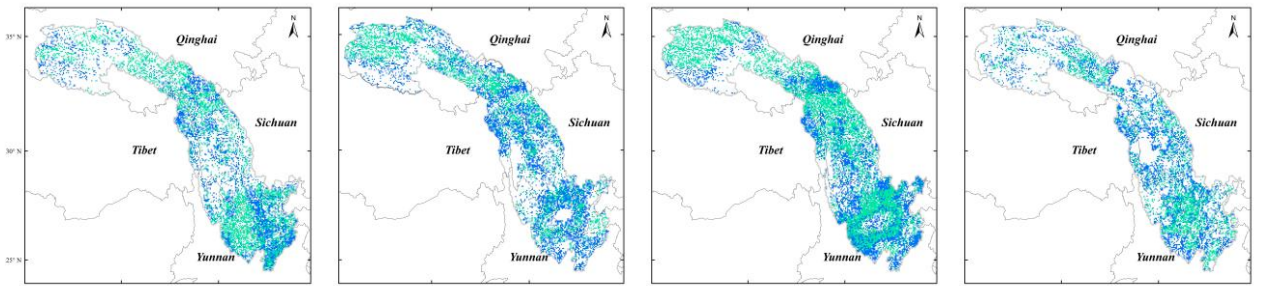
56543



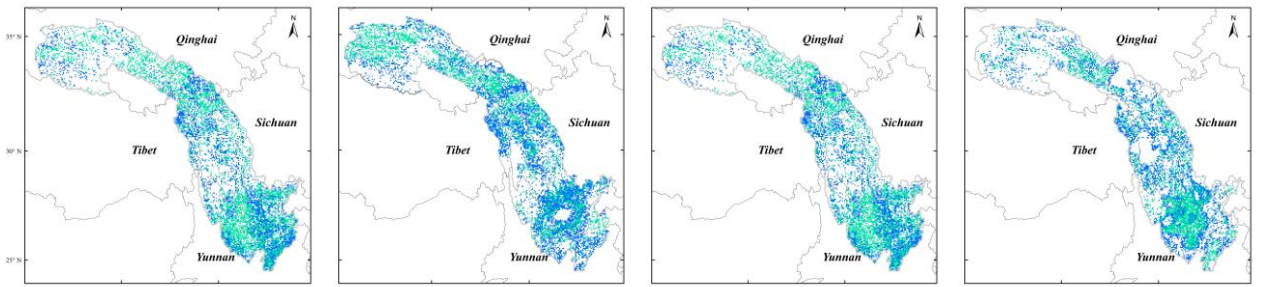
56565



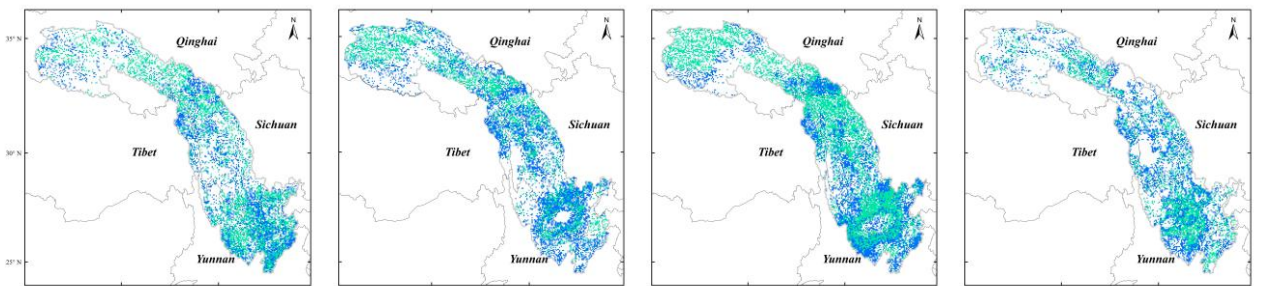
56571

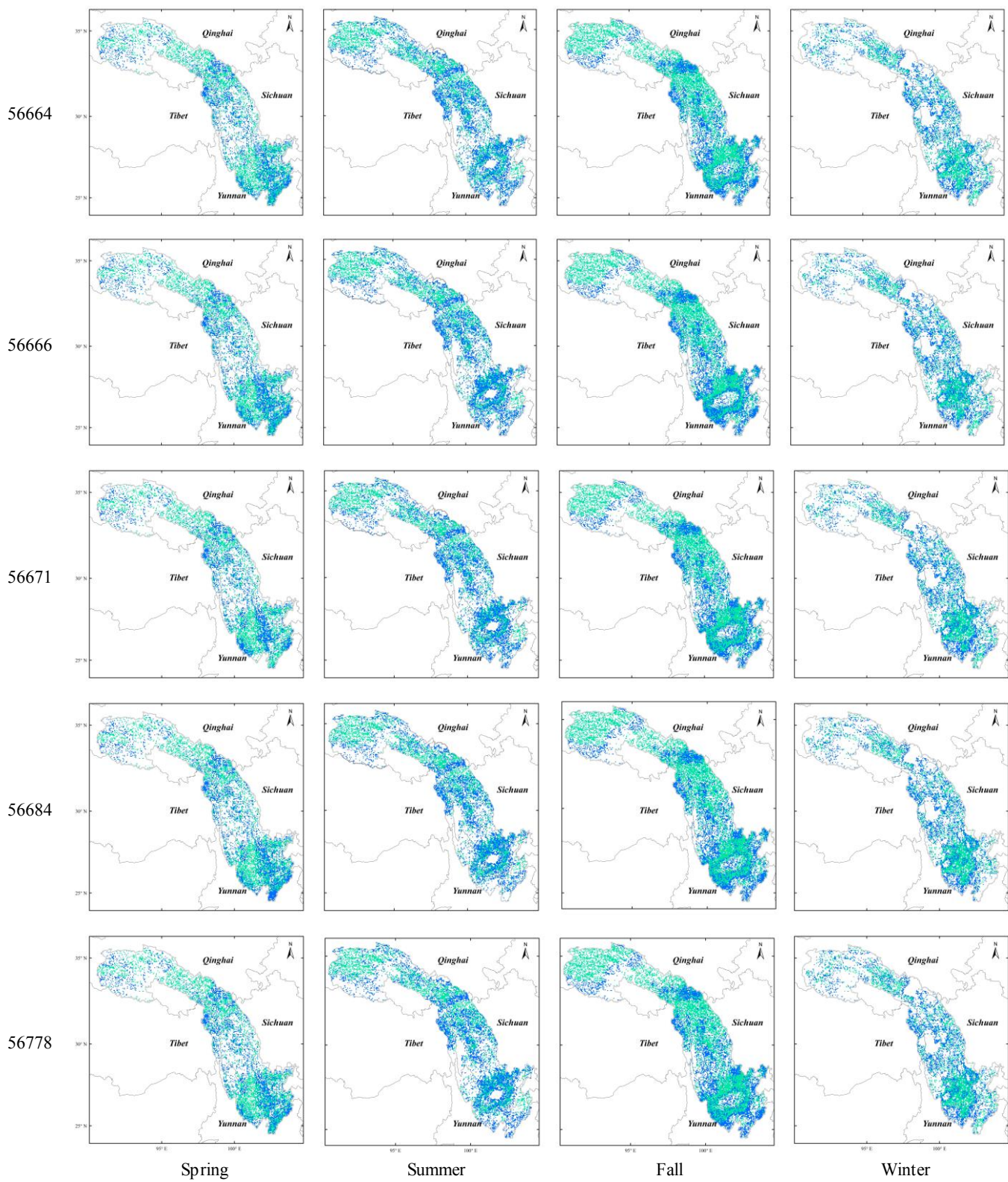


56586



56651





608

609

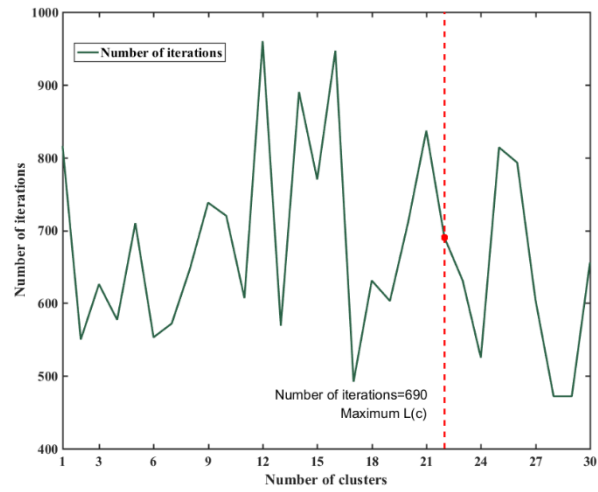
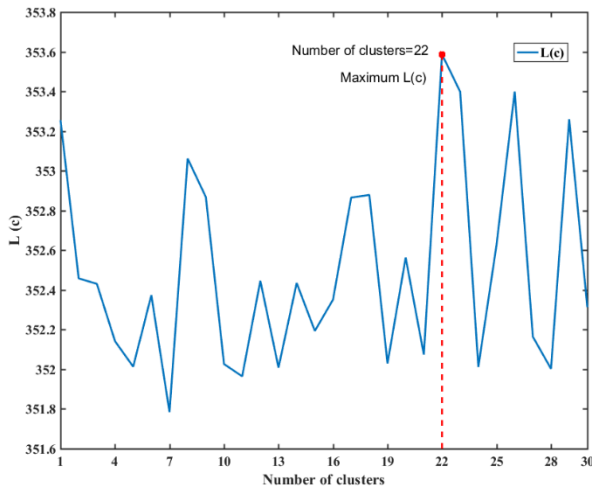
610

Figure D1 Spatial distribution of each class of pixels adjusted by each rule using the WHU-SGCC method in the Jinsha River Basin.

611

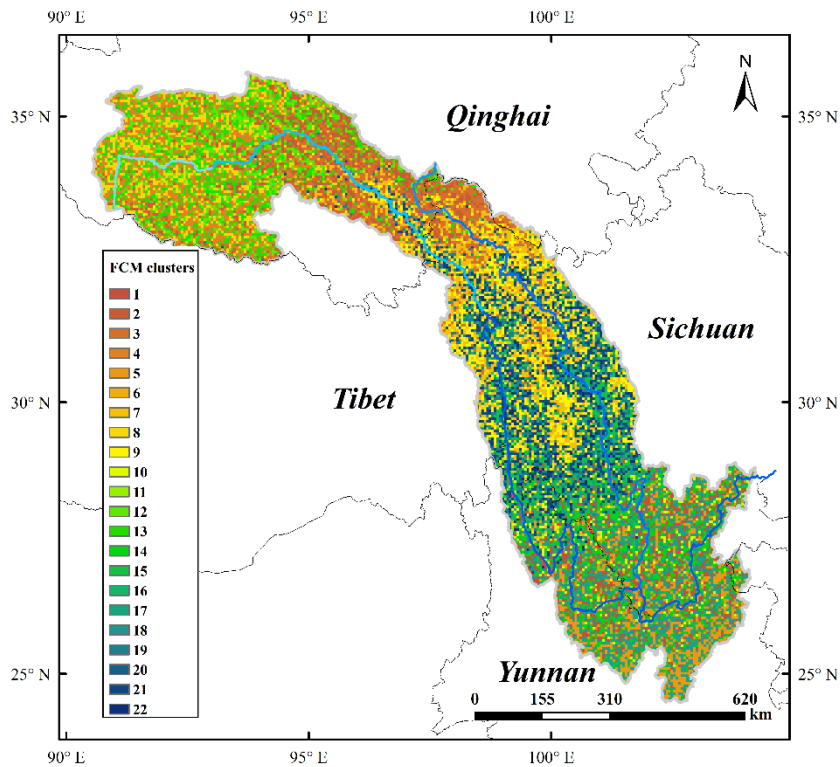
612

Appendix E: Spatial Clustering from the FCM method



613
614

Figure E1 Optimum number of clusters determined by the maximum $L(c)$ with the iterative process.



615
616

Figure E2 Spatial clustering as defined by the FCM method in the Jinsha River Basin.

617 This appendix shows how to set the number of clusters in the FCM method.

618 To adjust the pixels other than those of the gauge stations, the pixels that are statistically similar to the C1 pixels were
 619 selected. According to Rule 2, the C2 pixels were identified in a spatial area defined by the FCM method. In the following
 620 experiments of Rule 2, we set the parameters $m = 2, \epsilon = 0.00001$, and the maximum number of iterations was set 1000 (a
 621 sufficiently large value considering the algorithm efficiency). To determine the optimal numbers of clusters, the value of c was
 622 varied from 1 to 30 with an increment of 1. The values of $L(c)$ during the running of the FCM are shown in Fig E1. The optimum
 623 number of clusters was 22, and the number of iterations was 690 less than the maximum number of iterations.

624 Therefore, the number of clusters was set to 22, and the number of iterations was set to 1000 for full operation by means of
 625 the FCM. The spatial clustering results considering the terrain factors are shown in Fig. E2. In general, the spatial results of
 626 the FCM have many of the same characteristics as the areas defined by the terrain variations, especially with respect to the
 627 slope and runoff directions, which may influence the regional rainfall.

628 **7 Acknowledgments**

629 This work was supported by the National Natural Science Foundation of China program (no. 41771422), the Nature Science
630 Foundation of Hubei Province (no. 2017CFB616), the fundamental research funds for the central universities (no.
631 2042017kf0211), and the LIESMARS Special Research Funding.

632 The authors would like to thank data support: the Climate Hazards Group at the University of California, Santa Barbara, for
633 providing CHIRP and CHIRPS datasets (<http://chg.ucsb.edu/data/>), and the National Climate Center (NCC) of the China
634 Meteorological Administration (CMA) for providing the daily rain gauged observations and gridded precipitation observations
635 (<http://data.cma.cn/>). The authors also thank the PANGAEA Data Publisher for Earth & Environmental Science platform for
636 providing the storage to disseminate the data generated in this experiment.

637 The authors are grateful for the editor and anonymous reviewers for their useful suggestions that clearly improved this paper.

638 **References**

- 639 AghaKouchak, A., Behrangi, A., Sorooshian, S., Hsu, K., and Amitai, E.: Evaluation of satellite-retrieved extreme precipitation
640 rates across the central United States, *J. Geophys. Res.-Atmos.*, 116, 11, doi:10.1029/2010jd014741, 2011.
- 641 Agutu, N. O., Awange, J. L., Zerihun, A., Ndehedehe, C. E., Kuhn, M., and Fukuda, Y.: Assessing multi-satellite remote sensing,
642 reanalysis, and land surface models' products in characterizing agricultural drought in East Africa, *Remote Sens. Environ.*,
643 194, 287-302, doi:10.1016/j.rse.2017.03.041, 2017.
- 644 Ali, H., and Mishra, V.: Contrasting response of rainfall extremes to increase in surface air and dewpoint temperatures at urban
645 locations in India, *Sci Rep*, 7, 1228, doi:10.1038/s41598-017-01306-1, 2017.
- 646 Anders, A. M., Roe, G. H., Hallet, B., Montgomery, D. R., Finnegan, N. J., and Putkonen, J.: Spatial patterns of precipitation
647 and topography in the Himalaya, *Tectonics, Climate, and Landscape Evolution*, 398, 39-53, doi:10.1130/2006.2398(03),
648 2006.
- 649 Aonashi, K., Awaka, J., Hirose, M., Kozi, T., Kubota, T., Liu, G., Shige, S., Kida, S., Seto, S., Takahashi, N., and Takayabu,
650 Y. N.: GSMaP Passive Microwave Precipitation Retrieval Algorithm : Algorithm Description and Validation, *Journal of*
651 *the Meteorological Society of Japan*, 87A, 119-136, 10.2151/jmsj.87A.119, 2009.
- 652 Ashouri, H., Hsu, K.-L., Sorooshian, S., Braithwaite, D. K., Knapp, K. R., Cecil, L. D., Nelson, B. R., and Prat, O. P.:
653 PERSIANN-CDR: Daily Precipitation Climate Data Record from Multisatellite Observations for Hydrological and
654 Climate Studies, *Bulletin of the American Meteorological Society*, 96, 69-83, doi:10.1175/bams-d-13-00068.1, 2015.
- 655 Bai, L., Shi, C. X., Li, L. H., Yang, Y. F., and Wu, J.: Accuracy of CHIRPS Satellite-Rainfall Products over Mainland China,
656 *Remote Sens.*, 10, 28, doi:10.3390/rs10030362, 2018.
- 657 Beck, H. E., Vergopolan, N., Pan, M., Levizzani, V., van Dijk, A. I. J. M., Weedon, G. P., Brocca, L., Pappenberger, F., Huffman,
658 G. J., and Wood, E. F.: Global-scale evaluation of 22 precipitation datasets using gauge observations and hydrological
659 modeling, *Hydrology and Earth System Sciences*, 21, 6201-6217, 10.5194/hess-21-6201-2017, 2017.
- 660 Beck, H. E., Wood, E. F., Pan, M., Fisher, C. K., Miralles, D. G., van Dijk, A. I. J. M., McVicar, T. R., and Adler, R. F.: MSWEP
661 V2 Global 3-Hourly 0.1 degrees Precipitation: Methodology and Quantitative Assessment, *Bulletin of the American*
662 *Meteorological Society*, 100, 473-502, 10.1175/bams-d-17-0138.1, 2019.
- 663 Behrangi, A., Andreadis, K., Fisher, J. B., Turk, F. J., Granger, S., Painter, T., and Das, N.: Satellite-Based Precipitation
664 Estimation and Its Application for Streamflow Prediction over Mountainous Western US Basins, *J. Appl. Meteorol.*
665 *Climatol.*, 53, 2823-2842, doi:10.1175/jamc-d-14-0056.1, 2014.
- 666 Berndt, C., Rabiei, E., and Haberlandt, U.: Geostatistical merging of rain gauge and radar data for high temporal resolutions
667 and various station density scenarios, *Journal of Hydrology*, 508, 88-101, doi:10.1016/j.jhydrol.2013.10.028, 2014.
- 668 Cattani, E., Merino, A., Guijarro, J. A., and Levizzani, V.: East Africa Rainfall Trends and Variability 1983-2015 Using Three

669 Long-Term Satellite Products, *Remote Sens.*, 10, 26, doi:10.3390/rs10060931, 2018.

670 Chen, F. W., and Liu, C. W.: Estimation of the spatial rainfall distribution using inverse distance weighting (IDW) in the middle
671 of Taiwan, *Paddy Water Environ.*, 10, 209-222, 10.1007/s10333-012-0319-1, 2012.

672 Chen, J., Brissette, F. P., Chaumont, D., and Braun, M.: Finding appropriate bias correction methods in downscaling
673 precipitation for hydrologic impact studies over North America, *Water Resources Research*, 49, 4187-4205,
674 doi:10.1002/wrcr.20331, 2013.

675 Derin, Y., Anagnostou, E., Berne, A., Borga, M., Boudevillain, B., Buytaert, W., Chang, C.-H., Delrieu, G., Hong, Y., Hsu, Y.
676 C., Lavado-Casimiro, W., Manz, B., Moges, S., Nikolopoulos, E. I., Sahu, D., Salerno, F., Rodriguez-Sanchez, J.-P.,
677 Vergara, H. J., and Yilmaz, K. K.: Multiregional Satellite Precipitation Products Evaluation over Complex Terrain, *J.*
678 *Hydrometeorol.*, 17, 1817-1836, 10.1175/jhm-d-15-0197.1, 2016.

679 Duan, Z., Liu, J. Z., Tuo, Y., Chiogna, G., and Disse, M.: Evaluation of eight high spatial resolution gridded precipitation
680 products in Adige Basin (Italy) at multiple temporal and spatial scales, *Sci. Total Environ.*, 573, 1536-1553,
681 doi:10.1016/j.scitotenv.2016.08.213, 2016.

682 Dunn, J. C.: A fuzzy relative of the ISODATA Process and Its Use in Detecting Compact Well-Separated Clusters, *Journal of*
683 *Cybernetics*, 3, 32-57, 1973.

684 Durre, I., Menne, M. J., Gleason, B. E., Houston, T. G., and Vose, R. S.: Comprehensive Automated Quality Assurance of
685 Daily Surface Observations, *J. Appl. Meteorol. Climatol.*, 49, 1615-1633, doi:10.1175/2010jamc2375.1, 2010.

686 Funk, C., Peterson, P., Landsfeld, M., Pedreros, D., Verdin, J., Shukla, S., Husak, G., Rowland, J., Harrison, L., Hoell, A., and
687 Michaelsen, J.: The climate hazards infrared precipitation with stations-a new environmental record for monitoring
688 extremes, *Sci. Data*, 2, 21, doi:10.1038/sdata.2015.66, 2015 a.

689 Funk, C., Verdin, A., Michaelsen, J., Peterson, P., Pedreros, D., and Husak, G.: A global satellite-assisted precipitation
690 climatology, *Earth Syst. Sci. Data*, 7, 275-287, 10.5194/essd-7-275-2015, 2015 b.

691 Funk, C., Peterson, P., Landsfeld, M., Pedreros, D., Verdin, J., Rowland, J., Bo, E., Husak, G. J., Michaelsen, J. C., and Verdin,
692 A. P.: A Quasi-Global Precipitation Time Series for Drought Monitoring Data Series 832, *Usgs Professional Paper, Data*
693 *Series*, 2014.

694 Genuer, R., Poggi, J. M., Tuleau-Malot, C., and Villa-Vialaneix, N.: Random Forests for Big Data, *Big Data Res.*, 9, 28-46,
695 doi:10.1016/j.bdr.2017.07.003, 2017.

696 Hou, A. Y., Kakar, R. K., Neeck, S., Azarbarzin, A. A., Kummerow, C. D., Kojima, M., Oki, R., Nakamura, K., and Iguchi, T.:
697 The Global Precipitation Measurement Mission, *Bulletin of the American Meteorological Society*, 95, 701-722,
698 10.1175/bams-d-13-00164.1, 2014.

699 Huffman, G. J., Adler, R. F., Bolvin, D. T., Gu, G., Nelkin, E. J., Bowman, K. P., Hong, Y., Stocker, E. F., and Wolff, D. B. :
700 The TRMM multisatellite precipitation analysis (TMPA): Quasi-global, multiyear, combined-sensor precipitation
701 estimates at fine scales, *J. Hydrometeorol.*, 8, 38-55, 10.1175/jhm560.1, 2007.

702 Huffman, G. J., Adler, R. F., Bolvin, D. T., and Nelkin, E. J.: The TRMM Multi-Satellite Precipitation Analysis (TMPA), in:
703 *Satellite Rainfall Applications for Surface Hydrology*, edited by: Gebremichael, M., and Hossain, F., Springer Netherlands,
704 Dordrecht, 3-22, 2010.

705 Huffman, G. J., D. T. Bolvin, D. Braithwaite, K. Hsu, R. Joyce, P. Xie.: NASA Global Precipitation Measurement Integrated
706 Multi-satellite Retrievals for GPM (IMERG), NASA Algorithm theoretical basis document (ATBD) version 5.2., 35 pp.
707 https://pmm.nasa.gov/sites/default/files/document_files/IMERG_ATBD_V5.2.pdf, 2018.

708 Johnson, R. W.: *An Introduction to the Bootstrap*, Chapman & Hall/CRC Press, 49-54 pp., 1998.

709 Joyce, R. J., Janowiak, J. E., Arkin, P. A., and Xie, P. P.: CMORPH: A method that produces global precipitation estimates
710 from passive microwave and infrared data at high spatial and temporal resolution, *J. Hydrometeorol.*, 5, 487-503,
711 10.1175/1525-7541(2004)005<0487:camtpg>2.0.co;2, 2004.

712 Joyce, R. J., and Xie, P.: Kalman Filter-Based CMORPH, *J. Hydrometeorol.*, 12, 1547-1563, 10.1175/jhm-d-11-022.1, 2011.

713 Katsanos, D., Retalis, A., and Michaelides, S.: Validation of a high-resolution precipitation database (CHIRPS) over Cyprus
714 for a 30-year period, *Atmospheric Research*, 169, 459-464, doi:10.1016/j.atmosres.2015.05.015, 2016a.

715 Katsanos, D., Retalis, A., Tymvios, F., and Michaelides, S.: Analysis of precipitation extremes based on satellite (CHIRPS)
716 and in situ dataset over Cyprus, *Natural Hazards*, 83, 53-63, doi:10.1007/s11069-016-2335-8, 2016b.

717 Kummerow, C., Barnes, W., Kozu, T., Shiue, J., and Simpson, J.: The Tropical Rainfall Measuring Mission (TRMM) sensor
718 package, *J. Atmos. Ocean. Technol.*, 15, 809-817, doi:10.1175/1520-0426(1998)015<0809:ttrmmt>2.0.co;2, 1998.

719 Long, D., and Singh, V. P.: Assessing the impact of end-member selection on the accuracy of satellite-based spatial variability
720 models for actual evapotranspiration estimation, *Water Resources Research*, 49, 2601-2618, doi:10.1002/wrcr.20208,
721 2013.

722 Lu, G. Y., and Wong, D. W.: An adaptive inverse-distance weighting spatial interpolation technique, *Comput. Geosci.*, 34,
723 1044-1055, 10.1016/j.cageo.2007.07.010, 2008.

724 Maggioni, V., and Massari, C.: on the performance of satellite precipitation products in riverine flood modeling: A review,
725 *Journal of Hydrology*, 558, 214-224, 10.1016/j.jhydrol.2018.01.039, 2018.

726 Maggioni, V., Meyers, P. C., and Robinson, M. D.: A Review of Merged High-Resolution Satellite Precipitation Product
727 Accuracy during the Tropical Rainfall Measuring Mission (TRMM) Era, *J. Hydrometeorol.*, 17, 1101-1117, 10.1175/jhm-
728 d-15-0190.1, 2016.

729 Mahmoud, M. T., Al-Zahrani, M. A., and Sharif, H. O.: Assessment of global precipitation measurement satellite products over
730 Saudi Arabia, *Journal of Hydrology*, 559, 1-12, 10.1016/j.jhydrol.2018.02.015, 2018.

731 Martens, B., Cabus, P., De Jongh, I., and Verhoest, N. E. C.: Merging weather radar observations with ground-based
732 measurements of rainfall using an adaptive multiquadric surface fitting algorithm, *Journal of Hydrology*, 500, 84-96,
733 doi:10.1016/j.jhydrol.2013.07.011, 2013.

734 Nash, J. E., Sutcliffe, J. V.: River flow forecasting through conceptual models, Part I - A discussion of principles, *Journal of*
735 *Hydrology*, 10, 282-290, doi.org/10.1016/0022-1694(70)90255-6, 1970.

736 Nogueira, S. M. C., Moreira, M. A., and Vulpato, M. M. L.: Evaluating Precipitation Estimates from Eta, TRMM and CHIRPS
737 Data in the South-Southeast Region of Minas Gerais State-Brazil, *Remote Sens.*, 10, 16, doi:10.3390/rs10020313, 2018.

738 Ning, S., Wang, J., Jin, J., and Ishidaira, H.: Assessment of the Latest GPM-Era High-Resolution Satellite Precipitation
739 Products by Comparison with Observation Gauge Data over the Chinese Mainland, *Water*, 8, 481-497,
740 doi:10.3390/w8110481, 2016.

741 Paredes-Trejo, F. J., Barbosa, H. A., and Kumar, T. V. L.: Validating CHIRPS-based satellite precipitation estimates in
742 Northeast Brazil, *J. Arid. Environ.*, 139, 26-40, doi:10.1016/j.jaridenv.2016.12.009, 2017.

743 Prakash, S.: Performance assessment of CHIRPS, MSWEP, SM2RAIN-CCI, and TMPA precipitation products across India,
744 *Journal of Hydrology*, 571, 50-59, 10.1016/j.jhydrol.2019.01.036, 2019.

745 Pessoa, F. C. L., Blanco, C. J. C., and Gomes, E. P.: Delineation of homogeneous regions for streamflow via fuzzy c-means in
746 the Amazon, *Water Pract. Technol.*, 13, 210-218, doi:10.2166/wpt.2018.035, 2018.

747 Roy, T., Gupta, H. V., Serrat-Capdevila, A., and Valdes, J. B.: Using satellite-based evapotranspiration estimates to improve
748 the structure of a simple conceptual rainfall–runoff model, *Hydrology and Earth System Sciences*, 21, 879-896,
749 doi:10.5194/hess-21-879-2017, 2017.

750 Skofronick-Jackson, G., Petersen, W. A., Berg, W., Kidd, C., Stocker, E. F., Kirschbaum, D. B., Kakar, R., Braun, S. A.,
751 Huffman, G. J., Iguchi, T., Kirstetter, P. E., Kummerow, C., Meneghini, R., Oki, R., Olson, W. S., Takayabu, Y. N.,
752 Furukawa, K., and Wilhelm, T.: The Global Precipitation Measurement (GPM) Mission for Science and Society, *Bulletin*
753 *of the American Meteorological Society*, 98, 1679-1695, 10.1175/bams-d-15-00306.1, 2017.

754 Shen, G. Y., Chen, N. C., Wang, W., and Chen, Z. Q.: High-resolution daily precipitation estimation data from WHU-SGCC

755 method: A novel approach for blending daily satellite (CHIRP) and precipitation observations over the Jinsha River Basin.
756 PANGAEA, <https://doi.pangaea.de/10.1594/PANGAEA.900620>, 2019.

757 Simanton, J. R., and Osborn, H. B.: RECIPROCAL-DISTANCE ESTIMATE OF POINT RAINFALL, *Journal of the*
758 *Hydraulics Division-Asce*, 106, 1242-1246, 1980.

759 Simpson, J., Adler, R. F., and North, G. R.: A PROPOSED TROPICAL RAINFALL MEASURING MISSION (TRMM)
760 SATELLITE, *Bulletin of the American Meteorological Society*, 69, 278-295, doi:10.1175/1520-
761 0477(1988)069<0278:aptrmm>2.0.co;2, 1988.

762 Sokol, Z.: The use of radar and gauge measurements to estimate areal precipitation for several Czech River basins, *Stud.*
763 *Geophys. Geod.*, 47, 587-604, doi:10.1023/a:1024715702575, 2003.

764 Su, F. G., Gao, H. L., Huffman, G. J., and Lettenmaier, D. P.: Potential Utility of the Real-Time TMPA-RT Precipitation
765 Estimates in Streamflow Prediction, *J. Hydrometeorol.*, 12, 444-455, doi:10.1175/2010jhm1353.1, 2011.

766 Thiemig, V., Rojas, R., Zambrano-Bigiarini, M., and De Roo, A.: Hydrological evaluation of satellite-based rainfall estimates
767 over the Volta and Baro-Akobo Basin, *Journal of Hydrology*, 499, 324-338, doi:10.1016/j.jhydrol.2013.07.012, 2013.

768 Trejo, F. J. P., Barbosa, H. A., Penaloza-Murillo, M. A., Moreno, M. A., and Farias, A.: Intercomparison of improved satellite
769 rainfall estimation with CHIRPS gridded product and rain gauge data over Venezuela, *Atmosfera*, 29, 323-342,
770 doi:10.20937/atm.2016.29.04.04, 2016.

771 Tung, Y. K.: POINT RAINFALL ESTIMATION FOR A MOUNTAINOUS REGION, *J. Hydraul. Eng.-ASCE*, 109, 1386-
772 1393, 10.1061/(asce)0733-9429(1983)109:10(1386), 1983.

773 Ushio, T., Sasashige, K., Kubota, T., Shige, S., Okamoto, K. i., Aonashi, K., Inoue, T., Takahashi, N., Iguchi, T., Kachi, M.,
774 Oki, R., Morimoto, T., and Kawasaki, Z.-I.: A Kalman Filter Approach to the Global Satellite Mapping of Precipitation
775 (GSMaP) from Combined Passive Microwave and Infrared Radiometric Data, *Journal of the Meteorological Society of*
776 *Japan*, 87A, 137-151, 10.2151/jmsj.87A.137, 2009.

777 Ushio, T., and Kachi, M.: Kalman filtering applications for global satellite mapping of precipitation (GSMaP), in: *Satellite*
778 *rainfall applications for surface hydrology*, Springer, 105-123, 2010.

779 Verdin, A., Rajagopalan, B., Kleiber, W., and Funk, C.: A Bayesian kriging approach for blending satellite and ground
780 precipitation observations, *Water Resources Research*, 51, 908-921, 2015.

781 Vila, D. A., de Goncalves, L. G. G., Toll, D. L., and Rozante, J. R.: Statistical Evaluation of Combined Daily Gauge
782 Observations and Rainfall Satellite Estimates over Continental South America, *J. Hydrometeorol.*, 10, 533-543,
783 doi:10.1175/2008jhm1048.1, 2009.

784 Wang, P. H.: PATTERN-RECOGNITION WITH FUZZY OBJECTIVE FUNCTION ALGORITHMS - BEZDEK,JC, *SIAM*
785 *Rev.*, 25, 442-442, 1983.

786 Xie, P., Joyce, R., Wu, S., Yoo, S.-H., Yarosh, Y., Sun, F., and Lin, R.: Reprocessed, Bias-Corrected CMORPH Global High-
787 Resolution Precipitation Estimates from 1998, *J. Hydrometeorol.*, 18, 1617-1641, 10.1175/jhm-d-16-0168.1, 2017.

788 Xu, L., Chen, N., Zhang, X., Chen, Z., Hu, C., and Wang, C.: Improving the North American multi-model ensemble (NMME)
789 precipitation forecasts at local areas using wavelet and machine learning, *Clim. Dyn.*, 53, 601-615, 10.1007/s00382-018-
790 04605-z, 2019.

791 Yang, T. T., Asanjan, A. A., Welles, E., Gao, X. G., Sorooshian, S., and Liu, X. M.: Developing reservoir monthly inflow
792 forecasts using artificial intelligence and climate phenomenon information, *Water Resources Research*, 53, 2786-2812,
793 doi:10.1002/2017wr020482, 2017.

794 Yang, Z., Hsu, K., Sorooshian, S., Xu, X., Braithwaite, D., and Verbist, K. M. J.: Bias adjustment of satellite-based precipitation
795 estimation using gauge observations: A case study in Chile, *Journal of Geophysical Research: Atmospheres*, 121, 3790-
796 3806, doi:10.1002/2015jd024540, 2016.

797 Yuan, Z., Xu, J. J., and Wang, Y. Q.: Projection of Future Extreme Precipitation and Flood Changes of the Jinsha River Basin

798 in China Based on CMIP5 Climate Models, *Int. J. Environ. Res. Public Health*, 15, 17, 10.3390/ijerph15112491, 2018.

799 Zambrano-Bigiarini, M., Nauditt, A., Birkel, C., Verbist, K., and Ribbe, L.: Temporal and spatial evaluation of satellite-based
800 rainfall estimates across the complex topographical and climatic gradients of Chile, *Hydrology and Earth System Sciences*,
801 21, 1295-1320, doi:10.5194/hess-21-1295-2017, 2017.

802 Zhang, X., and Chen, N. C.: Reconstruction of GF-1 Soil Moisture Observation Based on Satellite and In Situ Sensor
803 Collaboration Under Full Cloud Contamination, *Ieee Transactions on Geoscience and Remote Sensing*, 54, 5185-5202,
804 10.1109/tgrs.2016.2558109, 2016.

805 Zhang, Y. R., Sun, A., Sun, H. W., Gui, D. W., Xue, J., Liao, W. H., Yan, D., Zhao, N., and Zeng, X. F.: Error adjustment of
806 TMPA satellite precipitation estimates and assessment of their hydrological utility in the middle and upper Yangtze River
807 Basin, China, *Atmospheric Research*, 216, 52-64, 10.1016/j.atmosres.2018.09.021, 2019.